Budapest University of Technology and Economics
Faculty of Civil Engineering
Department of Structural Mechanics

EFFECT OF PREBUCKLING DEFORMATIONS ON THE LATERAL TORSIONAL BUCKLING OF DOUBLY SYMMERTIC BEAMS: INFLUENCE OF TORSIONAL RIGIDITY, END SUPPORTS, AND INTERMEDIATE SUPPORTS

PhD Dissertation

GHAITH ABU REDEN

Supervised by

Dr. Sándor Ádány

Budapest, 2025

Abstract

Classical solutions for the LTB of beams which are widely used nowadays assume a perfectly straight beam when the buckling occurs. In the reality however, prebuckling deformations exist. Although not too numerous, several studies showed that prebuckling deformations can have a significant effect on the values of critical moment. However, these studies are limited to the most basic case but still give several analytical solutions for the seemingly same case. Furthermore, the effect of torsional rigidity, end supports, and intermediate lateral supports are hardly discussed or not discussed at all within the context of prebuckling deformations. Finally, there are very little studies that used a general numerical method (FEM) to study the effect of prebuckling deformations.

This study aims towards deepening the understanding of the LTB considering prebuckling deformations by considering several factors: (i) causes of discrepancies in the literature, (ii) effect of torsional rigidity (open vs closed sections), (iii) effect of end supports, and (iv) effect of intermediate lateral and torsional supports. Both analytical and numerical approaches are taken. For the analytical solutions, the energy method is used. For the numerical solutions, the Finite Element Method (FEM) is employed using both beam and shell elements, and two types of analysis: the geometrically nonlinear with imperfections analysis (GNIA), and the linear buckling analysis (LBA). However, since the LBA does not account for prebuckling deformations, a specialized iterative process that alternate between static analysis and buckling analysis is proposed. The iterative LBA and GNIA methods were shown to yield similar results.

Several interesting results were found. First, the sources of discrepancies in the literature were shown to come from various options during the derivations, as well as simplifications/assumptions that are either appropriate or not depending on the case, which means there is no definite single critical moment formula that works for all cases. Furthermore, it was found that the torsional rigidity plays an important role in how the prebuckling deformations affect the critical moment. The end supports were also shown to have a significant influence on the effect of prebuckling deformations, with some end supports causing a decrease in critical moment due to prebuckling deformations rather than an increase. The intermediate lateral supports were also shown to have a significant influence, which is caused by a ‘switch’ in the buckling shape depending on which type of intermediate support is used. A comprehensive shape analysis study was conducted to further understand the behaviors. Other support conditions, loading conditions, or cross sections can be investigated in future studies.

Contents

Chapter 1: Introduction

1.1 Lateral Torsional Buckling (LTB)

Although thin-walled steel structural members offer the advantage of high carrying capacity with relatively low weights, they have some disadvantages, one of the most notable being the instabilities due to local and global buckling. Several types of instabilities can occur to steel structural members, such as: flexural buckling [1], lateral torsional buckling [2], local buckling [3], pure torsional buckling [4], distortional buckling [5], or combined types of buckling, such as: interaction buckling [6] and coupled instabilities [7].

In this research, the *lateral-torsional buckling* (LTB) is discussed. The beam deflection takes place in the plane of the loading (referred to as *primary displacement*), and the deflection gradually increases (approximately linearly) as the load increases. Even if the material is perfectly elastic, which is assumed here, stable equilibrium in the primary displaced shape is not possible for an arbitrary load, since at a certain load level, the member starts to develop rapidly increasing lateral displacements (referred to as *secondary displacement*) characterized by twisting rotations and translations perpendicular to the plane of loading as shown in Figure 1-1.

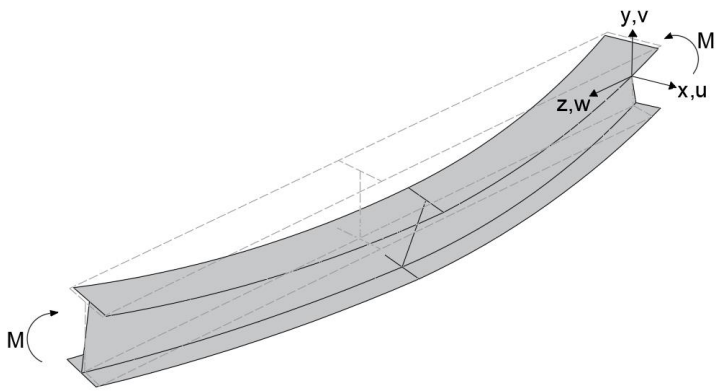

Figure 1-1: Lateral torsional buckling (LTB) of a steel beam.

One of the earliest publications discussing the topic was back in 1899 [2] which did not use the term *lateral torsional buckling* directly but discussed the instability of thin flat bars by a “combined lateral displacement and twist”. It is mentioned that the torsional rigidity is the main affecting factor of such failure, rather than the flexural rigidity. Another early work was [8], which was done by Stephen P. Timoshenko and discussed the failure due to the lateral displacement of a rod, which is always accompanied by a twisting or overturning. It is

mentioned that such a rod would have two very different principal moments of inertia and is subjected to bending forces in the direction of the greater stiffness.

In fact, Timoshenko was one of the main contributors in the field of LTB, he published various papers on the topic [8,9,10]. Later in his book [11], Timoshenko discussed the LTB of beams under various conditions, such as beams in pure bending, simply supported, cantilevers, beams with narrow rectangular cross sections, as well as other cases. LTB, or the Lateral Buckling as referred to in the book, occurs when the beam is subjected to bending in the plane of the highest moment of inertia, by the lateral buckling (in the direction of the plane of the lowest moment of inertia). Differential equations are established assuming a perfect non-deflected beam, and a closed formed solutions are provided for the critical moment for several cases. These formulae are still (more or less) being used until this day in many design codes and practices. It is also to mention that other early works also investigated the same topic, such as [12].

1.2 Energy method

The energy method for the stability of structures involves assessing the potential energy of a deformed structure to determine if small perturbations will increase or decrease the energy, indicating stability or instability, respectively [11, 13]. Which is based on the Lagrange-Dirichlet theorem [14], stating that a system is at equilibrium in a certain state when the total potential energy of the system is at the absolute minimum at that state [15, 16]. In the context of buckling, this would involve determining the total potential energy of the structural element under certain loading and boundary conditions, which includes a combination of strain energy due to deflection, as well as external potential energy due to applied load [17]. Many studies used the energy method for the calculation of the critical load for LTB of beams by assuming shape functions and deriving the energy formulation [18-21].

For the calculation of potential energy, the strain energy is first calculated. The strain energy of a member under bending is equal to the integration of stress times the strain over the volume of the beam [22]. This can be broken down into components of curvatures and stiffnesses as it will be shown in following chapters. Expressions for the curvature in both directions, as well as the twisting curvature are needed, as can be obtained from [23]. The curvature in the longitudinal direction is also used for the calculation of the external energy. The calculation of the curvatures involves establishing a proper transformation matrix from the global to local coordinates [24], as well as establishing shape functions which satisfy the

boundary conditions. In this study, various transformation matrices, leading to different curvature functions are considered. This will be shown in detail in Chapter 2.

1.3 Linear Buckling Analysis (LBA)

One of the most commonly used techniques for the prediction of buckling loads is what is known as the Linear Buckling Analysis (LBA). The word Linear comes from the assumption of linear material behavior and small deformations. It focuses on the initial stability of the structure, and not on the post-buckling behavior [40, 41]. LBA determines the bucking loads and their corresponding buckling modes of a structure. This is done by solving an eigenvalue problem, in this context, the critical loads, as their corresponding eigenvectors, which are the buckling shapes associated with these critical loads. The eigenvalue problem can be expressed as

$$(K - \lambda K_g)\phi = 0 \tag{1}$$

with K being the stiffness matrix, $K_g$being the geometric stiffness matrix, λ being the eigenvalues representing the buckling loads, and ϕ the eigenvectors representing the buckling modes [42,43].

1.4 Geometrically Nonlinear Analysis with Imperfections (GNIA)

Although Linear Buckling Analysis is a good way for predicting the possible buckling loads and their associated buckling modes, it is very limited and can be only used for initial estimates, as it considers a perfect geometry and does not deal with the prebuckling, or post buckling behaviors. On the other hand, another method for the assessment of the stabilities of structures is the Geometrically Nonlinear with Imperfections Analysis (GNIA) method [44]. The concept was probably first applied by Young [45] for columns and was later extended to other types of buckling. GNIA can be a useful tool for predicting the load-bearing capacity, as first proposed in [46]. The approach and resulting formula, known as the Ayrton-Perry approach/formula, are named after the authors.

This approach is the basis of the European buckling curves, which were proposed by [47], and which are still in use in the current Eurocode standards, e.g. [48], for both column buckling and LTB. It is a nonlinear method which can account for large deformations, as well as initial imperfections. This makes it more capable of predicting real life behaviors of the structure. However, it should be noted that material nonlinearity is not considered in this

method, making it distinct from the Geometrically and Materially Nonlinear with Imperfections method (GMNIA) [49].

The GNIA method often uses a numerical method for the solution, typically the FEM method. Compared to the LBA method, the GNIA is more computationally demanding since the solution follows the load path, resulting in many sub-steps of which the stiffness matrix is updated constantly, with an iterative process in each load step. This process makes it not as widely used as much as the LBA, especially when large deformations and the post buckling behavior are not of the greatest importance. However, it is a powerful tool for research purposes, or for special structures [50,51].

.

Chapter 2: Effect of Prebuckling Deformations

2.1 Overview

Although classical solutions still used nowadays consider a perfect beam when the buckling occurs, neglecting prebuckling deformations, it was observed in previous studies that the primary (in-plane) deflections might influence the solution of LTB, since when the buckling occurs, the structure is already in a deflected state. If this deflected shape (i.e., *prebuckling deflection*) is considered in the LBA, the associated critical load is different from the one obtained from an undeflected shape. It is reasonable to assume that prebuckling deflection is never zero, however, whether it has an important or negligible effect on the buckling depends on the structure. It is worth emphasizing here that prebuckling deflections are not the same as imperfections, since they are due to the loading, and exist even if the original structure is perfect.

When prebuckling deflections are considered, the problem cannot be expressed as an eigen-value problem, since the critical load value is dependent on the deflected shape, but the deflected shape is dependent on the load (which, when buckling occurs, must be equal to the critical load). Still, the problem remains solvable under certain circumstances and with certain simplifications. In fact, the effect of the prebuckling deflection was included even in the very first analytical solution for the LTB problem by Michell, in [2]. Later, the problem was discussed by several researchers [52-77], as will be discussed in detail in this chapter.

There seems to be a consensus in the available literature that the prebuckling deformations increase the critical moment, and that the increase is dominantly determined by the lateral rigidity of the beam. However, there are some discrepancies, both in the proposed analytical expressions and in the numerical results. The research presented herein is focused on understanding the role of prebuckling deflections on LTB, exploring the source of the contradictory results in the literature. This chapter is dedicated to the basic case, which is: single-span beams subjected to uniform moment, the cross-section is doubly symmetric, the bending is about the major axis of the cross-section, and the end supports are pinned (forked) in the direction of the minor axis bending.

In Section 2.2, a detailed review of the literature is provided, and in Section 2.3 the various steps of the analytical derivation are presented, highlighting when it is appropriate to do certain assumptions/simplifications. Section 2.4 gives the critical moment formula variants and provides elementary numerical results to illustrate the effect of the introduced assumptions and/or simplifications. Finally, the results are discussed in section 2.5.

2.2 Literature review

In this Section, a literature review is provided, focusing on literature where the effect of prebucking deflections on the LTB of doubly-symmetric beams is discussed. While acknowledging the researchers who have contributed to this topic would be commendable, the primary reason of the detailed review is that the available papers are not too numerous, but still include slightly different formulae for the seemingly same case, as well as include certain contradictory statements or suggestions.

As far as is known, the effect of pre-buckling deformations on the lateral-torsional buckling of beams was first reported by Michell [2]. In his paper, differential equations (D.E.-s) are formulated and solved for various beam-column cases, and two simple experiments are reported to validate the theoretical results. A particular case considered in the derivations is the *basic case*. A solution is derived for the critical moment M_{cr}, written (using the notations normally used nowadays) as:

$$M_{cr} = M_{rc0} \Big/ \sqrt{\left(1 - \frac{EI_y}{EI_x}\right)} \qquad \text{with } M_{cr0} = \frac{\pi}{L}\sqrt{EI_y GJ} \tag{1}$$

where M_{cr0} is the critical moment without the effect of prebuckling deformations, I_x and I_y are the second moments of area for the x (major) and y (minor) axes, respectively (see Fig. 1-1), J is the torsional inertia, L is the length of the beam, and E and G are the Young's modulus and shear modulus, respectively. It is to observe that the warping effect is totally disregarded. The results obtained from this formula are in line with later results if the cross-section has a small warping constant, e.g., in the case of a narrow rectangular section.

In fact, while the paper does not explicitly state this limitation to narrow rectangular shapes, such members are considered in the conducted experiments. Another remark is that the paper does not discuss the "effect of prebuckling deformations" separately, i.e., there is no distinct solution provided with and without prebuckling deformations; instead, it explicitly assumes the presence of prebuckling deformations and solves the equations accordingly. Another early work was done by Prandtl [52], who also established the D.E.-s for the LTB problem (without considering warping), and also solved them for a few cases, but without considering the prebuckling deflections.

An important contribution to LTB was made by Timoshenko [8], where the effect of warping for thin-walled members in twist was first introduced in the context of I-section members. Timoshenko published the first critical moment formula with considering warping, particularly for I-shaped members [53]. The formula is essentially identical to the one known nowadays, though in [53] it is formally different and expressed specifically for I-shaped beams only. It is:

$$M_{cr0} = \frac{\pi}{L}\sqrt{EI_y GJ\left(1 + \frac{\pi^2 EI_w}{GJL^2}\right)} \tag{2}$$

where I_w is the warping modulus. Later, in [10] a solution is presented for clamped-clamped beams (without the prebuckling effect).

Chwalla [54] formulated the D.E.-s of the beam-column buckling problem considering the warping effect and accounting for the prebuckling deflections, and provided closed-form solutions for several cases. Regarding the effect of prebuckling deformations, the derivation is presented for the basic case with narrow rectangular sections, leading to the following formula:

$$M_{cr} = M_{cr0} \Big/ \sqrt{\left(1 - \frac{EI_y}{EI_x}\right)\left(1 - \frac{2GJ}{EI_x}\right)} \tag{3}$$

with M_{cr0} as given by Eq. (1). In [54], it is also proposed to introduce an equivalent lateral bending stiffness to consider the effect of prebuckling deflections, suggesting that the proposed equivalent bending stiffness can be employed to any LTB case. It is also commented that GJ/EI_x is typically small, therefore, can be neglected.

LTB is discussed by Davidson [55], also for I-sections (and as special cases: narrow rectangular sections). Analytical solutions for both without and with considering the prebuckling deflections are given, assuming elastic end supports with separate stiffnesses for the global rotation of the beam ends (about the minor axis) and rotation of the flanges (which latter one could be "translated" to today's terminology as elastic warping support). Analytical solutions are given, but typically not in closed format, due to the complexity of the problem. Explicit formulae can be derived only for some simple cases, e.g., if the supports stiffnesses are zero (i.e., forked supports) and $I_w = 0$ (e.g., rectangular narrow section), the derivation leads to the following formula:

$$M_{cr} = M_{cr0} \Big/ \sqrt{\left(1 - \frac{EI_y}{EI_x}\right)\left(1 - \frac{GJ}{EI_x}\right)} \tag{4}$$

with M_{cr0} as given by Eq. (1). This is nearly (but not exactly) identical to the solution in [6].

The next appearance of the same problem is in [56] by Pettersson, focusing on mono-symmetric cross-sections. The displacement functions of beams subjected to combined loading (biaxial bending and torsion) are derived. Mostly simply supported beams are considered, but 3-span beams are also discussed. Critical moment expressions with and without the prebuckling deflection are provided for a few cases. For rectangular section beams under uniform major-axis moment, the derived formula is identical to the one in [55], see (Eq. 4).

In [57], Kerensky and his colleagues summarized the background of the then-current British Standard, and for the calculation of critical moment, a formula with considering the effect of prebuckling deflection was proposed, using the $1/\sqrt{1 - I_y/I_x}$ factor as in Eq. (1). A few years later, Clark and Knoll extended the critical moment formula for a few cases [58]. For clamped beams with narrow rectangular cross-sections, they derived the formula as follows:

$$M_{cr} = M_{cr0}\left(1 - \frac{EI_y}{EI_x}\right) \Big/ \sqrt{\left(1 - \frac{EI_y}{EI_x}\right)\left(1 - \frac{GJ}{EI_x}\right)} \qquad \text{with } M_{cr0} = \frac{2\pi}{L}\sqrt{EI_y GJ} \tag{5}$$

In the above equation, the M_{cr0} expression is the one normally used nowadays (if the warping effect is negligible), but the modification factor due to the prebuckling deflections is significantly different from those previously derived for the pinned-pinned case. This is, therefore, the first publication where the influence of the supports on the prebuckling effect is explicitly reported. Moreover, a formula is derived for a doubly-symmetric I-section beam in [58], where M_{cr0} is identical to that derived by Timoshenko, and the modification factor accounting for the effect of prebuckling deflections is the same as that derived by Davidson.

The problem was revisited by Trahair and Woolcock. In [59] a set of D.E.-s with considering the effect of prebuckling deformations, assuming doubly symmetrical cross-sections and pinned end supports, is derived. The solutions for a few cases are discussed (mostly numerically). A closed-form solution is given for the basic case, which can be written as:

$$M_{cr} = M_{cr0} \Big/ \sqrt{\left(1 - \frac{EI_y}{EI_x}\right)\left(1 - \frac{GJ}{EI_x}\left(1 + \frac{\pi^2 EI_w}{GJL^2}\right)\right)} \tag{6}$$

where M_{cr0} is the same as proposed by Timoshenko, see Eq. (2).

The next important contribution is made by Vacharajittiphan, Trahair and Woolcock [60], where a general approach is introduced for describing the three-dimensional behavior of thin-walled members in bending, assuming doubly-symmetrical cross-sections. From the general description, a simplified set of D.E.-s is derived. Since the aim was to calculate the critical load, i.e., to capture the point of bifurcation of the equilibrium, it was assumed that the lateral and torsional displacements are infinitesimally small, while the primary (i.e., in the plane of the bending) displacements are moderately large. The simplifications are introduced accordingly, in a consistent way, as follows: the lateral and torsional displacements are approximated by linear terms, while the primary displacement is approximated by up to quadratic terms. The derived formula is identical to the one in [59], see Eq. (6).

Roberts and Azizia developed a beam finite element model for the analysis of thin-walled members with open cross-sections [61]. The used variational form of the problem is aimed to get weak (approximate) solutions numerically, as usual in any finite element implementation. Arbitrary open cross-sections, including asymmetrical ones, are considered. The developed beam finite element is based on Vlasov's thin-walled beam theory, and is employed to solve simple column and beam problems using an incremental-iterative solution scheme. Though the effect of prebuckling deformations is not specifically discussed, it is mentioned that "…when these nonlinear strains are incorporated in a general instability analysis …, the influence of pre-buckling displacements is automatically taken into account". A subsequent research [62] discusses the effect of prebuckling deformations, based on the same principles as in [61]. However, analytical solutions are also provided. For the basic case, a critical moment formula is derived, which is identical with the one in [59, 60]. An analytical solution for beams with monosymmetric T-shaped cross-sections, assuming that I_w is zero, is also provided.

The next noteworthy contribution is a pair of papers by Pi and Trahair [63-54]. In [63], the earlier work of Roberts and Azazian is criticized. The criticism is on the basis that the finite element solution provided in [61-62] leads to a quadratic eigenvalue problem due to the presence of second-order terms, and instead of using an iterative approach, the problem in [61] is solved as a linear eigenvalue problem. Other issues in [61] were addressed, too, such as the

consideration of "constant prebuckling in-plane rotations and curvatures" along each element, which is not an accurate representation, as well as the negligence of the additional moments the axial loads cause due to the presence of prebuckling deformations.

The geometrical description of the problem in [63] is similar to the one in [60], but there are some important differences and/or advancements. One is that energy equations are provided and used. Another one is that the equations are developed for mono-symmetrical cross-sections, too. Moreover, the geometric description is more accurate and/or general. Finally, more terms are included in the approximations (compared to [60]), though when it comes to the derivation of actual M_{cr} formulae, the kept nonlinear terms are more-or-less the same. Two new versions of M_{cr} formulae are derived and presented in [64], but only for the basic case. One formula, termed as "linearized", is obtained by neglecting "the terms containing the second-order prebuckling deformations … in the energy equation", as follows:

$$M_{cr} = M_{cr0} \Big/ \left[\left(1 - \frac{EI_y}{EI_x}\right) \left(1 - \frac{GJ}{2EI_x}\left(1 + \frac{\pi^2 EI_w}{GJL^2}\right)\right)\right] \tag{7}$$

This formula is immediately criticized, stating that this expression "overestimates the critical moment and shows that second-order terms in the energy equation should not be neglected". The other, believed to be more accurate, formula is as follows:

$$M_{cr} = M_{cr0} \Big/ \sqrt{\left(1 - \frac{EI_y}{EI_x}\right) \left(1 - \frac{GJ}{2EI_x}\left(1 + \frac{\pi^2 EI_w}{GJL^2}\right)\right)} \tag{8}$$

In both of the above formulae M_{cr0} is identical to the one proposed by Timoshenko, see Eq. (2).

Eq. (8) is almost identical to the ones published in [59-61]. The only difference is the appearance of a '2' in the denominator of the $GJ/2EI_x$ term. The authors mention this slight difference, but do not explain or discuss. It is to mention, that later, in the book of Trahair [65], Eq. (8) is presented. (It is to note that, in [64], an M_{cr} formula is proposed for mono-symmetric cross-sections. It is not clear how it is obtained, but it is clearly different from the one derived by Roberts and Azizian [62] for mono-symmetric sections).

In [64], the analytical and numerical results are compared to those obtained from experiments. The test-based critical values are determined by the so-called Southwell-plot technique. Looking at the results, it is fair to say that: (i) the linearized formula is clearly incorrect, (ii) the experimental results are perhaps somewhat closer to the numerical ones if the

prebuckling deflections are considered, (iii) but the experimental results are not convincing regarding the effect of prebuckling deflections.

Though in [66], the LTB problem is not discussed, it is worth mentioning here because the paper expresses some criticism regarding the mathematical background of the derivations in [63].

In [67], Andrade and Camotim discuss the LTB of prismatic and tapered beams, both with and without the effect of prebuckling deflections. The developed and utilized formulation includes some approximations. It is suggested that the prebuckling effect can be taken into consideration by the $1/\sqrt{1 - I_y/I_x}$ factor, same as in [2,57].

Machado and Cortinez also investigated doubly-symmetric beams considering the effect of prebuckling deflections [68]. The novelty in this research is the consideration of transverse shear deformations, both along the major and minor axes, assuming laminated material. Variational principles are used, and closed-form solutions are provided. As a special case, if the shear deformations are neglected, the solution is identical to that given in [63]. Various transverse load cases are investigated, including the load height effect on simply supported single-span beams and cantilevers. The general observation is that the shear deformations decrease the critical loads, while the prebuckling deflections increase it. (Note, the effect of various laminations is also discussed.)

Mohri and Potier-Ferry studied doubly- and mono-symmetric beams under various loading conditions, including transverse loading with varying load application heights. In [69], D.E.-s considering the effect of prebuckling deflections are developed and solved. In the basic case, the same solution as in [60] is obtained. It is also commented that in engineering practice it is acceptable to account for the prebuckling effect by the $1/\sqrt{1 - I_y/I_x}$ factor.

In [70], Torkamani and Roberts derived new energy equations for flexural-torsional and lateral-torsional buckling of thin-walled beam-columns. The equations are very similar to those in [63]. There are a few differences, however, in how the nonlinear displacements of an arbitrary cross-section point are approximated. These differences are not discussed or explained. Some numerical examples are presented, one is related to LTB, but without special attention to the effect of prebuckling deflections.

Mohri, Damil, and Potier published another article on the same topic [71]. The theory is developed for general open cross-sections, using variational principles and D.E.-s, with the

focus being on monosymmetric I- and T-shaped sections. When considering doubly symmetric sections, it is again suggested that the prebuckling effect can be considered by the $1/\sqrt{1-I_y/I_x}$ factor.

In [72], a new version of the weak formulation of the lateral buckling problem is published by Attard and Kim. The kinematic assumptions are similar to those presented in earlier papers, and the novelty is the consideration of hyperelastic materials. The derived general formulae are utilized to re-derive an M_{cr} formula for the basic case, which is found to be identical to the one presented in [60]. (Also, they try to derive the M_{cr} formula for mono-symmetric cross-sections; in their results, the derivation leads to a cubic equation from which M_{cr} cannot be expressed in closed format. However, this formula is clearly different from that in [62] or in [64].)

The topic is discussed by Erkmen and Attard in [73], considering the shear deformations (similarly as discussed earlier in [68]). As for the analytical solution, the earlier formula for the basic doubly-symmetric case is repeated, where the effect of shear is said to be nonexistent. However, numerical (finite element) solutions are also provided and compared with results from the analytical ones. It is noted that "in order to induce bifurcation type post-buckling behavior, an initial small horizontal load is applied in the nonlinear analysis". The numerical results, hence, were obtained by nonlinear incremental analysis, not eigen-value analysis. It is declared that the analytical closed-form solution "is a lower bound to the results based on the nonlinear analysis procedure". In other words, the authors declare that the effect of prebuckling deformations is even larger than what is predicted by the analytical formulae. The question is discussed again by Mohri, Damil and Potier-Ferry [74], but the discussion and conclusions are rather similar to those of [71].

In [75], the LTB behavior of U-shaped sections (i.e., unlipped channel) is discussed by Beyer et al. The energy method is used, and the effect of prebuckling deflections is considered. The main focus of the paper is on minor-axis bending. For major axis bending (which is similar to a doubly symmetrical section), the prebuckling effect is considered by the $1/\sqrt{1-I_y/I_x}$ factor.

In the next related study, conducted by Pezeshky and Mohareb [76], the main focus is on the distortional deformations, though shear deformations are optionally considered, too. Variational principles are employed, but closed-form solutions are not provided. From the

numerical results it can be deduced that the shear deformations have small effect, but the distortional deformations noticeably reduce the M_{cr}/M_{cr0} ratio.

A more recent relevant paper is published by Su et al, see [77]. Their paper discusses the effect of prebuckling deformations, but the subject is essentially different from classic structures in structural engineering. The studied structure is the so-called "serpentine interconnect", which is a beam with a serpentine-shaped axis. The prebuckling deflections are huge compared to classic structures, accordingly, the effect of prebuckling deformations is drastic. Some analytical solutions and numerical examples are shown. As a special case, the classic LTB problem is considered, to which a closed-form solution is derived. The beam is assumed to have a rectangular cross-section, but not necessarily narrow rectangular. The warping effect is not directly considered. The obtained closed-form solution for the critical moment is identical to the one first derived in [55], with the only difference being that the torsion constant is different. The method is developed essentially for numerical solutions. It is worth mentioning that some of the numerical results predict higher values than the analytical solution, suggesting that the analytical solution is not perfectly precise.

Finally, the most recent paper investigating the effect of prebuckling deformations was done by Zhang and Kim [78]. The study employed finite element method with various numerical techniques for predicting the critical moment, namely: linear buckling analysis, geometrically nonlinear analysis, and a linear buckling analysis with an iterative solution to account for prebuckling deformations. The study found that the linear buckling analysis does not provide accurate solutions, which is expected since it doesn't account for prebuckling effects, and the nonlinear and iterative linear solutions provide more accurate critical moment predictions, with the iterative linear solution being far less demanding computationally. It is to mention that although the paper says that the "iterative LTB analysis method is newly proposed", a similar method was proposed earlier in [76, 82].

The main observations from the literature can be summarized as follows.

- The vast majority of research considers simply supported beams with forked supports. Cantilever beams and clamped beams occur in a few papers, but other support conditions are not discussed at all.
- There seems to be a consensus that the prebuckling deflection has a positive effect on LTB, i.e., the prebuckling deflection increases the critical moment. Moreover, there is

an agreement that the increase is primarily influenced by the ratio of the weak to strong axis moments of inertias.

- Most of the papers agree that the increase due to prebuckling deflections can approximately be expressed by the $1/\sqrt{1-I_y/I_x}$ factor. More precise formulae are given in several papers, and there are small discrepancies between these formulae. In a few papers, it is suggested that the available formula underestimates the critical moment.
- In most of the papers, it is implicitly assumed or explicitly stated that the provided formula to consider the prebuckling effect is generally valid. There is one single paper in which it is suggested that the critical moment increase is affected by the supports.
- The discrepancies between the papers are not limited to differences between the provided closed-form solutions for the critical moment with prebuckling effect, differences can also be observed in the underlying basic mechanical-mathematical formulae. In certain papers, criticism can be found regarding the content of other papers.
- Experimental work specifically devoted to the effect of prebuckling deflection is rather scarce; the existing experimental results are not convincing.
- In the literature there is hardly any attempt to use general numerical methods such as the shell finite element method, to verify the analytical results or the developed specific numerical formulations.

2.3 Analytical solution for the basic case

2.3.1 General

- Shape functions

In this study, the energy method is used. The total potential is expressed in terms of displacements. Thus, the displacements have to be assumed. In case of LTB, the secondary displacements are the lateral translation and twisting rotation, u and φ. The shape functions must satisfy the boundary conditions. For example, in the case of forked supports, the assumed displacement functions are simple half sinewaves:

$$u(z) = u_m sin\frac{\pi z}{L}$$
$$\varphi(z) = \varphi_m sin\frac{\pi z}{L} \tag{9}$$

where u_m and φ_m are the displacement amplitudes, and L is the beam length, see Fig. 2.1. (Further classic support cases will be considered in Section 2.4).

The primary (prebuckling) displacement is the in-plane deflection due to loading. Although it is not included in the energy method solution, it has an influence on the strains and curvatures, which influence is disregarded in classic LTB solutions. The primary displacements can be expressed by classic equations of the strength of materials. For example, in the basic case the beam is simply supported at both ends and subjected to uniform moment along the length, accordingly, the primary displacement of the beam's system line can be described by a quadratic function:

$$v(z) = \frac{v_m 4z(L-z)}{L^2} \quad \text{with} \quad v_m = \frac{M_x L^2}{8EI_x} \tag{10}$$

where v_m is the maximum vertical displacement, and M_x is the applied uniform bending moment.

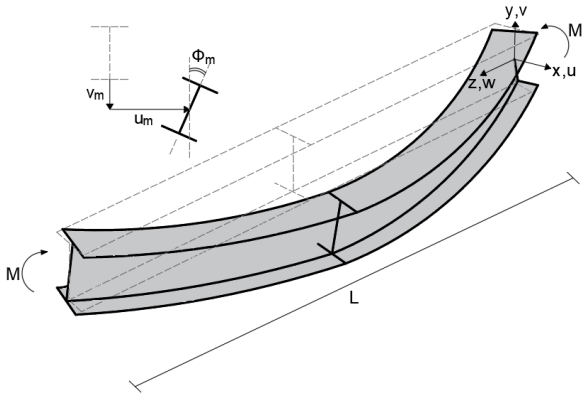

Figure 2.1: Coordinate system, displacements.

- Total potential

The total potential (Π) is expressed as the sum the strain energy (S) and the work (W) of the stresses on the nonlinear strains.

$$\Pi = S + W \tag{11}$$

where

$$W = \int_0^L \int_A \varepsilon_z \frac{M_x}{I_x} y dA\, dz \tag{12}$$

$$S = \frac{1}{2}\int_0^L \int_A \left(EI_y {\kappa_y}^2 + EI_w {\kappa_{zd}}^2 + GJ {\kappa_z}^2\right) dA\, dz \tag{13}$$

In the strain energy expression, κ_y is the curvature in the lateral direction, (i.e., the rate of change of the tangent of the system line in the lateral direction,) κ_z is the rate of change of the twist angle, and κ_{zd} is the rate of change of κ_z. In the work expression, M_x is the applied moment, ε_z is the nonlinear longitudinal normal strain due to displacements. Both the ε_z longitudinal strain and the κ curvatures must be expressed on the deformed geometry, which requires the transformation between the deformed and undeformed coordinate systems. In the relevant literature, multiple solutions can be found, as will be discussed later.

- Curvatures

The T_R rotation matrix can be obtained by the u, v and φ displacement functions, and once obtained, the curvatures (on the deformed geometry of the beam) can be expressed. The expressions are, see [60-64]:

$$\begin{aligned} \kappa_x &= l_z \frac{dl_y}{ds} + m_z \frac{dm_y}{ds} + n_z \frac{dn_y}{ds} \\ \kappa_y &= l_x \frac{dl_z}{ds} + m_x \frac{dm_z}{ds} + n_x \frac{dn_z}{ds} \\ \kappa_z &= l_y \frac{dl_x}{ds} + m_y \frac{dm_x}{ds} + n_y \frac{dn_x}{ds} \end{aligned} \tag{14}$$

where the elements of T_R are direction cosines:

$$T_R = \begin{bmatrix} l_x & l_y & l_z \\ m_x & m_y & m_z \\ n_x & n_y & n_z \end{bmatrix} \tag{15}$$

The derivation with respect to length '*s*' can be approximated by the derivation with respect to the longitudinal coordinate '*z*'. It is also to note that the actual expressions for the curvatures are fairly long, and approximations are necessary, as will be discussed later.

- Longitudinal normal strain

To calculate the work of the loads/stresses, strains are needed. Assuming that there are longitudinal stresses only (as usual in any beam-model-based solution), only the longitudinal normal strain is needed, which is derived from the translations. According to the Green-Lagrange starin tensor, the strain can be expressed as:

$$\varepsilon_z = \frac{\partial w_{xy}}{\partial z} + \frac{1}{2}\left(\left(\frac{\partial u_{xy}}{\partial z}\right)^2 + \left(\frac{\partial v_{xy}}{\partial z}\right)^2 + \left(\frac{\partial w_{xy}}{\partial z}\right)^2\right) \tag{16}$$

where u_{xy}, v_{xy}, and w_{xy} are the translation at an arbitrary cross-section point. As it is typical in classic buckling solutions, the $\left(\partial w_{xy}/\partial z\right)^2$ nonlinear term is neglected. All translations must be interpreted on the deflected geometry. According to e.g., [63], the translations of an arbitrary cross-section point (at the x, y position, with sectoral coordinate ω) can be expressed as:

$$\begin{bmatrix} u_{xy} \\ v_{xy} \\ w_{xy} \end{bmatrix} = \begin{bmatrix} u \\ v \\ w \end{bmatrix} + T_R \begin{bmatrix} x \\ y \\ -\omega\kappa_z \end{bmatrix} - \begin{bmatrix} x \\ y \\ 0 \end{bmatrix} \tag{17}$$

where u, v, and w are the translations at the centroid (and due to double symmetry, the shear center and centroid coincide). T_R is substituted into Eq. (17) to calculate u_{xy}, v_{xy}, and w_{xy} , then they are substituted into the strain expression Eq. (16). Without further simplifications, the final formula is extremely long (with many dozens of terms). However, many of these terms are zero if the cross-section is doubly-symmetric, due to the fact that y is measured from the centroid. As a result, the integral of all the terms in ε_z that are independent of y or contain y^2 are equal to zero. In other words, only the terms that are linearly dependent on y are necessary to consider. With this, the expression for ε_z is greatly simplified, but still might be long, hence, some approximations might be reasonable.

- Equation system, critical load

The expressions for the curvatures and longitudinal strain can be substituted into the total potential formula. After the integrations, the total potential is expressed in terms of the displacement parameters, i.e., the displacement amplitudes u_m and φ_m. Note, v_m is not an independent displacement parameter, since it is defined by M_x, see Eq. (10). According to the theorem of stationarity of total potential, equilibrium exists if the total potential is stationary, i.e.:

$$\frac{\partial \Pi}{\partial u_m} = 0 \quad \frac{\partial \Pi}{\partial \varphi_m} = 0 \tag{18}$$

The above expressions form a system of two equations. Applying certain simplifications (which will be discussed later), the equations are linear, and can be written in matrix format as:

$$[\boldsymbol{C}] \begin{bmatrix} u_m \\ \varphi_m \end{bmatrix} = 0 \tag{19}$$

where $\boldsymbol{C}$ is a 2×2 coefficient matrix dependent on M_x. A nontrivial solution of the homogeneous system of linear equation exists if the coefficient matrix is singular, i.e., its determinant equals to zero.

$$\det(\boldsymbol{C}) = 0 \tag{20}$$

This condition can be satisfied if M_x takes specific value(s), which is (are) the critical moment(s) M_{cr}. To be able to solve the $\det(\boldsymbol{C}) = 0$ equation, further approximations might be necessary, as discussed in the following Section.

2.3.2 Variants and approximations in the derivation

- Transformation matrix

Using the rotational angles α, β and φ about the x, y and z axis, respectively, the rotation matrix can be expressed. If the rotations are large and no approximations are introduced, it is relatively easy to define the transformation matrix by the sines and cosines of the rotational angles; in this case, however, the order of how the rotations around the three axes occur matters. On the other hand, if the rotations are (very) small, the cosines can be taken as 1, and the sines can be approximated by the value of the angle; leading to the T_R transformation matrix being simple and independent of the order of the rotations. However, to solve the LTB problem with prebuckling deflections, moderately large rotations must be assumed. Essentially, the sine and cosine of an angle are approximated using the Taylor series expansion up to quadratic terms.

There are two ways in the relevant papers to express the transformation matrix. In [60], it can be understood that the rotations around x, y and z are applied one by one, then the sine and cosine terms are approximated by Taylor series, and in the transformation matrix, the linear terms and some quadratic terms are kept. Regarding the quadratic terms, the approximation is based on the logic that the secondary displacements are infinitesimally small (hence β and φ are small), but the primary displacement is moderately large (hence α is moderately large). Accordingly, only the quadratic terms associated with α are kept. The resulting transformation matrix is as follows:

$$T_{R,angle}^{Va} = \begin{bmatrix} 1 & -\varphi & \beta \\ \varphi + \alpha\beta & 1 - \frac{1}{2}\alpha^2 & -\alpha \\ -\beta + \alpha\varphi & \alpha & 1 - \frac{1}{2}\alpha^2 \end{bmatrix} \tag{21}$$

Papers [63] and [66] present a different version of T_R. Though [63] and [66] use different mathematical apparatus, the same transformation matrix is derived when expressed by the angles, as follows:

$$T_{R,angle}^{Pi} = \begin{bmatrix} 1-\frac{1}{2}\beta^2-\frac{1}{2}\varphi^2 & -\varphi+\frac{1}{2}\alpha\beta & \beta+\frac{1}{2}\alpha\varphi \\ \varphi+\frac{1}{2}\alpha\beta & 1-\frac{1}{2}\alpha^2-\frac{1}{2}\varphi^2 & -\alpha+\frac{1}{2}\beta\varphi \\ -\beta+\frac{1}{2}\alpha\varphi & \alpha+\frac{1}{2}\beta\varphi & 1-\frac{1}{2}\alpha^2-\frac{1}{2}\beta^2 \end{bmatrix} \tag{22}$$

The rotation angles must be expressed using the displacement functions. The angle about the longitudinal axis is directly given by the φ function. For α and β, there are two alternatives in the literature. The simplest approximation, used in [60], is:

$$\begin{aligned} \alpha &= -\frac{dv}{dz} = -v' \\ \beta &= \frac{du}{dz} = u' \end{aligned} \tag{23}$$

In [15] and [18], however, α and β are approximated more accurately as:

$$\begin{aligned} \alpha &= -\frac{dv}{dz}+\frac{1}{2}\varphi\frac{du}{dz} = -v'+\frac{1}{2}\varphi u' \\ \beta &= \frac{du}{dz}+\varphi\frac{dv}{dz} = u'+\frac{1}{2}\varphi v' \end{aligned} \tag{24}$$

To obtain the necessary transformation matrix, Eq. (23) or Eq. (24) must be substituted into either Eq. (21) or Eq. (22). In [60], Eq. (23) is substituted into Eq. (21) which leads to a transformation matrix as follows:

$$T_R^{Va} = \begin{bmatrix} 1 & -\varphi & u' \\ \varphi-u'v' & 1-\frac{1}{2}(v')^2 & v' \\ -u'-v'\varphi & -v' & 1-\frac{1}{2}(v')^2 \end{bmatrix} \tag{25}$$

However, if Eq. (24) is substituted into Eq. (22), it leads to a transformation matrix with entries up to 4th-order terms, and it is reasonable to introduce approximations. If the 4th-order terms are eliminated, the resulting matrix is as follows:

$$T_R^{3rd} = \begin{bmatrix} 1-\frac{1}{2}(u')^2-\frac{1}{2}\varphi^2-\frac{1}{2}u'v'\varphi & -\varphi-\frac{1}{2}u'v'+\frac{1}{4}(u')^2\varphi-\frac{1}{4}(v')^2\varphi & u'+\frac{1}{4}u'\varphi^2 \\ \varphi-\frac{1}{2}u'v'+\frac{1}{4}(u')^2\varphi-\frac{1}{4}(v')^2\varphi & 1-\frac{1}{2}(v')^2-\frac{1}{2}\varphi^2+\frac{1}{2}u'v'\varphi & v'+\frac{1}{4}v'\varphi^2 \\ -u'-v'\varphi+\frac{1}{4}u'\varphi^2 & -v'+u'\varphi+\frac{1}{4}v'\varphi^2 & 1-\frac{1}{2}(u')^2-\frac{1}{2}(v')^2 \end{bmatrix} \quad (26)$$

In [66], the transformation matrix is essentially similar to Eq (26), but some 3rd-order terms are eliminated, namely from entries (1,3) and (2,3). The resulting matrix is then:

$$T_R^{To} = \begin{bmatrix} 1-\frac{1}{2}(u')^2-\frac{1}{2}\varphi^2-\frac{1}{2}u'v'\varphi & -\varphi-\frac{1}{2}u'v'+\frac{1}{4}(u')^2\varphi-\frac{1}{4}(v')^2\varphi & u' \\ \varphi-\frac{1}{2}u'v'+\frac{1}{4}(u')^2\varphi-\frac{1}{4}(v')^2\varphi & 1-\frac{1}{2}(v')^2-\frac{1}{2}\varphi^2+\frac{1}{2}u'v'\varphi & v' \\ -u'-v'\varphi+\frac{1}{4}u'\varphi^2 & -v'+u'\varphi+\frac{1}{4}v'\varphi^2 & 1-\frac{1}{2}(u')^2-\frac{1}{2}(v')^2 \end{bmatrix} \quad (27)$$

In [63], the transformation matrix is similar to Eq. (26) or Eq. (27), but further simplified as:

$$T_R^{Pi} = \begin{bmatrix} 1-\frac{1}{2}(u')^2-\frac{1}{2}\varphi^2-\frac{1}{2}u'v'\varphi & -\varphi-\frac{1}{2}u'v'+\frac{1}{2}(u')^2\varphi & u' \\ \varphi-\frac{1}{2}u'v'-\frac{1}{2}(v')^2\varphi & 1-\frac{1}{2}(v')^2-\frac{1}{2}\varphi^2+\frac{1}{2}u'v'\varphi & v' \\ -u'-v'\varphi+\frac{1}{2}u'\varphi^2 & -v'+u'\varphi+\frac{1}{2}v'\varphi^2 & 1-\frac{1}{2}(u')^2-\frac{1}{2}(v')^2 \end{bmatrix} \quad (28)$$

It can be noticed that the 3rd-order terms are eliminated from (1,3) and (2,3), plus, the entries (1,2) and (3,2) are modified. This modification is not mentioned, hence not commented in the paper.

Several further variants of the matrix could be defined, depending on what terms are eliminated or kept. Since it is a widely used engineering approximation to eliminate all the 3rd-order terms, the second-order approximation is provided here as follows:

$$T_R^{2nd} = \begin{bmatrix} 1-\frac{1}{2}(u')^2-\frac{1}{2}\varphi^2 & -\varphi-\frac{1}{2}u'v' & u' \\ \varphi-\frac{1}{2}u'v' & 1-\frac{1}{2}(v')^2-\frac{1}{2}\varphi^2 & v' \\ -u'-v'\varphi & -v'+u'\varphi & 1-\frac{1}{2}(u')^2-\frac{1}{2}(v')^2 \end{bmatrix} \quad (29)$$

- Curvatures

Using one of the above transformation matrices and considering Eqs. (14-15), the curvatures can be expressed in terms of the displacement functions. The obtained formulae are long. For example, using T_R^{Pi}, the curvature formulae have 9, 7 and 11 terms for κ_x, κ_y, and κ_z, respectively. Most of the terms are higher-order. If the linear and quadratic terms are kept, the

curvatures are expressed (from almost any of the above-mentioned variants, with the exception of T_R^{Va}) as follows:

$$\kappa_x = -v'' + \varphi u''$$
$$\kappa_y = u'' + \varphi v'' \tag{30}$$
$$\kappa_z^{gen} = \varphi' - \frac{1}{2}u'v'' + \frac{1}{2}u''v'$$

On the other hand, the κ_z curvature obtained from T_R^{Va} is slightly different:

$$\kappa_z^{Va} = \varphi' - u'v'' \tag{31}$$

It is to note that in [61-62], another equation is used for κ_z (derived differently, not directly from a transformation matrix) as follows:

$$\kappa_z^{Ro} = \varphi' - u'v'' + u''v' \tag{32}$$

It is to observe that there is agreement in the literature on how to express κ_y, while various variants for κ_z exist. In κ_x, the 2nd-order term is sometimes eliminated, however, this has no effect on the critical moment formula, since κ_x is not directly employed in the derivations.

- Longitudinal strain

Following the steps described in Section 2.3.1.4, the longitudinal normal strain is expressed through the displacements of the beam's system line. The actual expression depends on the considered rotation matrix, but typically has one first-order term, one second-order term, several third-order terms, and several fourth-order terms. According to the logic of the linear buckling analysis, the first-order term should be disregarded. It might also be reasonable to neglect the fourth-order terms. With these eliminations, there is a second-order term and some third-order terms. A few possible expressions are given here, as follows.

From T_R^{2nd}:

$$\varepsilon_z^{2nd} = \left(\varphi u'' - \varphi\varphi' v' - \frac{1}{2}(u')^2 v'' - (v')^2 v'' - \frac{1}{2}u'u''v'\right) y \tag{33}$$

From T_R^{3rd} or T_R^{To}:

$$\varepsilon_z^{3rd} = \left(\varphi u'' + \frac{1}{4}\varphi^2 v'' - \frac{1}{2}(u')^2 v'' - (v')^2 v'' - \frac{1}{2}\varphi\varphi' v' - \frac{1}{2}u'u''v'\right) y \tag{34}$$

From T_R^{Pi}:

$$\varepsilon_z^{Pi} = \left(\varphi u'' + \frac{1}{2}\varphi^2 v'' - \frac{1}{2}(u')^2 v'' - (v')^2 v'' - \frac{1}{2}u'u''v'\right) y \tag{35}$$

In [61-63], ε_z^{Pi} is further simplified by keeping one single 3rd-order term only, as follows.

$$\varepsilon_z^{Pi,simple} = \left(\varphi u'' + \frac{1}{2}\varphi^2 v''\right) y \tag{36}$$

From T_R^{3rd} or T_R^{To}, but with keeping only one 3rd-order term similarly to the previous case:

$$\varepsilon_z^{3rd,simple} = \left(\varphi u'' + \frac{1}{4}\varphi^2 v''\right) y \tag{37}$$

From any T_R , if only the single second-order term is kept:

$$\varepsilon_z^{2nd,simple} = (\varphi u'') y \tag{38}$$

- Approximations due to cross-section characteristics

If the cross-section is open, it is reasonable to introduce approximations (which will be referred to as 'open') as follows:

$$\left(\frac{EI_w/L^2}{EI_x}\right)^2 \cong 0 \quad \left(\frac{GJ}{EI_x}\right)^2 \cong 0 \quad \frac{GJ(EI_w/L^2)}{(EI_x)^2} \cong 0 \tag{39}$$

The formulae can be further simplified (which option will be referred to as 'open-simple') assuming that:

$$\frac{EI_w/L^2}{EI_x} \cong 0 \quad \frac{GJ}{EI_x} \cong 0 \tag{40}$$

If the cross-section is closed, the warping is negligible, but the Saint-Venant torsion rigidity is significant, hence the following approximation might be used (referred to as option 'closed'):

$$\frac{EI_w/L^2}{EI_x} \cong 0 \tag{41}$$

The formulae can further be simplified (resulting in option 'closed-simple') assuming that:

$$\frac{EI_w/L^2}{EI_x} \cong 0 \quad \left(\frac{GJ}{EI_x}\right)^2 \cong 0 \tag{42}$$

- Optional reduction of equation degree

Even if the above-discussed approximations are introduced, the final equation, i.e., Eq. (20), from which the critical moment can be calculated, is of 4th-degree. Since there is no cubic term in the equation, it can still be solved, and a closed-form expression (even if long) can be obtained for M_{cr}. However, in the literature the higher-degree terms are always eliminated and finally the critical moment is calculated from a simplified quadratic equation.

2.4 Critical moment variants

2.4.1 Open sections

The derivation of the critical moment can be completed as summarized in Section 2.3.1, but the final result (e.g., final expression for the critical moment) is dependent on various details. The determining factors are as follows: the T_R, the curvatures, the longitudinal strain, the assumed stiffness ratios of the cross-section, and the potential elimination of higher-degree M_{cr} terms in the final equation.

The elements of T_R matrix are combined from the displacement functions and their derivatives. The curvatures and the longitudinal normal strain are also expressed by the combination of the displacement functions and their derivatives. In most structural engineering stability problems, when displacement functions and/or derivatives are combined, it is appropriate to eliminate cubic or higher-order terms.

However, the literature suggests that to have the critical moment with prebuckling deflections, third-order terms are required, too, in the T_R transformation matrix, and in the ε_z strain, but it is not clear which cubic terms are necessary. Moreover, in the literature, I-shaped and (narrow) rectangular sections are discussed, and some stiffness values are assumed to be small (compared to others), but – in many cases – without introducing a consistent assumption system. Closed sections with high torsional rigidity (e.g., RHS) are not discussed, therefore, it remains unknown how the assumed stiffness ratios affect the results.

Finally, the M_{cr} formulae in the literature are solutions of quadratic equations. However, this is possible only if the higher-degree M_{cr} terms are eliminated. It is questionable whether the effect of this simplification can always be justified. The solution for M_{cr} is, therefore, very far from being unambiguous; this explains why various formulae are found in various papers. Actually, several dozens of different M_{cr} formulae could be derived. A few possible formulae are presented here, to demonstrate which options lead to the formulae found in the literature,

and how the details of the derivations influence the final results. First, open cross-sections are considered, therefore ‘open‘ and ’open-simple‘ options are employed. The considered derivation variants are summarized in Table 2.1.

Variant (ref) is the reproduction of the simplest formula, shown in several papers, e.g., [2,67,69,71,75], which will be used here as a reference. Variant (a) is the reproduction of the Pi-Trahair formula as in [64]. Variant (b) is the reproduction of the formula in [60] and [62]. Variant (c) is obtained by applying the geometric approximations proposed by [66]. Variant (d) is similar to (c), but the simplified formula is employed for the longitudinal strain (similarly to the simplified longitudinal strain formula by Pi-Trahair). Variant (e) is obtained by a consistent quadratic approximation in each step (i.e., eliminating the cubic terms systematically). The variants denoted by (+) are included here in order to observe the influence of neglecting or considering the 4th-degree term in the final equation. Accordingly, variant (a+) is similar to (a), but the final equation is 4th-degree, and variant (c+) is similar to (c), but the final equation is 4th-degre. It is to note that in the case of variants (a+) and (c+), M_{cr} is calculated from a 4-th-degree equation; the obtained formulae can be expressed in closed format, but they are relatively long, thus, not presented here.

Table 2.1: Summary of options considered for DSI sections

vari-ant	transf. matrix	curvatures	nonlinear longit. strain	cross-section model	final equation	Eq.
(ref)	T_R^{2nd}	κ_y and κ_z^{gen}	$\varepsilon_z^{Pi,simple}$	open simple	quadratic	(43)
(a)	T_R^{Pi}	κ_y and κ_z^{gen}	$\varepsilon_z^{Pi,simple}$	open	quadratic	(44)
(b)	no T_R	κ_y and κ_z^{Ro}	$\varepsilon_z^{Pi,simple}$	open	quadratic	(45)
(c)	T_R^{To} or T_R^{2nd}	κ_y and κ_z^{gen}	ε_z^{3rd}	open	quadratic	(46)
(d)	T_R^{To}	κ_y and κ_z^{gen}	$\varepsilon_z^{3rd,simple}$	open	quadratic	(47)
(e)	T_R^{2nd}	κ_y and κ_z^{gen}	$\varepsilon_z^{2nd,simple}$	open	quadratic	(48)
(a+)	T_R^{Pi}	κ_y and κ_z^{gen}	$\varepsilon_z^{Pi,simple}$	open	4th-degree	-
(c+)	T_R^{To}	κ_y and κ_z^{gen}	ε_z^{3rd}	open	4th-degree	-

The obtained formulae are as follows:

$$M_{cr}^{(ref)} = M_{cr0} \Big/ \sqrt{1 - \frac{EI_y}{EI_x}} = M_{cr0} \Big/ \sqrt{1 - \frac{I_y}{I_x}} \tag{43}$$

$$M_{cr}^{(a)} = M_{cr0} \Big/ \sqrt{\left(1 - \frac{EI_y}{EI_x} - \frac{GJ}{2EI_x} - \frac{\pi^2 EI_w}{2EI_x L^2} + \frac{GJEI_y}{2(EI_x)^2} + \frac{\pi^2 EI_w EI_y}{2(EI_x)^2 L^2}\right)} \tag{44}$$

$$M_{cr}^{(b)} = M_{cr0} \Big/ \sqrt{\left(1 - \frac{EI_y}{EI_x} - \frac{GJ}{EI_x} - \frac{\pi^2 EI_w}{EI_x L^2} + \frac{GJEI_y}{(EI_x)^2} + \frac{\pi^2 EI_w EI_y}{(EI_x)^2 L^2}\right)} \tag{45}$$

$$M_{cr}^{(c)} = M_{cr0} \Big/ \sqrt{\left(1 - \frac{EI_y}{EI_x} - \frac{2GJ}{EI_x} - \frac{2\pi^2 EI_w}{EI_x L^2} + \frac{GJEI_y}{2(EI_x)^2} + \frac{\pi^2 EI_w EI_y}{2(EI_x)^2 L^2}\right)} \tag{46}$$

$$M_{cr}^{(d)} = M_{cr0} \Big/ \sqrt{\left(1 - \frac{3EI_y}{2EI_x} - \frac{GJ}{2EI_x} - \frac{\pi^2 EI_w}{2EI_x L^2} + \frac{GJEI_y}{2(EI_x)^2} + \frac{\pi^2 EI_w EI_y}{2(EI_x)^2 L^2}\right)} \tag{47}$$

$$M_{cr}^{(e)} = M_{cr0} \Big/ \sqrt{\left(1 - \frac{2EI_y}{EI_x} - \frac{GJ}{2EI_x} - \frac{\pi^2 EI_w}{2EI_x L^2} + \frac{GJEI_y}{2(EI_x)^2} + \frac{\pi^2 EI_w EI_y}{2(EI_x)^2 L^2}\right)} \tag{48}$$

In all the above equations:

$$M_{cr0} = \frac{\pi}{L}\sqrt{EI_y\left(GJ + \frac{\pi^2 EI_w}{L^2}\right)} \tag{49}$$

It is obvious that the expressions for M_{cr} are dependent on the details of the derivation, leading to different M_{cr} formulae. To be able to evaluate the differences, a simple numerical study is provided (Fig. 2.2).

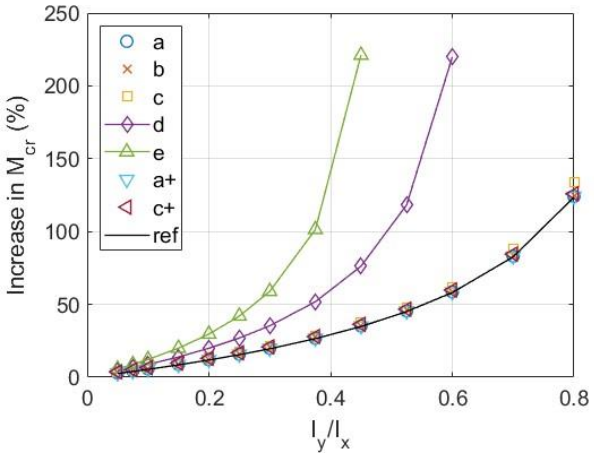

Figure 2.2: Open sections: moment increase due to prebucking deflection.

Obviously, the critical moment values are dependent on the cross-section properties, the beam length, and the material constants, however, here the focus is on the effect of the

derivation details, therefore, hypothetical cross-sections are used with assumed stiffness ratios. Considering typical doubly-symmetric I-shaped steel sections, it can be observed that GJ/EI_x is around (or smaller) than 0.01. Also, $\pi^2 EI_w/L^2/EI_x$ is around (or smaller) than 0.001. By assuming these rigidity ratios, the solution becomes independent of the length and material. The critical moment increase, i.e., the $(M_{cr} - M_{cr0})/M_{cr0}$ values are plotted in Fig. 2.2 for various, practically relevant I_y/I_x ratios.

Since for the given basic case of LTB, the solutions by [64], i.e., (a) and by [60], i.e., (b) are re-derived by various researchers, it is fair to assume that these solutions are reasonably correct. It can be observed that variant (c) results are very similar to those from (a) and (b). The numerical studies presented in the next chapter validate this conclusion, too. It is clear that the simplest, so-called reference formula yields nearly the same results. This means that it is reasonable to use 'open-simple' option in practical cases (at least in the basic case). Moreover, the results seem to justify the suggestion from various papers that the effect of prebuckling deflection can be accounted for by the $1/\sqrt{1 - I_y/I_x}$ factor. Mathematically, however, this is simply due to the fact that the $EI_w/L^2/EI_x$ and GJ/EI_x rigidity ratios are small for practical I-shaped steel sections.

It is clear from the M_{cr} formulae that no real root exists if I_y/I_x is large in any variant. In most variants, the $I_y/I_x = 1$ is the point of singularity; while in variants (d) and (e), the singularity occurs for much smaller value of I_y/I_x. Moreover, for medium I_y/I_x values, variant (d) and (e) lead to results very different from any other variants. Therefore, variant (d) and (e) can be judged as incorrect. The results suggest that in these options, some important terms are missing from the displacement approximations, leading to poor approximation(s) of the function(s), which finally leads to poor prediction for the critical moment. It can be also observed that the 4th-degree moment term in the final equation has very little effect. This is particularly true when comparing (a) and (a+); though the M_{cr} values are not equal, the difference is extremely small.

2.4.2 Closed sections

Unlike in open sections, the torsion rigidity is significant in closed sections, and this has an effect on the M_{cr} formulae. Two of the above-mentioned variants are therefore re-calculated, using 'closed' and 'closed-simple' cross-section approximations. Namely: variant (a) and variant (c) are considered, (a1) and (c1) being the simplified, (a2) and (c2) being the more

complex ones. Moreover, the effect of eliminating the 4th-degree term in the final equation is illustrated in variants (a1) and (c1): if the 4th-degree term is kept, the resulting variants are identified as (a1+) and (c1+), respectively. The characteristics of the variants are summarized in Table 2.2.

Table 2.2: Summary of options considered for RHS sections

vari-ant	transf. matrix	curvatures	nonlinear longit. strain	cross-section model	final equation	Eq.
(a1)	T_R^{Pi}	κ_y and κ_z^{gen}	$\varepsilon_z^{Pi,simple}$	closed-simple	quadratic	(50)
(a2)	T_R^{Pi}	κ_y and κ_z^{gen}	$\varepsilon_z^{Pi,simple}$	closed	quadratic	(51)
(c1)	T_R^{To} or T_R^{2nd}	κ_y and κ_z^{gen}	ε_z^{3rd} or ε_z^{2nd}	closed-simple	quadratic	(52)
(c2)	T_R^{To} or T_R^{2nd}	κ_y and κ_z^{gen}	ε_z^{3rd} or ε_z^{2nd}	closed	quadratic	(53)
(a1+)	T_R^{Pi}	κ_y and κ_z^{gen}	$\varepsilon_z^{Pi,simple}$	closed-simple	4th-degree	-
(c1+)	T_R^{To} or T_R^{2nd}	κ_y and κ_z^{gen}	ε_z^{3rd} or ε_z^{2nd}	closed-simple	4th-degree	-

The obtained formulae are summarized as follows:

$$M_{cr}^{(a1)} = M_{cr0} \Big/ \sqrt{1 - \frac{EI_y}{EI_x} - \frac{GJ}{2EI_x} + \frac{EI_y GJ}{2(EI_x)^2}} = M_{cr0} \Big/ \sqrt{\left(1 - \frac{EI_y}{EI_x}\right)\left(1 - \frac{GJ}{2EI_x}\right)} \tag{50}$$

$$M_{cr}^{(a2)} = M_{cr0} \Big/ \sqrt{1 - \frac{EI_y}{EI_x} - \frac{GJ}{2EI_x} + \frac{EI_y GJ}{2(EI_x)^2} + \frac{9(GJ)^2}{48(EI_x)^2} - \frac{\pi^2 (GJ)^2}{48(EI_x)^2}} \tag{51}$$

$$M_{cr}^{(c1)} = M_{cr0} \Big/ \sqrt{1 - \frac{EI_y}{EI_x} - \frac{2GJ}{EI_x} + \frac{EI_y GJ}{2(EI_x)^2}} \tag{52}$$

$$M_{cr}^{(c2)} = M_{cr0} \Big/ \sqrt{1 - \frac{EI_y}{EI_x} - \frac{2GJ}{EI_x} + \frac{EI_y GJ}{2(EI_x)^2} + \frac{9(GJ)^2}{48(EI_x)^2} - \frac{\pi^2 (GJ)^2}{48(EI_x)^2}} \tag{53}$$

Fig. 2.3 shows that the effect of GJ is non-negligible in the case of closed sections; in fact, it increases the M_{cr}/M_{cr0} ratio. However, usually, the higher-degree terms with GJ have very small effect. Though variants (a) and (c) have been found to be very similar for open cross-sections, they lead to rather different M_{cr}/M_{cr0} ratios for closed sections, particularly if the final equation is quadratic. The 4th-degree moment term in the final equation has noticeable effect; in variant (a) the effect is relatively small, but in variant (c) it seems to be absolutely necessary to keep the 4th-degree moment term, otherwise the results look unrealistic.

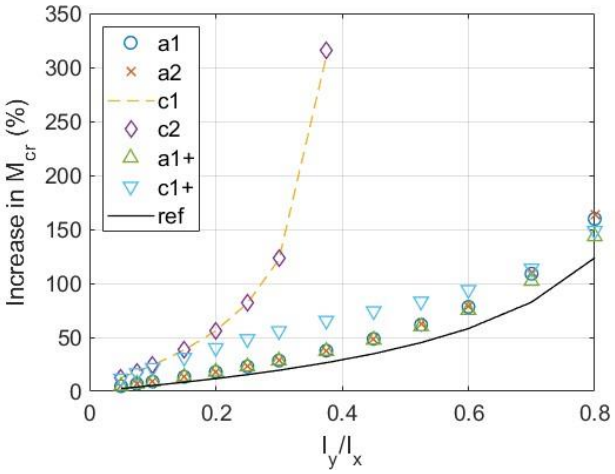

Figure 2.3: Closed sections: moment increase due to prebucking deflection.

2.5 Summary

In this chapter, analytical solutions for the lateral-torsional buckling of thin-walled beams, considering the effect of prebuckling deformations, were discussed. Doubly symmetric beams with various end supports, as well as cross sections with low and high torsional rigidities were considered. The critical moment formulae proposed in earlier papers for simply supported beams subjected to uniform moment were re-derived, identifying the important decision points which can/will influence the final formula.

In the analytical derivations, the transformation of displacements is necessary due to the 3D rotations of the system line of the beam. Since the rotations are not necessarily small, the transformation can be realized in multiple ways. Moreover, in the course of the derivations, many higher-order terms show up, and some of them are important, while others are not. It is not self-evident which terms should be kept and which terms can be eliminated; earlier papers show a significant scatter in this regard. Moreover, in certain publications some inconsistencies can be found. All these factors lead to variations in the end results.

Both the derivations presented in this chapter and the in-depth study of the literature suggest that approximations should be done carefully since they might lead to erroneous results if done improperly. The results suggest that in the curvatures, up to second-order terms are necessary and enough to consider. In the longitudinal normal strain, however, 3rd-order terms are necessary too. It might be enough to consider selected 3rd-order term(s), but they need to be carefully selected. Regarding the transformation matrix, though in certain cases it is enough to

consider the second-order terms only, but in other cases higher-order terms are necessary, too; therefore, considering the 3rd-order terms is recommended.

In the following chapters, further analytical derivations are performed for other cases (different end supports and intermediate supports), the approximations done by Pi-Trahair [63,64] are employed for these derivations since it was found in this chapter that they lead to reasonable results for the cases included in the scope of this study.

Chapter 3: Effect of End Supports

3.1 Overview

In the previous chapter, a detailed literature review is provided, which revealed that (i) there are some contradictory statements and suggestions in the literature; (ii) the effect of end supports is hardly considered; and (iii) there was hardly any attempt to use general finite element tools to investigate the prebuckling effect on LTB. Later in Chapter 2, the contradictions were addressed, and a detailed overview of the analytical derivations, as well as the various resulting formulae is given. In this chapter, the investigation is expanded to include other end support conditions, as well as numerical methods.

Nowadays, numerical methods are widely used in the engineering practice and research. The most typical method is the *finite element method* (FEM). In this chapter, the FEM is used, with both beam and shell FEM elements. If the problem is idealized, by assuming elastic behavior without imperfections, the analysis is then called *linear buckling analysis* (LBA). In the case of LTB, the critical load is usually expressed as the *critical moment*, which is the topic of discussion here. Another commonly used approach for the buckling analysis is the previously mentioned GNIA (see Chapter 1), which will also be used in this chapter.

Analytical considerations suggest that the maximum load from GNIA, if the imperfection is very small, converges to the critical load from LBA [45,80]. However, when GNIA is performed numerically, discrepancies are experienced, e.g., the moment where instability occurs can be smaller or larger than the critical moment from LBA [44]. One of the potential reasons of these discrepancies is the so-called prebuckling deflections, which is the main focus in this investigation.

In Section 3.2, the scope of the study is discussed, showing the parameters considered in the study. In Section 3.3, the analytical derivations from Chapter 2 are expanded to include other boundary conditions, and several critical moment formulae are provided. In section 3.4, the numerical methods (LBA and GNIA), as well as the FEM models are discussed. The results from the various methods are presented and discussed in section 3.5. Though in general, the numerical and analytical results show reasonable coincidence, some differences are experienced, which are discussed in Section 3.6 and 3.7. Section 3.6 discusses the effect of the length of the beam, and section 3.7 discusses the localized deformations.

3.2 Scope

In this study, single-span girders are analyzed with doubly symmetric steel cross-sections. The girder (Fig. 3.1) is prismatic and originally straight. The beam is subjected to uniform moment about the major axis, and various boundary conditions have been considered. The critical moments without and with considering the in-plane deflections have been calculated (leading to M_{cr0} and M_{cr}, respectively). Analytical and numerical methods have been applied, as follows: (i) analytical formulae derived in Chapter 2, as well as further formulae for other boundary conditions derived in this chapter, (ii) LBA analysis by beam FEM, (iii) LBA by shell FEM, (iv) GNIA by beam FEM, and (v) GNIA by shell FEM.

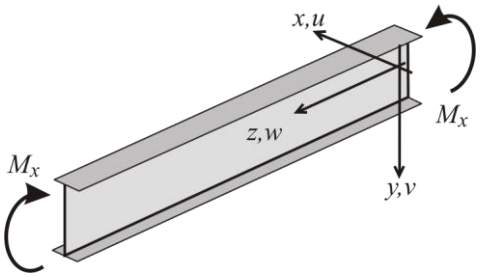

Figure 3.1: Beam configuration, coordinates, displacements.

A key objective here is to investigate the effect of end supports. Accordingly, various classic boundary condition combinations have been considered as summarized in Table 3.1. The main two variables are the rotation and warping, the latter one being the distortion of the cross-sectional plane along the beam's length due to non-uniform torsion [83]. In the table 'P' indicates a free condition (i.e., "pinned"), and 'F' indicates a fixed condition, while 'r' and 'w' specify whether the fixity is for rotation (about the minor axis *y*) or warping.

Table 3.1: Boundary conditions combination.

	Left end		Right end		notation
	rot.	warp.	rot.	warp.	
1	P	P	P	P	PrPw-PrPw
2	F	F	F	F	FrFw-FrFw
3	P	F	P	F	PrFw-PrFw
4	F	P	F	P	FrPw-FrPw
5	P	P	F	F	PrPw-FrFw

It is important to underline that the transverse translations (along *x* and *y*) as well as the twisting rotation around the longitudinal axis are always prevented at both ends, the longitudinal translation is always prevented at one end, and the rotation about the major axis *x* is always free.

Two cross-section types are considered: doubly-symmetric I-shaped sections (DSI), and rectangular hollow sections (RHS). The reviewed literature suggests that the ratio of the weak to strong axis moments of inertia (I_y/I_x) is the main influencing factor of the in-plane deflection effect; the cross-sections of the study have been defined accordingly, including a wide range of I_y/I_x ratios. Another important aspect is that unlike the beam element FEM or analytical solutions, the shell element solution is affected by local deformations. However, if the beam is long enough and the plates are thick enough, these local deformations are less influential. Since the aim of the study is to compare the various methods, relatively long beams and thick plates are employed.

In the case of DSI, the flange width is 200 mm, the flange and web thicknesses are 20 and 12 mm, respectively, while the total section depth (out-to-out) is a variable so that the I_y/I_x ratio would be in the range of 0.05 to 0.75. In the case of RHS, the section width is 150 mm (out-to-out), the flange and web thicknesses are 30 and 10 mm, respectively, the total section depth (out-to-out) varies, so that the I_y/I_x ratio would be in the range of 0.03 to 0.75. The actual section depth values and inertia ratio values are summarized in Table 3.2.

Table 3.2: Section depths and inertia ratios

DSI		RHS	
depth (mm)	I_y/I_x	depth (mm)	I_y/I_x
150	0.75	150	0.75
160	0.65	160	0.66
180	0.49	180	0.53
200	0.39	200	0.43
300	0.15	300	0.22
400	0.08	400	0.13
500	0.05	500	0.09
		1000	0.03

Regarding the length of the beam, a pilot study was conducted in which different lengths were analyzed for various boundary conditions. It was found that the RHS section experiences higher local deformations, requiring longer beams to reduce them. It was found that for the DSI, a length of 15 meters, and for the RHS, 30 meters, are suitable for keeping the local deformations small, even though it is not possible to completely eliminate them. (It is to note that the effect of beam length and localized deformations are discussed in Section 3.6). For the

material, a classic isotropic steel is considered, with a Young's modulus equal to 210000 MPa, and Poisson's ratio equal to 0.3.

3.3 Analytical solutions

This section extends the analytical derivations for the various boundary conditions proposed in Chapter 2. Critical moment formulae are derived for each support condition, both for open cross-sections with small torsional rigidity, and for closed cross-sections with large torsional rigidity. The derivation options are selected so that the final formulae would be as simple as possible. For the cross-section, options 'open-simple' and 'closed-simple' are used, and the final equation is simplified to a quadratic equation. Due to these simplifications, the longitudinal strain can be either $\varepsilon_z^{Pi,simple}$ or ε_z^{3rd}. Finally, κ_y and κ_z^{gen} are used for the curvatures.

It is to note that the formulae are presented only for open cross-section, though numerical result will be shown for both open and closed sections. It should also be noted that the resulting formulae are dependent on the assumed displacement functions. Here, to each support condition critical moment formulae are initially derived assuming a single trigonometric term in the displacement functions, However, it was found that the 'single-term' formulae are inaccurate in certain cases, therefore, more refined formulae are derived for selected cases, using 3 trigonometric terms (i.e., '3-term' solutions).

3.3.1 FrFw-FrFw

In this case, the weak-axis rotation and warping are fixed at both ends of the beam.

- Single-term solution

If a single trigonometric term is used, the simplest displacement functions that satisfy the support conditions are as follows:

$$\begin{aligned} u(z) &= u_m \frac{1}{2}\left(1 - \cos\frac{2\pi z}{L}\right) \\ \varphi(z) &= \varphi_m \frac{1}{2}\left(1 - \cos\frac{2\pi z}{L}\right) \end{aligned} \tag{54}$$

where u_m and φ_m are the displacement amplitudes (in this case, at the middle of the beam).

The M_{cr0} without prebuckling deflections is:

$$M_{cr0,1t} = \frac{\pi}{0.5L}\sqrt{EI_y\left(GJ + \frac{\pi^2 EI_w}{(0.5L)^2}\right)} \tag{55}$$

The formula for the critical moment is:

$$M_{cr,1t} = M_{cr0,1t}\Big/\sqrt{\left(1 - \frac{EI_y}{EI_x}\right)\left(1 + 2\frac{EI_y}{EI_x}\right)} \tag{56}$$

It is interesting to observe that while $M_{cr0,1t}$ for FrFw-FrFw can be determined from PrPw-PrPw using an equivalent length $(0.5L)$, this is not true for $M_{cr,1t}$. The simple engineering explanation is that in the case of M_{cr0} the solution is determined by the $u(z)$ and $\varphi(z)$ functions only, both having two half-waves, while in the case of M_{cr} the solution is influenced by the primary deflection, too, which has only one single half-wave.

- three-term solution

The solution can be enhanced by considering further similar terms in the displacement approximation. However, only a few terms can be added if closed-form results are desired. The results suggest that additional terms are more important for the rotation, thus, a reasonable possible approximation is as follows:

$$\begin{aligned} u(z) &= u_m \frac{1}{2}\left(1 - \cos\frac{2\pi z}{L}\right) \\ \varphi(z) &= \varphi_m\left[\frac{1}{2}\left(1 - \cos\frac{2\pi z}{L}\right) + r_2\left(1 - \cos\frac{4\pi z}{L}\right) + r_3\left(1 - \cos\frac{6\pi z}{L}\right)\right] \end{aligned} \tag{57}$$

Where r_2 and r_3 are scalar parameters to be determined. (It is to note that in the 3-term displacement assumption u_m and φ_m are not the displacement amplitudes anymore). After performing the derivations, the critical moment without the prebuckling deflections is:

$$\begin{aligned} M_{cr0,3t} &= \frac{\pi}{0.5L}\sqrt{EI_y\left(\alpha_G GJ + \alpha_w \frac{\pi^2 EI_w}{(0.5L)^2}\right)} \\ \alpha_G &= 1 + 16{r_2}^2 + 36{r_3}^2 \\ \alpha_w &= 1 + 64{r_2}^2 + 256{r_3}^2 \end{aligned} \tag{58}$$

If the prebuckling deflection is considered, the critical moment expression is as follows:

$$M_{cr,3t} = M_{cr0,3t} \Big/ \sqrt{\left(1 - \frac{I_y}{I_x}\right)\left(1 + 2\frac{I_y}{I_x}(1 + 4r_2 + 4r_3 + 6{r_2}^2 + 6{r_3}^2 + 8r_2 r_3)\right)} \tag{59}$$

Note, if $r_2 = r_3 = 0$, the 3-term formulae simplify to the single-term solution. Due to symmetry, the critical moments can be plus or minus; the positive ones are taken as the critical moment.

- Moment increase due to the prebuckling deflection

In order to calculate the increase due to the prebuckling deflection, the minimum values of both M_{cr0} and M_{cr} are to be found. Regarding M_{cr0}, it is obvious that $M_{cr0,3t}$ takes its minimal value if $r_2 = r_3 = 0$; i.e., $M_{cr0,min} = M_{cr0,1t}$. Regarding M_{cr}, first, the minimum of the $M_{cr,3t}$ expression should be found; mathematically, the following equation system should be solved:

$$\frac{\partial M_{cr,3t}}{\partial r_2} = 0 \quad \frac{\partial M_{cr,3t}}{\partial r_3} = 0 \tag{60}$$

Unfortunately, this equation system cannot be solved analytically. As a simplification, the first equation is solved by assuming $r_3 = 0$, from which r_2 is obtained (which is a reasonable approximation, since r_3 is supposed to be a rather small number). Then, the second equation can be solved. Eliminating the higher-order terms of r_2 and r_3, the following expressions can be derived:

$$\begin{aligned} r_2 &= \frac{EI_y(GJL^2 + 4\pi^2 EI_w)}{GJL^2\left(4EI_x + 5EI_y\right) + 4\pi^2 EI_w\left(16EI_x + 29EI_y\right)} \\ r_3 &= \frac{EI_y(GJL^2 + 4\pi^2 EI_w)(1 + 2r_2)}{GJL^2\left(9EI_x + 15EI_y\right) + 4\pi^2 EI_w\left(81EI_x + 159EI_y\right)} \end{aligned} \tag{61}$$

The above formulae suggest that r_2 and r_3 increase as the beam length increases and/or the inertia ratio increases. A practical upper bound is 1/9 and 11/216 for r_2 and r_3, respectively, which belong to $L \to \infty$ and $I_y/I_x = 1$. A mathematical lower bound for both r_2 and r_3 are zero, when $L = 0$ and $I_y/I_x = 0$. This also means that in any practical case the minimum M_{cr} value can be obtained from the 3-term solution, i.e., $M_{cr,min} = M_{cr,3t}$ with the r_2 and r_3 values from Eq. (61). Another observation is that both r_2 and r_3 are small numbers, but r_3 is smaller than r_2. This justifies the approximate approach employed in the derivation. (Furthermore, this makes it possible to further simplify Eq. (59), e.g., by eliminating some or all the higher-order terms of r_3 and/or r_2.). Finally, the moment increase can be calculated as $(M_{cr} - M_{cr0})/M_{cr0}$.

3.3.2 FrPw-FrPw

This is the case where the weak-axis rotation is fixed, and warping is free at both ends of the beam.

- Single-term solution

If a single trigonometric term is used, the simplest displacement functions that satisfy the support conditions are as follows:

$$u(z) = u_m \frac{1}{2}\left(1 - \cos\frac{2\pi z}{L}\right)$$
$$\varphi(z) = \varphi_m \sin\frac{\pi z}{L} \tag{62}$$

The critical moment without the prebuckling deflections is:

$$M_{cr0,1t} = \frac{3\pi}{8}\frac{\pi}{0.5L}\sqrt{EI_y\left(GJ + \frac{\pi^2 EI_w}{L^2}\right)} \tag{63}$$

The critical moment with the prebuckling deflections is:

$$M_{cr,1t} = M_{cr0,1t} \Big/ \sqrt{\left(1 - \frac{EI_y}{EI_x}\right)\left(1 + \left(\frac{9\pi^2}{16} - 1\right)\frac{EI_y}{EI_x}\right)} \tag{64}$$

The $M_{cr0,1t}$ formula can be interpreted as follows: the equivalent length for twisting is $1.0L$, (which can directly be concluded from the assumed displacement function), while the equivalent length for the lateral translation is $(4/3\pi)L = 0.4244L$, i.e., smaller than what could be predicted from the shape function. However, detailed numerical analysis results suggest that this solution is not precise, and the real critical moment is somewhat smaller, which can be approximated by a more refined displacement function assumption, as follows.

- three-term solution

Better results can be obtained (and still, the critical moments can be expressed in closed format) if the displacements are approximated as follows:

$$u(z) = u_m \frac{1}{2}\left(1 - \cos\frac{2\pi z}{L}\right)$$
$$\varphi(z) = \varphi_m \left[\sin\frac{\pi z}{L} + r_2 \sin\frac{3\pi z}{L} + r_2 \sin\frac{5\pi z}{L}\right] \tag{65}$$

where r_2 and r_3 are scalar parameters to be determined.

The solution without the prebuckling deflection is:

$$M_{cr0,3t} = \alpha_y \frac{\pi}{0.5L}\sqrt{EI_y\left(\alpha_G GJ + \alpha_w \frac{\pi^2 EI_w}{(0.5L)^2}\right)}$$

$$\alpha_y = \frac{105\pi}{8(35 - 63r_2 - 25r_3)} \tag{66}$$

$$\alpha_G = 1 + 9{r_2}^2 + 25{r_3}^2$$

$$\alpha_w = 1 + 81{r_2}^2 + 625{r_3}^2$$

The critical moment with prebuckling deflections can be derived similarly, and the $M_{cr,3t}/\,M_{cr0,3t}$ratio can be expressed as follows:

$$M_{cr,3t} = M_{cr0,3t}\Big/\sqrt{\left(1 - \frac{I_y}{I_x}\right)\left(1 + \frac{I_y}{I_x}\left(\frac{11025\pi^2(1 + {r_2}^2 + {r_3}^2)}{16(35 - 63r_2 - 25r_3)^2} - 1\right)\right)} \tag{67}$$

Again, if $r_2 = r_3 = 0$, both critical moment formulae simplify to the single-term solutions.

- Moment increase due to the prebuckling deflection

To calculate the increase due to the prebuckling deflection, the minimum values of both M_{cr0} and M_{cr} are to be found. For this support, the minimum point of either formula is not obvious. Regarding $M_{cr0,3t}$, the following equation system must be solved:

$$\frac{\partial M_{cr0,3t}}{\partial r_2} = 0 \quad \frac{\partial M_{cr0,3t}}{\partial r_3} = 0 \tag{68}$$

This can be done analytically, and the following expressions are obtained:

$$r_2 = -\frac{GJ + \frac{\pi^2 EI_w}{L^2}}{5GJ + 45\frac{\pi^2 EI_w}{L^2}} = -\frac{GJL^2 + \pi^2 EI_w}{5GJL^2 + 45\pi^2 EI_w}$$

$$r_3 = -\frac{GJ + \frac{\pi^2 EI_w}{L^2}}{35GJ + 875\frac{\pi^2 EI_w}{L^2}} = -\frac{GJL^2 + \pi^2 EI_w}{35GJL^2 + 875\pi^2 EI_w} \tag{69}$$

It can be observed that r_2 and r_3 depend on the length (and the torsion properties), but both are bounded. If $L \to 0$, then r_2 and r_3 takes the values -1/45 and -1/875, respectively. If $L \to \infty$, then r_2 and r_3 approaches -1/5 and -1/35, respectively. Theoretically, the minimum point of the $M_{cr,3t}$ formula can be found by setting the partial derivatives to zero. Practically however, the $M_{cr,3t}$ expression is too complex, and closed-form analytical solution for r_2 and

r_3 cannot be obtained. It is reasonable to assume, however, that the same r_2 and r_3 which minimize $M_{cr0,3t}$ will approximately minimize $M_{cr,3t}$, too. However, it cannot be easily predicted whether the minimal critical moments belong to the single-term or 3-term solutions. That is why, finally, the minimal critical moment values can be obtained as $M_{cr0,min} = min(M_{cr0,1t}, M_{cr0,3t})$ and $M_{cr,min} = min(M_{cr,1t}, M_{cr,3t})$ with r_2 and r_3 values from Eq. (69). Then, the moment increase can be.

3.3.3 PrFw-PrFw

This is the case where the weak-axis rotation is free, and warping is fixed at both ends of the beam.

- Single-term solution

If a single trigonometric term is used, the simplest displacement functions that satisfy the support conditions are as follows:

$$u(z) = u_m \sin\frac{\pi z}{L}$$
$$\varphi(z) = \varphi_m \frac{1}{2}\left(1 - \cos\frac{2\pi z}{L}\right) \tag{70}$$

The critical without the prebuckling deflections is:

$$M_{cr0,1t} = \frac{3\pi}{8}\frac{\pi}{L}\sqrt{EI_y\left(GJ + \frac{\pi^2 EI_w}{(0.5L)^2}\right)} \tag{71}$$

The critical moment with the prebuckling deflections is:

$$M_{cr,1t} = M_{cr0,1t} \Big/ \sqrt{\left(1 - \frac{EI_y}{EI_x}\right)\left(1 + \frac{EI_y}{EI_x}\left(\frac{27\pi^2}{256} - 1\right)\right)} \tag{72}$$

Since $27\pi^2/256 - 1 = 0.0409$, this formula is nearly identical to the reference solution. This implies that the warping fixity does not cause a significant change in how the prebuckling deflection influences the critical moment. The $M_{cr0,1t}$ formula can be interpreted as follows: the equivalent length for twisting is $0.5L$, (which can directly be concluded from the assumed displacement function), while the equivalent length for the lateral translation is $(8/3\pi)L = 0.8488L$, i.e., the warping restraint has some supporting effect for the lateral translations, too. However, detailed numerical analysis results suggest that this solution is not precise, and the real critical moment is somewhat smaller, which can be approximated by a more refined displacement function assumption.

- three-term solution

Similar to other cases, the displacements can be approximated more precisely as follows:

$$u(z) = u_m \sin\frac{\pi z}{L}$$
$$\varphi(z) = \varphi_m \left[\frac{1}{2}\left(1 - \cos\frac{2\pi z}{L}\right) + r_2\left(1 - \cos\frac{4\pi z}{L}\right) + r_3\left(1 - \cos\frac{6\pi z}{L}\right)\right] \tag{73}$$

where r_2 and r_3 are scalar parameters to be determined. The solution without the prebuckling deflection is:

$$M_{cr0} = \alpha_y \frac{\pi}{L}\sqrt{EI_y\left(\alpha_G GJ + \alpha_w \frac{\pi^2 EI_w}{(0.5L)^2}\right)}$$
$$\alpha_y = \frac{105\pi}{8(35 + 56r_2 + 54r_3)} \tag{74}$$
$$\alpha_G = 1 + 16{r_2}^2 + 36{r_3}^2$$
$$\alpha_w = 1 + 64{r_2}^2 + 324{r_3}^2$$

The solution with the prebuckling deflection is:

$$M_{cr,3t} = M_{cr0,3t} \Big/ \sqrt{\left(1 - \frac{I_y}{I_x}\right)\left(1 + \frac{I_y}{I_x}\alpha_r\right)}$$
$$\alpha_r = \frac{11025\pi^2(3 + 8r_2 + 8r_3 + 16r_2r_3 + 12{r_2}^2 + 12{r_3}^2)}{256(35 + 56r_2 + 54r_3)^2} - 1 \tag{75}$$

Note, if $r_2 = r_3 = 0$, the formulae simplify to the single-term solutions, but this would not lead to the lowest critical moments.

- Moment increase due to the prebuckling deflection

The expressions for r_2 and r_3 that minimize $M_{cr0,3t}$ (and approximately minimize $M_{cr,3t}$), can be obtained similarly as presented in the previous section. The resulting expressions are as follows:

$$r_2 = \frac{GJ + \frac{\pi^2 EI_w}{(0.5L)^2}}{10GJ + 40\frac{\pi^2 EI_w}{(0.5L)^2}} = \frac{GJL^2 + 4\pi^2 EI_w}{10GJL^2 + 160\pi^2 EI_w} \tag{76}$$

$$r_3 = \frac{3GJ + 3\frac{\pi^2 EI_w}{(0.5L)^2}}{70GJ + 630\frac{\pi^2 EI_w}{(0.5L)^2}} = \frac{3GJL^2 + 12\pi^2 EI_w}{70GJL^2 + 2520\pi^2 EI_w}$$

Both r_2 and r_3 are bounded: r_2 is between 1/40 and 1/10, while r_3 is between 1/210 and 3/70. The minimal critical moment values can then be obtained as $M_{cr0,min} = (M_{cr0,1t}, M_{cr0,3t})$ and $M_{cr,min} = (M_{cr,1t}, M_{cr,3t})$.

3.3.4 PrPw-FrFw

This is the case where the weak-axis rotations and warping are fixed at one end, and free at the other. It turns out that assumed displacement functions with single trigonometric terms lead to reasonably good solutions, thus, no more refined solutions are shown here. The assumed displacement functions are deducted from the flexural buckling solution of a pinned-clamped column, as follows:

$$\begin{aligned} u(z) &= u_m \left(\sin\frac{\pi z}{KL} - \frac{z}{L}\sin\left(\frac{\pi}{K}\right)\right) \\ \varphi(z) &= \varphi_m \left(\sin\frac{\pi z}{KL} - \frac{z}{L}\sin\left(\frac{\pi}{K}\right)\right) \end{aligned} \tag{77}$$

where K can be interpreted as an equivalent (i.e., buckling) length factor. Mathematically, the condition $\frac{\pi}{K} = \tan(\frac{\pi}{K})$ must be satisfied, from which the approximate value of K is 0.6992. The M_{cr0} without prebuckling deflections is:

$$M_{cr0,1t} = \frac{\pi}{0.6992L}\sqrt{EI_y\left(GJ + \frac{\pi^2 EI_w}{(0.6992L)^2}\right)} \tag{78}$$

The M_{cr} with prebuckling deflections is:

$$M_{cr,1t} = M_{cr0,1t} \Big/ \sqrt{\left(1 - \frac{EI_y}{EI_x}\right)\left(1 + \frac{2EI_y}{3EI_x}\right)} \tag{79}$$

The moment increase can be calculated similarly., simply taking the single-term solutions, i.e., $M_{cr0,min} = M_{cr0,1t}$ and $M_{cr,min} = M_{cr,1t}$.

3.3.5 Reference solution

Furthermore, a simplified analytical solution (proposed in several papers by various researchers) for the simple case is also considered. From this, the M_{cr}/M_{cr0} ratio will be referred to as the *reference ratio* and is expressed as follows:

$$\frac{M_{cr}}{M_{cr0}} = 1 \Big/ \sqrt{\left(1 - \frac{I_y}{I_x}\right)} \tag{80}$$

The increase in the critical moment due to the prebuckling deflection – which will be referred to here as *reference increase* – is expressed as:

$$\frac{M_{cr} - M_{cr0}}{M_{cr0}} = 1 \Big/ \sqrt{\left(1 - \frac{I_y}{I_x}\right)} - 1 \tag{81}$$

3.4 Numerical solutions

3.4.1 Iterative LBA on deflected beam

If classic LBA is conducted by FEM, (i) first, the stresses are calculated on the undeflected structure from the given loading (i.e., a linear static analysis is performed), (ii) then, the geometric stiffness matrix is calculated considering the stress distribution obtained in the previous step, (iii) then, the loads/stresses are scaled to find the critical values by solving the generalized eigen-value problem of the structure. Obviously, this process does not include the effect of prebuckling deflections. A possible proposed way to include the prebuckling deflections is to perform LBA on a deflected beam by introducing an iterative procedure as follows.

Step #1: First, classic LBA is performed, and M_{cr} is calculated (which, in this step, will be equal to M_{cr0}).

Step #2: Static analysis is performed to get the deflected shape (i.e., the prebuckling shape), using the M_{cr} as the load from the previous Step.

Step #3: LBA is performed on the deflected shape, using the deflected shape from the previous step, from which a new value for M_{cr} is obtained.

Since the critical moment calculated in Step #3 (on the deflected beam) is different from the critical moment calculated in Step #1 (on the undeflected beam), Steps #2 and #3 should be repeated till convergence. Note, this iterative procedure is similar to the one applied in [76].

It can be understood that this iterative LBA is slightly different from the real behavior, since in the reality the stresses and deflections increase gradually as the load increases, whilst in the last step of the above iterative procedure (from which M_{cr} is finally obtained) there is a stress-free deflected beam on which the loads are applied, thus, the stress distribution as well

as the geometric stiffness matrix is theoretically different. However, in the case of the actual simple beam problem the stress distribution is hardly affected by the primary displacements, therefore, the above iterative LBA procedure can be considered as a rather accurate representation of the buckling with considering prebuckling deflections.

The above-described procedure is applicable whether the calculation uses a beam or shell FEM model. The convergence of M_{cr} through iterations is illustrated in Table 3.3, where the increase in the critical moment due to prebuckling deformations is shown in terms of the number of iterative steps. (The actual values belong to DSI section, PrPw-PrPw boundary conditions, and L=15 m length). Table 3.3 shows that the deeper the section is, the fewer iterations are required to achieve convergence. This is due to the smaller in-plane deflections in these sections, and, as a result, a smaller effect of prebuckling deformations.

Table 3.3: Increase in critical moments due to prebuckling deformation in terms of iterations.

No. of iteration steps	$I_y/I_x =$ 0.75	$I_y/I_x =$ 0.65	$I_y/I_x =$ 0.39
1	42.06%	35.40%	19.82%
2	62.93%	49.91%	24.13%
3	73.82%	56.10%	25.07%
4	79.63%	58.79%	25.28%
6	84.45%	60.47%	25.34%
8	85.87%	60.80%	25.34%
10	86.29%	60.86%	25.34%

In in Step #2 of the process, the static analysis should generally be nonlinear. The reason is that occasionally large deflections are experienced, and the deflected geometry is improperly captured by a linear analysis. In the linear analysis, the stiffness matrix is calculated for the undeflected (perfectly horizontal) beam, the whole load is applied to the member at once, and the equilibrium equation is solved. Even though one end is free to move axially, the calculated axial displacement would be zero, causing the actual length of the deflected beam to be larger compared to the original one. On the other hand, in the case of nonlinear analysis, the load is applied to the structure in an incremental way, and after the end of each incremental step, the stiffness matrix is updated, therefore the roller support displaces axially, and the total length of the beam remains (practically) unchanged. The total vertical deflections in the two cases are marginally different, however, the difference in the length of the deflected beam is the important factor since it modifies the curvature of the beam in the primary plane, which has a non-negligible effect on the critical moment of the – already curved – beam.

It was experienced that with using a higher number of load-steps, higher accuracies can be reached in the non-linear static analysis. Table 3.4 shows the percentages of error in the resulting M_{cr} when using different number of load steps. (When the number of steps is one, this represents the linear static analysis). Moreover, if the I_y/I_x ratio is small, the prebuckling deflections are small, and the linear and nonlinear static analysis lead to similar increase in M_{cr}. However, if the I_y/I_x is large enough, the influence of the nonlinearity is more visible.

Table 3.4: Error in M_{cr} in terms of load incremental steps.

Number of load steps	$I_y/I_x =$ 0.75	$I_y/I_x =$ 0.65	$I_y/I_x =$ 0.39
1	8.30%	4.37%	0.78%
2	3.88%	1.97%	0.35%
5	1.16%	0.58%	0.10%
10	0.06%	0.14%	0.03%
15	0.00%	0.00%	0.00%

3.4.2 GNIA with small initial imperfection

Another possible approach to numerically calculate the critical moment with considering the prebuckling effects is the geometrically nonlinear incremental analysis with initial imperfections (GNIA). The initial imperfection is necessary to initiate the secondary displacements, i.e., the buckling. For this reason, first, LBA is performed on the undeflected beam, then the (first mode) buckled shape – with proper scaling – is used as initial geometrically imperfect shape, and then the nonlinear analysis is performed, from which load-displacement curves can be established.

As it is well-known, if GNIA is performed, the secondary displacements (i.e., in this case, lateral translation and twisting rotation) are gradually increasing, therefore, there is no point of bifurcation, i.e., the critical moment cannot clearly be captured. However, if the initial imperfection is small, the load-displacement curve will have a relatively sharp "corner" point. This is illustrated in Fig. 3.2, where the total horizontal displacement at the reference point (i.e., the middle point of the beam) is plotted against the applied load, for three values of initial imperfection amplitude. (Note, the actual plot belongs to DSI section with $I_y/I_x = 0.49$, PrPw-PrPw supports.) It can be observed that when the initial amplitude is 0.001 mm (an extremely small value for a 15-m-long beam), the displacement increment significantly increases at the load step with approximately 1.3 mm of total translation, causing the tangent of the curve to

approach zero. The load value from such a step is chosen as the nominal critical moment. (In the example shown in Fig. 3.2, this load is well above M_{cr0}, and is very close to M_{cr} calculated by the iterative LBA procedure.)

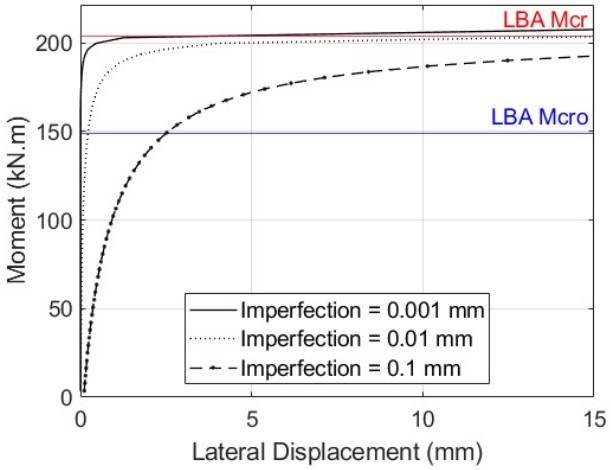

Figure 3.2: End moment vs. displacement of the reference point, for various values of initial imperfection

3.4.3 FEM models

- The models in general

When beam finite element analysis is performed, it is important to make sure that the employed beam element properly considers the warping and Saint-Venant torsion of thin-walled members. In this study the educational Mastan2 [84], and the commercial Ansys software [85] have been employed. Since the results of these two programs are nearly identical for the cases discussed, only the Ansys results are presented. The beams have been discretized into 32 beam finite elements along the length, and the load is applied as concentrated moments at the ends.

In the case of shell FE analysis, the student version of Ansys has been used. The applied finite element is the SHELL181. For the discretization of the model, the (average) element size was set to 40 mm. The end moments have been placed onto the model as equivalent distributed loads (i.e., line pressures) acting along the edges of the flanges and web of the member at the midline of the shell elements (Fig. 3.3). An important feature is that line pressure is perpendicular to the edges and remain so even when the structure deforms; therefore, the resultant of the loading (i.e., the bending moment) remains independent of the deflections.

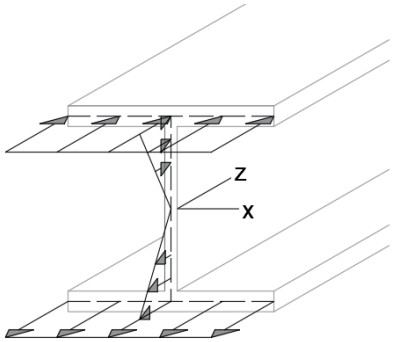

Figure 3.3: Line pressure applied to the shell model.

- Supports in beam FEM

Since in the analyses, the geometry is updated as part of the process (either in the case of iterative LBA or GNIA), and since the primary deflections can potentially be significant, it is a question whether the twisting rotations are interpreted in the fixed (i.e., global) coordinate system, or in a rotating (i.e., local) coordinate system aligned to the end cross-section. Both interpretations are reasonable but require different handling and lead to different results, since the twisting fixity, if applied in the global coordinate system, results in some fixity about the weak axis in the local (i.e., deflected) coordinate system.

If the rotations are interpreted in the global system, then the rotational fixity can directly be applied to the relevant DOF of the end cross-section. However, if the rotations are interpreted in the local system, some special support solution is needed. In this research, the rotations are typically interpreted in the local system and are realized by adding two small cantilevers along the local *y*' axis at the beam ends, which remain perpendicular to the longitudinal axis even when the beam is deflected. The twisting is then prevented by defining *x*-directional translational supports at the end of the cantilevers (Fig 3.4).

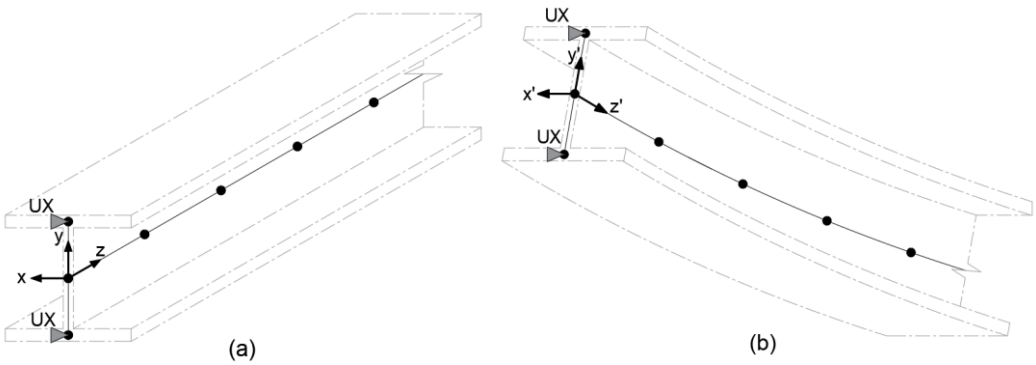

Figure 3.4: Support against local twisting rotation: (a) undeformed, (b) deformed.

It is to mention that, in the Fr case, this support defention problem does not exist because fixities about both the *y* and *z* axis exist, ensuring that both the minor-axis and twisting rotations are prevented, regardless in which coordinate system the rotations are interpreted. The interpretation of the twisting rotation has an important effect on the deflections. Fig. 3.5 shows four situations (the actual shown case is for the RHS section with L = 30 m), depending on whether the support is local or global (i.e., LS or GS), and whether the rotation is interpreted in the local or global system (i.e., LR or GR). Not surprisingly, the twisting rotation interpretation has noticeable influence on the calculated critical moment values.

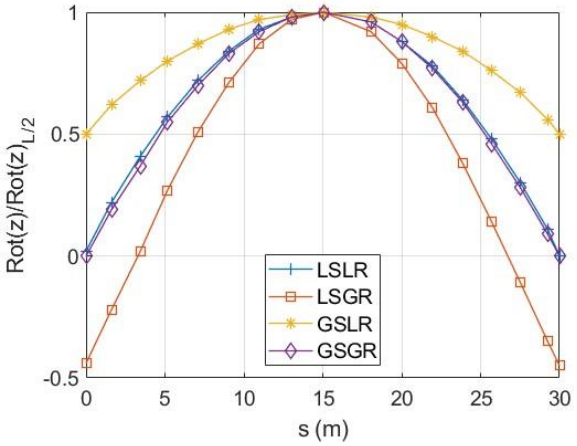

Figure 3.5: Local and global twisting rotations for the different support types.

To show the effect clearly, Table 3.5 shows the results of using either the global or the local supports: M_{cr0} (buckling moment without prebuckling deformations), and the increase in moment due to prebuckling deflections are given for the same case (which is RHS section with PrPw-PrPw supports). As can be observed, the M_{cr0} values are slightly affected, which is due to the extra flexibility provided by the small cantilevers.

Table 3.5: The effect of support type on the critical moments

I_y/I_x	Global Support M_{cr0} kNm	Local Support M_{cr0} kNm	Global Support incr (%)	Local Support incr (%)
0.53	432.2	430.6	11.39	75.47
0.43	461.1	459.4	7.39	58.08
0.22	518.4	516.4	0.82	25.73
0.13	575.1	572.7	-0.37	15.79
0.09	853.1	847.7	-0.65	11.05
0.03	1126.6	1115.9	-0.5	3.76

However, the increase in moment is strongly affected even if the I_y/I_x ratio is small. (It is fair to add that the support interpretation effect is much less significant in the case of DSI sections, primarily because the critical moments are smaller, hence the primary deflections are smaller, so that the difference between the local and global coordinate systems is small.) Though both the local and global supports might be meaningful, in the current studies local supports are applied as assumed in the analytical models.

- Supports in shell FEM

When shell FEM is used for the analysis of thin-walled members, it is not evident how the classic end supports (such as, pinned) can be realized. If the support is PrPw, two possible versions are considered.

Support #1: Each node of the end cross-sections is supported perpendicularly to the plate element as shown in Fig. 3.6(a). Note, such support is successfully used for the buckling analysis of thin-walled members, e.g., in [44,86].

Support #2: The end section nodes are supported against *x* or *y* translations, as shown in Fig. 3.6(b). Moreover, to reduce the localized deformations, all the nodes are restrained against twisting rotation, which is realized by introducing a master node which all the nodes at the end of the beam are rigidly linked to. (It is to note that the so-called master node is a separate node, i.e., not part of the member discretization, though in the case of DSI section its geometric location coincides with one of the nodes of the discretized member).

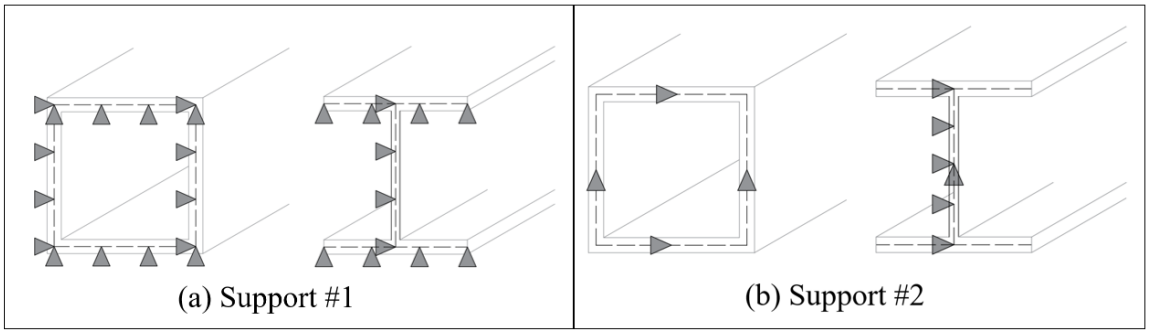

Figure 3.6: illustration of end supports in shell FE model for the DSI and RHS sections

If the beam axis is horizontal (i.e., undeflected beam), the two PrPw support versions are practically identical. However, both in the iterative LBA and GNIA, the geometry is updated, i.e., deflected beams are analyzed. As soon as the beam is deflected, the pressure load at the plate edges becomes inclined, and the vertical translational supports in Support #1 can directly take a portion of the loading, hence, the edge moment is not fully transferred to the

beam. On the other hand, in the case of Support #2, all the edge pressure load is directly transferred to the beam. The difference between Support #1 and #2 is reflected in the critical load values, too, as illustrated by Table 3.6, which is for the DSI section, PrPw-PrPw end supports, and a length of 15m.

Table 3.6: Increase in critical moment in terms of I_y/I_x for both support configurations

I_y/I_x	M_{cr0} kNm	Support #1 incr (%)	Support #2 incr (%)
0.75	147.8	86.29	229.17
0.65	148.2	60.80	128.81
0.49	149.1	36.54	51.80
0.39	150.0	25.33	30.81
0.15	1.55.3	7.96	8.16
0.08	159.3	3.77	3.86
0.05	166.2	2.22	2.16

Obviously, the larger the I_y/I_x, the larger the difference between the two support versions, which is due to the larger deflections. Though none of these support versions can be considered incorrect, Support #2 is employed in the further analysis, since this solution is comparable to the beam element model, and the analytical derivations.

In this study, 4 types of end supports are necessary to cover all support conditions in Table 1. (i) PrPw is realized as Support #2. (ii) In the case of PrFw support, the solution is similar to PrPw, but the additional warping support is introduced by forcing the linked nodes to follow the longitudinal translation of the master node. (iii) The FrPw support cannot easily be realized in a shell model, therefore, this support case was not considered in shell FEM analyses. (iv) FrFw is similar to PrFw, but, additionally, the master node is restrained against the rotation around the vertical axis (y).

3.5 Numerical results

3.5.1 Critical moments without prebuckling deformations

The results of M_{cr0} (without prebuckling deformations) are shown in Table 3.7 for the DSI sections, and Table 3.8 for the RHS sections. In these tables, “diff. ana.” refers to the difference in percentage between the analytical solution and the beam element solution, while “diff. shell FEM” refers to the difference between the shell and beam element solutions. It is shown that the beam FEM results are practically identical to the analytical ones for DSI sections. Furthermore, there is a systematic difference between the beam and shell FEM results,

the shell FEM leads to lower critical moments, which is due to the extra flexibility of the shell model, and in line with findings from other papers (e.g. [44,87]), with the shell model being able to produce non-beam-like deformations, such as localized bending deformations and/or cross-section distortion. The magnitude of these non-beam-like deformations depends on the geometry of the beam.

Table 3.7: M_{cr0} for DSI sections

I_y/I_x	PrPw-PrPw			FrFw-FrFw			PrFw-PrFw			FrPw-FrPw	
	beam FEM M_{cr0}	diff. ana.	diff shell FEM	beam FEM M_{cr0}	diff. ana.	diff shell FEM	beam FEM M_{cr0}	diff. ana.	diff shell FEM	beam FEM M_{cr0}	diff. ana.
	kN.m	%	%	kN.m	%	%	kN.m	%	%	kN.m	%
0.75	152	-0.02	-2.52	308	-0.09	-2.43	163	2.37	-2.41	307	0.08
0.65	152	-0.02	-2.62	310	-0.09	-2.55	164	2.25	-2.51	309	0.08
0.49	153	-0.02	-2.81	314	-0.08	-2.78	167	2.05	-2.74	313	0.07
0.39	155	-0.02	-2.91	319	-0.08	-2.90	170	1.88	-2.84	316	0.06
0.15	161	-0.02	-3.42	343	-0.08	-3.54	187	1.48	-3.46	335	0.09
0.08	168	-0.02	-4.91	372	-0.10	-5.40	205	1.38	-5.35	355	0.20
0.05	175	-0.02	-4.98	405	-0.10	-5.56	225	1.37	-5.48	405.3	0.35

Table 3.8: M_{cr0} for RHS sections

I_y/I_x	PrPw-PrPw			FrFw-FrFw			PrFw-PrFw			FrPw-FrPw	
	beam FEM M_{cr0}	diff. ana.	diff shell FEM	beam FEM M_{cr0}	diff. ana.	diff shell FEM	beam FEM M_{cr0}	diff. ana.	diff shell FEM	beam FEM M_{cr0}	diff. ana.
	kN.m	%	%	kN.m	%	%	kN.m	%	%	kN.m	%
0.75	432	0.02	-3.37	865	-0.08	-3.29	433	6.22	-3.46	865	0.19
0.66	461	0.01	-3.49	923	-0.09	-3.46	462	6.20	-3.55	923	0.19
0.53	518	0.07	-3.79	1038	-0.09	-3.94	520	6.28	-3.98	1038	0.19
0.43	575	0.01	-3.87	1151	-0.10	-4.10	577	6.24	-4.00	1151	0.19
0.22	853	0.01	-4.42	1708	-0.10	-5.62	857	6.73	-4.56	1708	0.18
0.13	1127	-0.05	-4.70	2255	-0.12	-7.25	1134	6.90	-4.89	2255	0.17
0.09	1398	-0.02	-7.26	2799	-0.13	-11.50	1409	7.19	-7.54	2799	0.15
0.03	2746	-0.03	-13.18	5501	-0.23	-27.05	2791	10.16	-13.77	5500	0.05

Regarding RHS, the analytical and beam element results for PrPw-PrPw and FrFw-FrFw (and also PrPw-FrFw, though not shown) coincide. Moreover, in the case of PrFw-PrFw and FrPw-FrPw slightly higher discrepancies are experienced, which suggests that the displacement

functions assumed in the analytical derivations (for these support cases) are approximate as explained in section 3.3. The differences between the shell and beam element seem to be higher in RHS compared to DSI. It can be concluded that the local deformations are larger when rotational or warping fixities are introduced, such as: (i) when the beam is shorter, (ii) when the beam is deeper, or (iii) in the case of RHS sections compared to DSI sections, resulting in lower M_{cr0} values in the shell element, compared to the beam element and analytical solutions.

3.5.2 Critical moments with prebuckling effect

The M_{cr} critical moments (with pre-buckling deflections) have been calculated by the iterative LBA as well as by GNIA methods, using both beam and shell element solutions. Then, M_{cr} values have been compared to M_{cr0} (without pre-buckling deflection). Figs. 3.7 to 3.11 show the increase in moment (i.e., difference between M_{cr} and M_{cro}) for the different boundary conditions. (Note, GNIA has been performed for DSI sections only. Also, FrPw-FrPw support case has not been considered in shell FEM.)

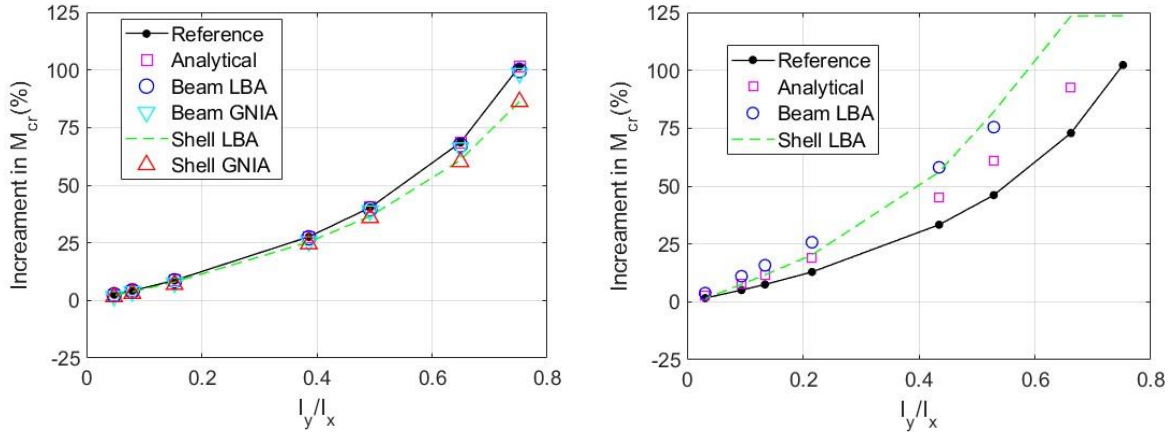

Figure 3.7: Critical moment increase, PrPw-PrPw, DSI (left) and RHS (right)

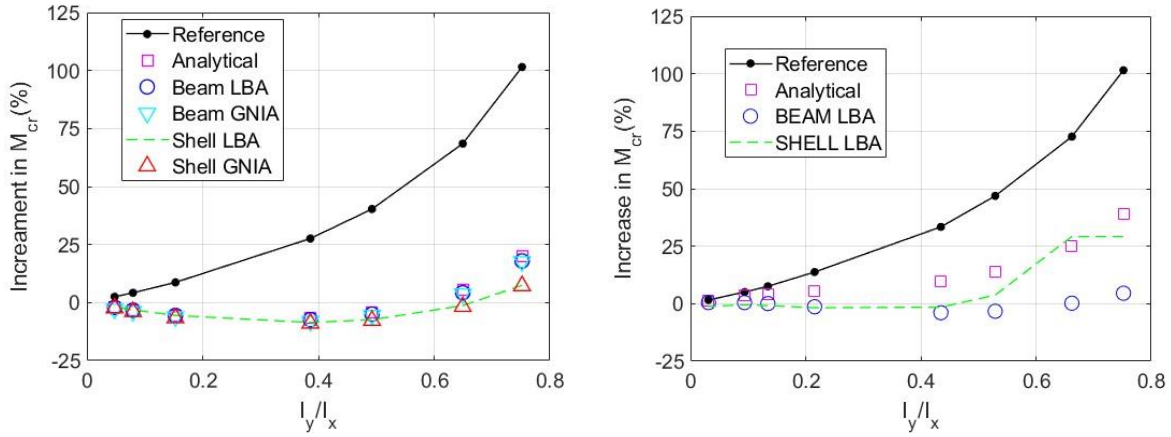

Figure 3.8: Critical moment increase, FrFw-FrFw, DSI (left) and RHS (right)

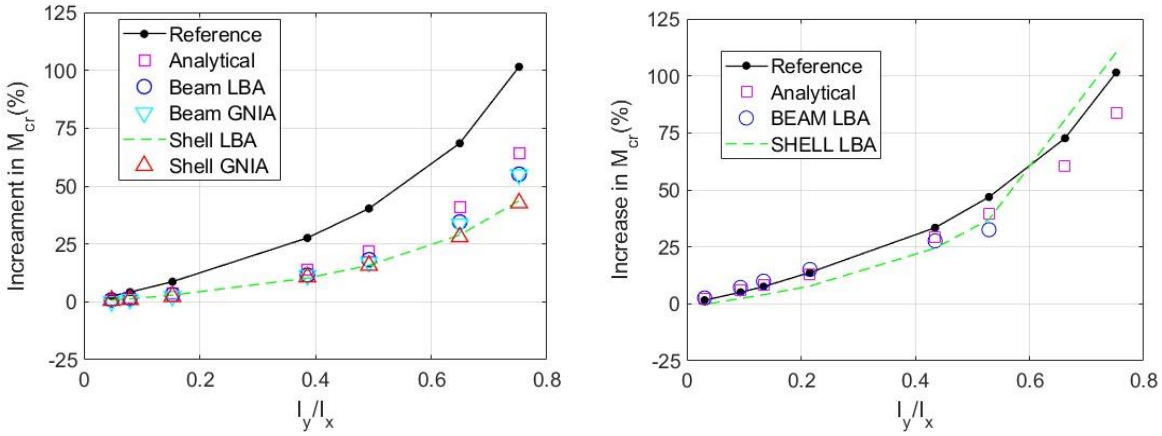

Figure 3.9: Critical moment increase, PrPw-FrFw, DSI (left) and RHS (right)

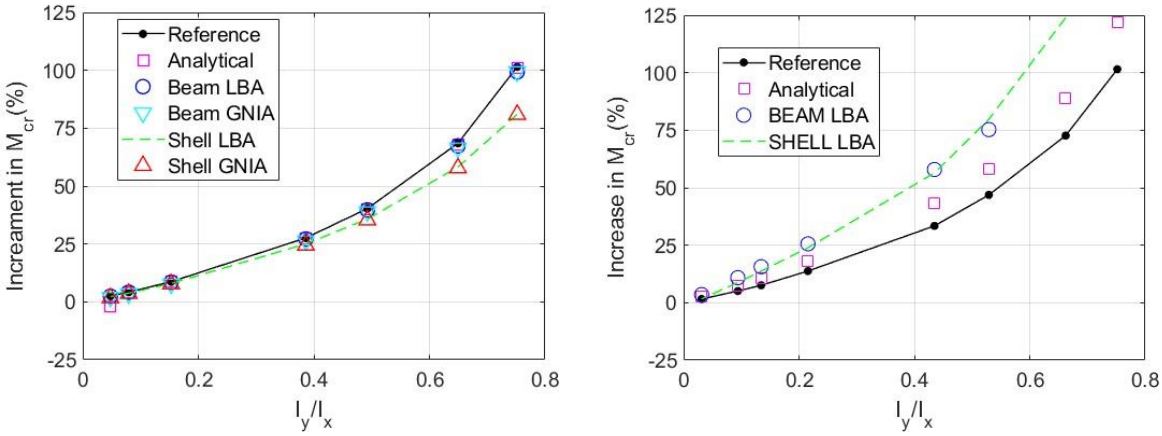

Figure 3.10: Critical moment increase, PrFw-PrFw, DSI (left) and RHS (right)

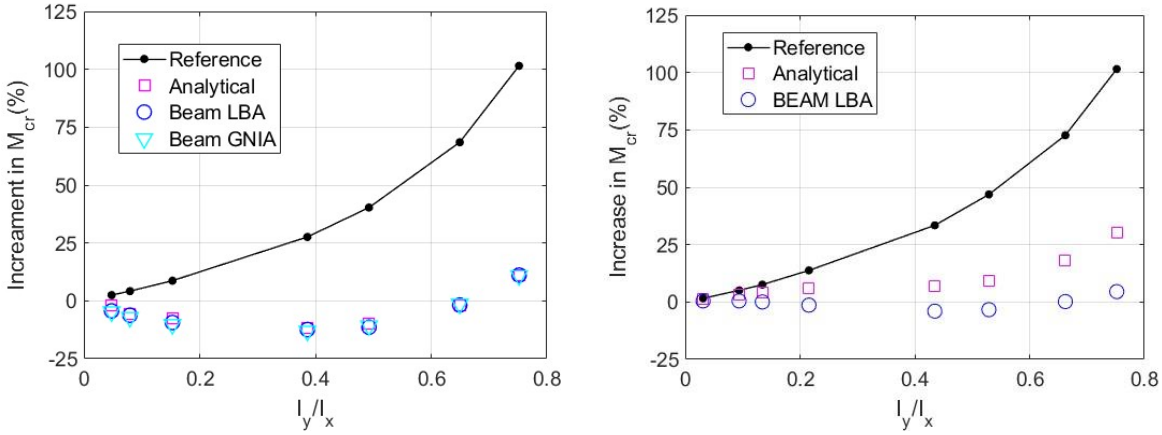

Figure 3.11: Critical moment increase, FrPw-FrPw, DSI (left) and RHS (right)

Several observations can be made from these plots. Firstly, there is a non-negligible difference between DSI and RHS. The critical moment increase is higher in RHS cross sections when compared to DSI. Furthermore, the end support has an important effect: while in the PrPw-PrPw case (which is overwhelmingly discussed in the literature), the reference increase

is nearly precise for DSI, the actual increase can be quite different for other boundary conditions.

In DSI, the increase is typically less than the reference, for all the other considered supports. In RHS, the increase can be smaller or larger than the reference, depending on the supports. Regarding the effect of end fixity, it is clear that rotation fixity has much higher effect than that of warping fixity. It is to highlight that in certain support conditions there is a decrease rather than an increase, i.e., the prebuckling effect decreases the critical moment, unlike what is suggested in the literature (the prebuckling deformations always increase the critical moment).

In general, good agreement between the methods is observed. The largest discrepancies are experienced for high I_y/I_x values (which are less willing to buckle, and therefore less important for the practice). When looking at the results of the numerical methods, LBA and GNIA lead to practically identical critical moment predictions for both the shell and beam element models, which justifies the applicability of the proposed iterative LBA method.

Also, in general, the agreement between the methods is better in the case of DSI compared to RHS. This is primarily due to the fact that the applied displacement approximations are less appropriate for sections with large torsional rigidity. It can be seen that the agreement is the highest between the beam FEM and the analytical solutions in the case of DSI. Even in these cases, however, smaller discrepancies are found. These discrepancies can be attributed primarily to the approximate nature of the assumed displacement functions in the analytical solutions.

Finally, in some cases, the shell model results are considerably different from those from the other methods. This seems to be particularly true in the case of RHS. These discrepancies can be attributed to the localized deformations, which are always present in shell FEM, and which seem to have an even higher effect when prebuckling deformations are considered, as will briefly be discussed in the next section.

3.6 On the effect of beam length

All the numerical results presented above are calculated for specific beam lengths, i.e., 15 m and 30 m for DSI and RHS beams, respectively. Looking at the simplified analytical solutions, the length is not included in the M_{cr}/M_{cr0} ratios. However, if more refined analytical derivations are applied (i.e., with less simplifications or approximations in the derivations, or

by having multiple terms in the assumed displacement functions), especially if some end fixity is introduced, too, the M_{cr}/M_{cr0} ratios become dependent on the beam length.

This is in accordance with the numerical results from the beam FEM solutions where length-dependency can also be observed, as illustrated by Fig. 3.13, where the increase in critical moment is plotted for DSI beams with FrFw-FrFw supports, with the selected section having I_y/I_x ratio of 0.49. It can be seen from Fig. 3.12 that unlike the single-term analytical solution, all the other solutions show noticeable length-dependency when prebuckling deformations are considered. The beam FEM and the enhanced analytical solution show similar length dependencies, though the longer the beam is, the less well the results agree. The agreement could be improved by further enhancing the analytical solution, e.g., by adding more terms into the twisting function. In other words, more terms are needed for longer beams for an accurate solution.

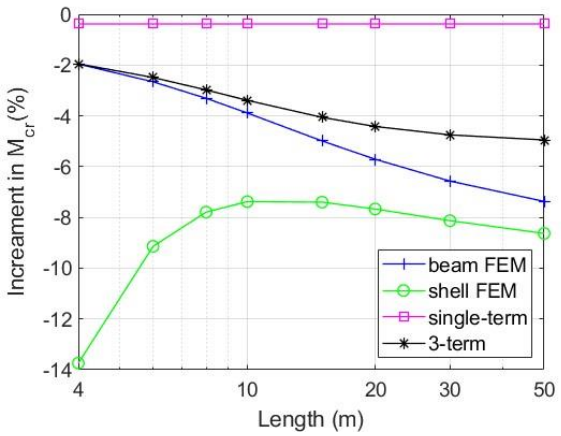

Figure 3.12: Effect of prebuckling deformations across the length.

At the same time, a more pronounced length-dependency is experienced in the shell FEM results. The critical moment increase from the shell FEM initially shows an increase with increasing the length, but then start to decrease, following the beam FEM behavior. The discrepancy between the tendencies in the case of short beams is due to the localized (i.e., non-beam-like) deformations, as discussed in the following Section. It should be mentioned that the effect of the local deformations exists in addition to the length effect included in the beam element solutions (when the beam is long enough for localized deformations to be negligible, the shell element solution follows the trend observed in the other solutions).

3.7 On the effect of localized deformations

The effect of beam length in the beam and analytical results is well explained by the analytical derivations. The further length-dependency in the shell FEM results is due to the localized (i.e., non-beam-like) deformations which are naturally allowed in shell FEM but excluded from beam FEM and analytical derivations. To demonstrate this in a simple and straightforward way, the so-called *local deformation index* (I_{LD}) has been introduced here, which is interpreted for a cross-section, i.e., can be calculated for any position along the beam, as:

$$I_{LD} = \frac{\varphi_{max} - \varphi_{avg}}{\varphi_{avg,max}} \tag{82}$$

where φ_{max} is the maximum twisting rotation in the cross-section, and φ_{avg} is the average twisting rotation of the cross-section, while $\varphi_{avg,max}$ is the maximum of the average rotations along all cross sections in the beam. Practically, these rotations can be obtained from the shell FEM results as nodal rotations around the longitudinal axis. After calculating the local deformation index for many cross-sections, the highest value can be used (i.e., $I_{LD,max}$) to characterize the magnitude of localized deformations of the whole beam by a single number. In most cases, the maximum value occurs at mid-length where the deformations are the largest. Table 3.9 shows the maximum local deformation index for beams with various lengths.

Table 3.9: I_{LD} across the length for both DSI and RHS cross sections

Length (m)	I_{LD} across the length (%)			
	DSI		RHS	
	PrPw-PrPw	FrFw-FrFw	PrPw-PrPw	FrFw-FrFw
4	7.25	10.09	87.54	112.73
6	3.1	4.33	38.32	50.04
8	1.85	2.15	21.25	12.53
10	1.09	1.22	13.37	8.66
15	0.72	0.68	5.89	4.08
20	0.44	0.38	2.73	2.28
30	0	0	1.19	0.86
50	0	0	0	0.2

The table clearly shows that longer beams experience lower local deformations, making the solution approach the beam element solution, even if it is not possible to completely

eliminate the localized deformations from the shell element solutions, as shown in Fig. 3.12. Moreover, it can also be seen that the end fixity FrFw-FrFw results in higher levels of local deformations, which is also confirmed by the higher difference with the shell element and the beam element solutions experienced. Finally, it is evident that the RHS section has significantly higher local deformations when compared to the DSI section.

The general conclusion is that when restrictions are introduced to the movement of the beam (due to high torsional rigidity or rotational fixities), the beam is less susceptible to have pure LTB, and higher localized deformations are experienced as a result. The cross-section deformations can further be analyzed, e.g., how they are distributed over the cross-section or along the length. For example, it can be observed that in most cases, the web shows more localized deformations compared to the flanges, etc. Since, in this research classic lateral-torsional buckling is discussed, where non-beam-like deformations are negligibly small, the detailed investigation of the localized deformations is beyond the scope. Nevertheless, it is important to observe that such deformations can be experienced with shell FEM calculations, and they have noticeable influence on the buckling results.

3.8 Summary

In this chapter, the investigations of the effect of prebuckling deflections on lateral-torsional buckling of single-span beams from the previous chapter have been extended for other support conditions. Furthermore, numerical studies were also reported in addition to the analytical derivations. Several observations have been made.

Regarding the methods, the following conclusions can be drawn.

(i) Analytical solutions for various classic end supports can be obtained in closed format by properly selecting the shape functions that satisfy the conditions of these supports, for both open and closed sections. It was found that using only one trigonometric term in the shape functions for the simple (i.e., fork) supports case can lead to reasonable results. However, more trigonometric terms are needed for other boundary conditions.

(ii) Two numerical approaches were proposed and applied to calculate the critical moment of beams with considering prebuckling deflections. It was concluded that both the proposed iterative linear buckling analysis and the geometrically nonlinear analysis with (very) small imperfections lead to practically identical critical moments.

(iii) When numerical methods are used for the analysis of beams with prebuckling deflections, the loads and supports have to be carefully defined, considering that the deflections can occasionally be moderately large.

(iv) The results from beam and shell finite element models are similar, but there are always differences between them due to the localized (i.e., non-beam-like) deformations in shell models. It is fair to say, therefore, that beam elements are beneficial but might be problematic to use them for complicated problems; on the other hand, shell models can readily be applied to most thin-walled beam problems, but the results are influenced by the localized deformations.

Regarding the effect of prebuckling deflections, the most important conclusions are as follows.

(i) The effect of prebuckling deflection is small (and practically negligible) if the ratio of the lateral and primary flexural stiffness of the beam is small (i.e., the minor-axis moment of inertia of the cross-section is small compared to major-axis moment of inertia). However, in the cases of larger stiffness ratios, the prebuckling effect is non-negligible. Thus, the prebuckling deflection is confirmed to have an important contribution to the differences between the critical moments predicted by classic analytical formulae and by nonlinear finite element analyses.

(ii) The derived formulae clearly show that end supports have important effect. The suggestion of multiple previous papers that the prebuckling effect is always positive and the critical moment increase can be approximated by the $1/\sqrt{1-I_y/I_x}$ ratio can be confirmed only in the case of simply supported beams with small torsional rigidity (e.g., open thin-walled sections). In other end support cases the prebuckling effect is different and can even be negative. Moreover, the prebuckling effect is modified if the torsional rigidity is significant (e.g. closed thin-walled sections).

(iii) When prebuckling deformations are considered, the solution becomes length-dependent for some support conditions, with longer beams experiencing a reduced effect of prebuckling deformations, an effect that doesn't exist in classic solutions.

Thes results of this chapter reveal an important effect of the end supports regarding the effect of prebuckling deformations. However, it is a common practice to also introduce intermediate lateral supports, which is the focus of the next chapter. Since the beam FEM element was shown to predict the results efficiently faster than the shell element, it will be

mostly used, with some shell element results for confirmation purposes. Furthermore, although the DSI and RHS results are different, the trends are similar, which is why further investigations are limited to DSI sections. Finally, since the proposed iterative LBA method produced almost identical results to the GNIA, it is used for critical moment predictions, while the use of GNIA is limited to shape analysis (prebuckling behavior rather than the final result).

Chapter 4: Effect of Intermediate Supports

4.1 Overview

In this chapter, beams with intermediate lateral supports are investigated. It is to emphasize that the term 'intermediate lateral support' is used throughout this chapter in a broad sense, meaning any support along the beam length that acts against the development of the secondary displacements. Accordingly, lateral support can be a restraint against lateral translation or twisting rotation. Both types are considered in this research.

Intermediate lateral supports are well-documented for their ability to enhance lateral-torsional buckling (LTB) capacity or even prevent its occurrence. The influence of lateral supports has been extensively studied in the literature, with numerous papers exploring different aspects of the topic. Some studies focus on elastic behavior, while others investigate the ultimate response. Research varies in its consideration of continuous versus discrete supports, as well as rigid versus elastic support conditions. Additionally, various cross-sectional shapes have been examined, with beams modeled as prismatic, stepped, or tapered. A range of analytical, numerical, and experimental approaches have been employed. In particular, studies addressing the elastic behavior of beams with discrete lateral supports and doubly symmetric I-sections [88–101] have explored numerous aspects of this problem.

Examples are as follows: torsional or lateral (i.e. translational) support [88-90], the position of the support within the cross-section (e.g., top, bottom, centroid) [91-94], position or number of the support along the beam length, number of supports along the beam length [65,95], the effect of various simple and combined loading [96], how the stiffness of the support affects LTB if the support is elastic or what are the support requirements to avoid LTB [97-100], how the choice of the beam finite element affects the M_{cr} results in FEM solutions [101]. The provided list is not comprehensive, and, obviously, in many publications more than one aspect is discussed.

Upon reviewing the literature, it was found that beams with intermediate lateral supports have not been discussed at all with considering the effect of prebuckling deflections. In this chapter, therefore, the *combined effect* of the intermediate lateral supports and the prebuckling deflections is studied. The behavior considering the combined effect can be significantly different from the behavior when only one of them (i.e., either the prebuckling or the lateral support effect) is considered.

Section 4.2 presents the scope of the study. Section 4.3 presents the FEM models used, and section 4.4 presents the results of the numerical analysis, the results show complex behavior which is sometimes hard to interpret. To gain better understanding, analytical derivations have been performed, summarized in Section 4.5. All numerical and analytical results indicate that the structural behavior is primarily governed by the deformation shapes that develop during buckling (with and/or without considering the prebuckling deflections), therefore, in Section 4.6 the shapes are discussed along with comments on the effects of initial shape and values of initial imperfections. Section 4.6 discusses the practical efficiency of the intermediate supports.

4.2 Scope

This research focuses on thin-walled beams with intermediate lateral supports. The considered beam is similar to what was discussed in previous chapters (doubly symmetric, with a uniform moment distribution along its length, see Fig. 3.1). The middle cross-section of the beam is laterally supported, in one of the configurations as follows: Top flange Laterally Supported (TLS), Centroid Laterally Supported (CLS), Bottom flange Laterally Supported (BLS), and All the cross-section Laterally Supported (ALS).

Fig. 3.1 illustrates these cases. As a reference, the No Lateral Supports (NLS) case is considered, too. It is to emphasize that ‘lateral support’ means that the lateral translation is prevented at one (or multiple) cross-sections points, see Fig. 3.1. As a result, in the case of CLS the twisting rotation can freely occur; in the case of TLS and BLS the twisting rotation of the middle cross-section is not prevented but is linked to the lateral translations; while in the case of ALS the twisting rotation of the middle cross-section is fully prevented. In addition to the intermediate support, the end support conditions' effect has been studied, in a similar way as discussed in previous chapters. The considered beams were similar to those from previous chapters.

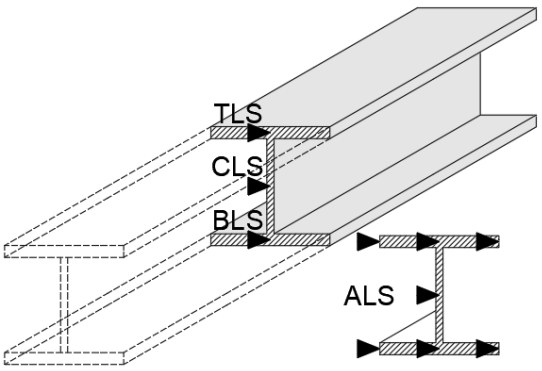

Figure 4.1: Intermediate lateral support types.

Beams with various lengths have also been considered, with the beam length L having a wide range between 2.5m and 50m. This length range covers the entire practical lengths for the given cross-section shape and dimensions, with some extreme cases produced for better understanding the behavior. Finally, for the material, a classic isotropic steel has been considered, with a Young's modulus equal to 210000 MPa, and Poisson's ratio equal to 0.3, which is similar to what was considered in previous chapters.

4.3 FEM models

For the Finite Element Method, similarly to previous chapters, the commercial FEM software Ansys APDL has been used, with primarily beam elements, but shell elements have been employed too for validation purposes. Similar end support conditions as in Chapter 3 were introduced. As for the intermediate support, only the CLS can be directly applied to an FE node in the beam element model. To apply the other intermediate supports, a cantilever, either at the bottom (BLS) or the top (TLS) of the beam, or both (ALS), has been created with a length equal to half the depth of the beam, and the lateral support being at the end node of the cantilever (Fig. 4.2).

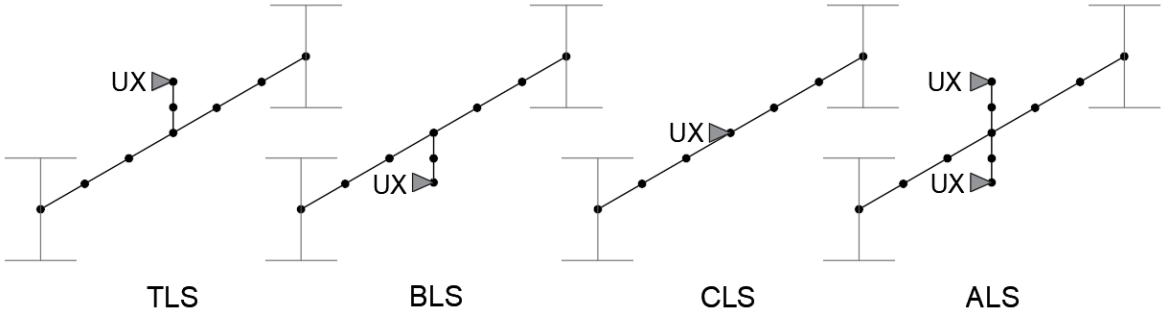

Figure 4.2: Intermediate lateral supports in the beam element model.

The shell FEM element used in this chapter is also the SHELL181 element available in ANSYS. The discretization, load application, as well as supports has been done in a similar manner as done previously. Regarding the intermediate lateral supports, they can directly be applied as nodal restraints against lateral translation.

4.4 Iterative LBA Results

4.4.1 The effect of intermediate lateral supports

The critical moment values with and without considering the effect of prebuckling deflection (M_{cr} and M_{cr0}, respectively) have been calculated for various cases. Here, the results calculated for 30-m-long beams with PrPw-PrPw end supports are presented in Fig. 4.3, where

the critical moment increase values are plotted in terms of the I_y/I_x ratios. The *reference moment increase*, is similar to what was proposed earlier (see eq. 81).

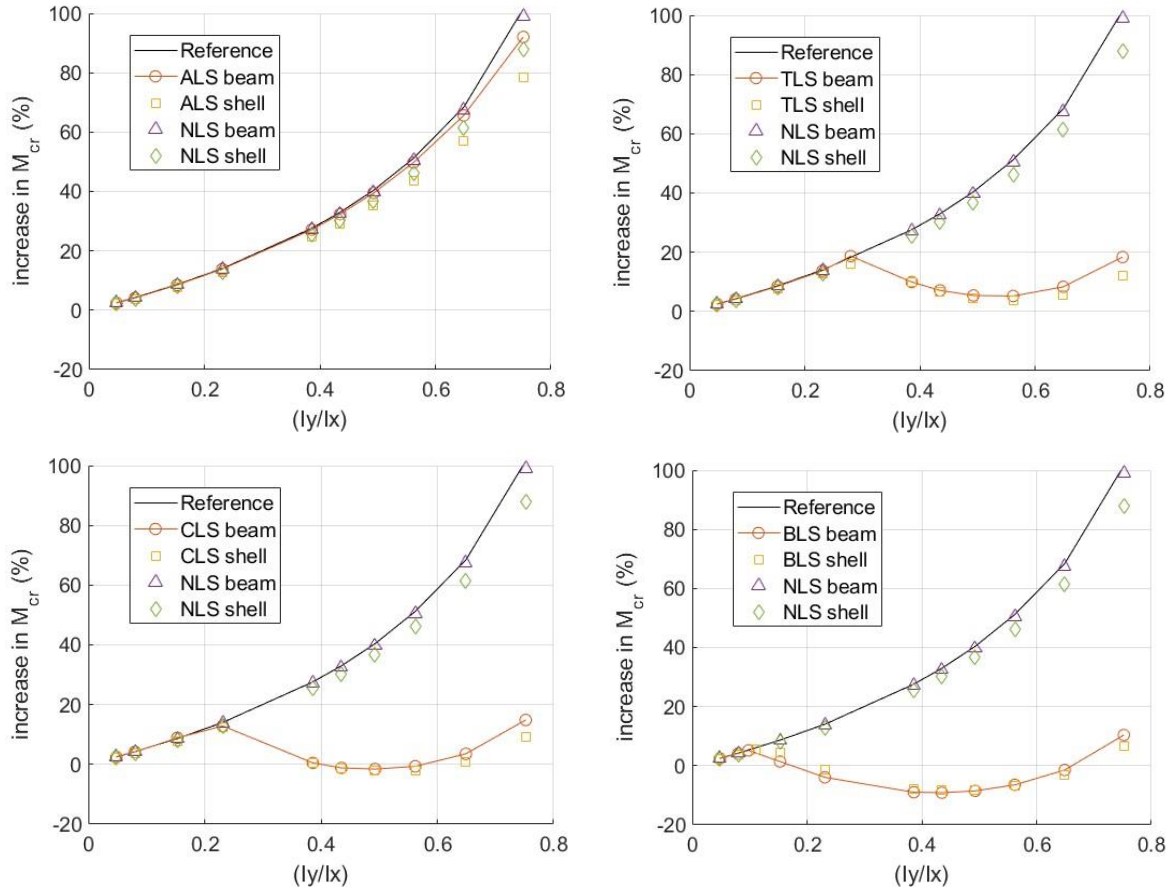

Figure 4.3: Critical moment increase due to prebuckling effect, with various intermediatelateral supports.

It can be observed that in the case of ALS type intermediate support, the moment increase curve closely follows the reference increase curve and/or the curve that belongs to a beam without any intermediate support. This means that ALS support has marginal effect on the moment increase (though, obviously, it has an important effect on the critical moment values).

For TLS, CLS, and BLS, the effect of lateral support on the moment capacity is minimal when the I_y/I_x ratio is small (i.e., for deep cross-sections). However, as the I_y/I_x ratio increases, intermediate lateral support plays a significant role in altering how prebuckling deflection influences the critical moment. In this context, a "small" I_y/I_x ratio is approximately 0.25 for the investigated cross-sections in the cases of TLS and CLS, while for BLS, it is considerably lower, around 0.1

Nevertheless, the large moment increase that can be observed in beams with simple end supports and no intermediate lateral support is significantly reduced by the presence of a lateral support, regardless the vertical position of it (with the exception of the ALS case). It can also be concluded that beam FEM and shell FEM results are similar, though not identical. The differences are primarily due to the non-beam-like deformations in the shell model, as discussed in Chapter 3. Since LTB is a global buckling phenomenon, i.e., without localized deformations, and since beam FEM is more efficient, no shell FEM results are shown in the subsequent sections.

4.4.2 Beams with intermediate lateral supports and various lengths

Earlier studies in the literature suggested that the effect of beam length on lateral-torsional buckling was negligible. However, Chapter 3 demonstrated that: (i) the beam length has a negligible effect only when the ends are simply supported and specific simplifying assumptions are applied in the analytical derivations; (ii) the effect remains small when the ends are simply supported; and (iii) a more significant influence of beam length is observed when the ends are partially or fully clamped. The results presented here further indicate that beam length has a pronounced effect when the beam is laterally supported by discrete supports, as illustrated in Figs. 4.4–4.5.

It is to mention that these results are for the PrPw-PrPw end supports case. In the case of TLS and CLS, the plotted curves usually have two parts, suggesting that there is a change of behavior at a certain I_y/I_x value. This I_y/I_x value strongly depends on the beam length. Furthermore, even if the curves for TLS and CLS cases are similar in shape, their tendencies are different: in the case of TLS, the longer the beam, the smaller the moment increase; in the case of CLS the trend is opposite: the longer the beam, the larger the moment increase.

Regarding BLS type lateral support, the right parts of the curves are visually like those of TLS or CLS, however, the length effect is different: the smallest moment increase values belong to medium length beams, while in the case of extraordinarily long or short beams the moment increase is larger. Moreover, in the left parts of the BLS curves it is hard to identify tendencies. Regarding the difference between M_{cr} and M_{cr0}, the location of the lateral support is crucial. In the case of TLS M_{cr} is always larger than M_{cr0}, hence the prebuckling deflection positively influences the critical moment. On the other hand, in the case of CLS and BLS, M_{cr}

can be smaller or larger than M_{cr0}, depending on beam length and the I_y/I_x ratio. Occasionally, the moment decrease can be significant up to 20-25% when the I_y/I_x ratio is around 0.4.

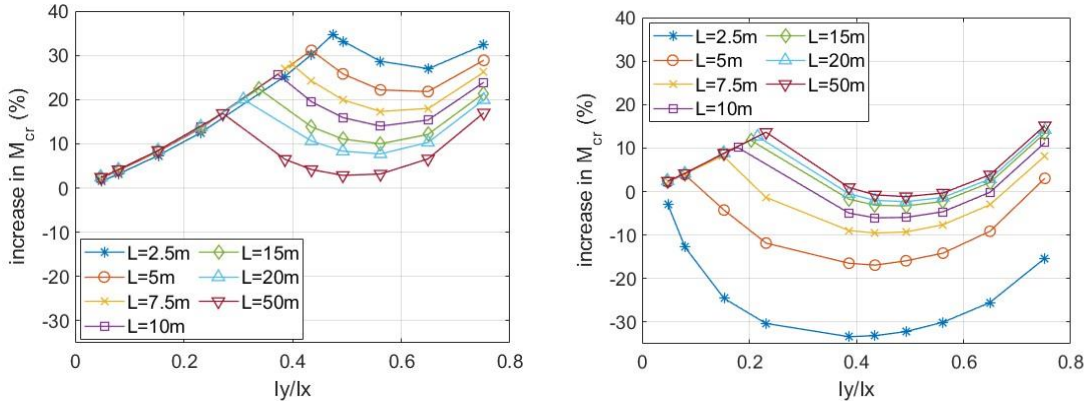

Figure 4.4: The effect of beam length on the moment increase: TLS (left) and CLS (right).

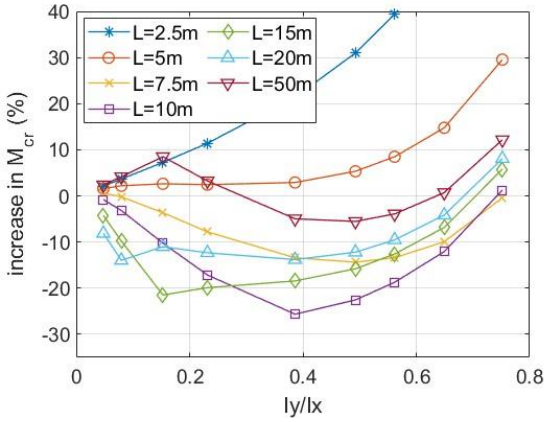

Figure 4.5: The effect of beam length on the moment increase: BLS support.

These experiences can better be explained by the buckling shapes, as will be discussed in detail in later sections.

4.4.3 The combined effects of intermediate supports and end supports

Since in Chapter 3, the importance of end supports has been revealed, the cases of intermediate lateral supports were considered for various end supports. The considered end support cases are similar to those from Chapter 3 (PrPw-PrPw, FrFw-FrFw, PrFw-PrFw, FrPw-FrPw, and PrPw-FrFw). Regarding the intermediate lateral supports, ALS, TLS, CLS, and BLS were considered. The calculations were completed by beam FEM, and the results for the 30-m-long beams are presented here, in Figs. 4.6-4.7. The main observations are as follows.

In the case of ALS, the warping fixity has marginal influence, while the rotation fixity (about the minor axis) reduces the moment increase. If the rotation is restrained at one end only, the results are in between the Pr-Pr and Fr-Fr cases. In general, the results show the same trends as those obtained for beams without intermediate lateral support. In the case of TLS/CLS/BLS, the trends from both cases of end supports and intermediate lateral supports can be observed. Regarding the end supports: the warping fixity has little effect while the rotational fixity reduces the 'increase' due to prebuckling deformations. Regarding the intermediate lateral supports, the curve has two parts as discussed earlier, with the same trends and discrepancies between these cases.

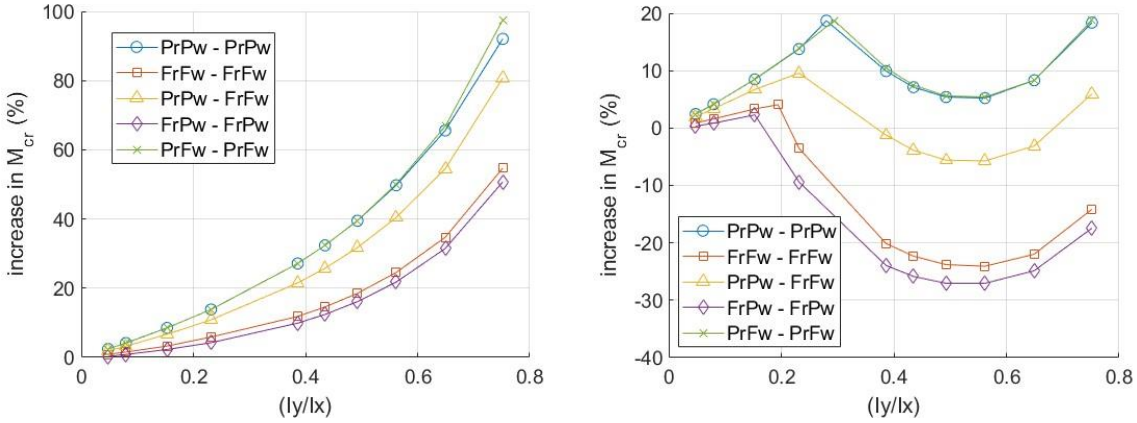

Figure 4.6: The effect of end supports: ALS (left) and TLS (right).

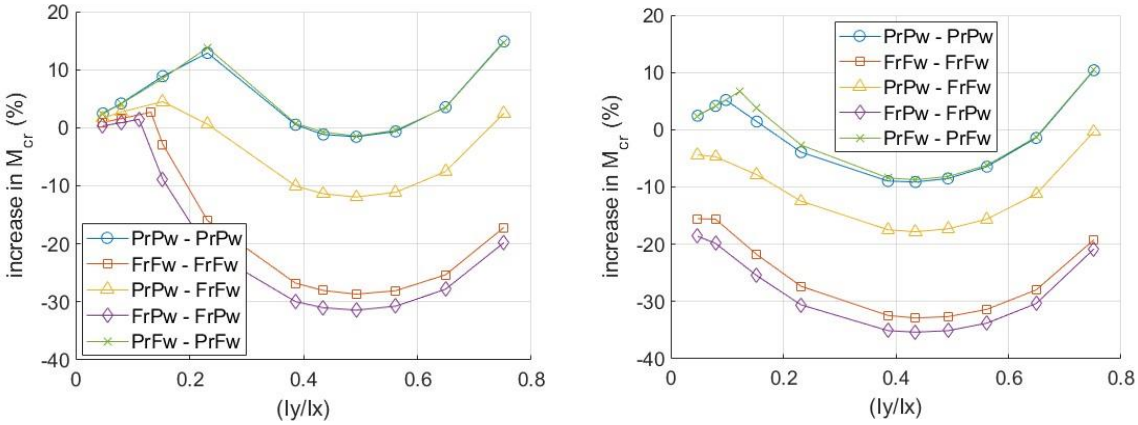

Figure 4.7: The effect of end supports: CLS (left) and BLS (right).

Furthermore, for each intermediate lateral support case, the cross section of which the 'switch' into the other part of the curve occurs is affected by the end support, with rotational supports generally causing the switch to occur at cross sections with lower I_y/I_x ratios. Since, in general, both the end fixity and the intermediate lateral support decreases M_{cr}, their

combined effect can cause it to be significantly smaller than M_{cr0}, the maximum decrease being 25-35%, depending on the lateral support position for the considered cases. (It is to note that for other beam lengths even larger moment degradation can be found.)

4.5 Analytical studies

4.5.1 Overview

To have better understanding of the experienced behavior, and to validate the obtained results, in this Section, analytical studies are presented: closed-form expressions for the critical moments with and without considering prebuckling deflections are derived and discussed. The analytical derivations closely follow those presented in Chapter 2. The key features can be summarized as follows.

The energy method is employed: the displacements are assumed, the potential energy function is established, and the minimum of the potential is searched for. During the derivations, approximations and simplifications are introduced, similarly as in Chapter 2. Furthermore, since the obtained formulae are usually complex, and since it is not the primary aim to provide formulae for all the relevant cases, the analytical solutions are derived for the PrPw-PrPw end supports only. To cover the intermediate lateral support cases considered, five candidates for the displacements are defined, as follows.

$$u^{(a)} = u_m sin\frac{2\pi z}{L}$$
$$\varphi^{(a)} = \varphi_m sin\frac{2\pi z}{L} \tag{83}$$

$$u^{(b)} = u_m\left(sin\frac{\pi z}{L} + sin\frac{3\pi z}{L}\right)$$
$$\varphi^{(b)} = \varphi_m\left(sin\frac{\pi z}{L} + sin\frac{3\pi z}{L}\right) \tag{84}$$

$$u^{(c)} = u_m\left(sin\frac{\pi z}{L} + \left(1 + \frac{\varphi_m}{u_m}\frac{h}{2}\right)sin\frac{3\pi z}{L}\right)$$
$$\varphi^{(c)} = \varphi_m\left(sin\frac{\pi z}{L}\right) \tag{85}$$

$$u^{(d)} = u_m\left(sin\frac{\pi z}{L} + sin\frac{3\pi z}{L}\right) \tag{86}$$

$$\varphi^{(d)} = \varphi_m \left(sin \frac{\pi z}{L} \right)$$

$$u^{(e)} = u_m \left(sin \frac{\pi z}{L} + \left(1 - \frac{\varphi_m}{u_m} \frac{h}{2} \right) sin \frac{3\pi z}{L} \right) \tag{87}$$

$$\varphi^{(e)} = \varphi_m \left(sin \frac{\pi z}{L} \right)$$

where u_m and φ_m are the displacement amplitudes.

It is to observe that (a) is point-symmetric (having two half-waves longitudinally for both u and φ), while the others are symmetric (having one or three half-waves longitudinally). Moreover, in the case of (a) and (b) both u and φ are zero at the middle of the beam; on the other hand, in the case of (c), (d) and (e) shapes u is zero only at a certain cross-section point while φ is non-zero at the middle of the beam. Depending on the position of lateral supports, some of the above shapes are kinematically possible, some not. This is summarized in Table 4.1, where 'Y' identifies the possible and 'N' identifies the not possible shapes, respectively.

Table 4.1: Assignment of support and shape functions.

	(a)	(b)	(c)	(d)	(e)
all	Y	Y	N	N	N
top	Y	Y	Y	N	N
centroid	Y	Y	N	Y	N
bottom	Y	Y	N	N	Y

To each assumed shape critical moments formulae with and without considering the prebuckling deflection can be derived, as summarized in the next Section. The analytical prediction for the lowest critical moment is the minimum among those that belong to the kinematically admissible shapes. For example, if the top flange is supported (TLS), (a), (b) and (c) shapes are possible, hence, the lowest (i.e., first mode) critical moments are obtained as:

$$M_{cr0}^{TLS} = \min\left(M_{cr0}^{(a)}, M_{cr0}^{(b)}, M_{cr0}^{(c)} \right)$$

$$M_{cr}^{TLS} = \min\left(M_{cr}^{(a)}, M_{cr}^{(b)}, M_{cr}^{(c)} \right) \tag{88}$$

The other support cases can be handled similarly.

4.5.2 Critical moment formulae

It is assumed here that the cross-section is doubly symmetric and open. To obtain simpler formulae for the critical moment, it is reasonable to introduce the following assumptions, similarly as in Chapter 2:

$$\frac{EI_w/L^2}{EI_x} \cong 0 \quad \frac{GJ}{EI_x} \cong 0 \tag{89}$$

To make the critical moment formulae more compact, the following symbols are introduced:

$$F_y = \frac{\pi^2 EI_y}{L^2} \quad F_w = \frac{\pi^2 EI_w}{L^2} \quad F_t = GJ \tag{90}$$

while the ratio of the lateral and vertical bending stiffness is:

$$r_{yx} = \frac{EI_y}{EI_x} \tag{91}$$

The critical moment formulae without the prebuckling deflection are listed as follows:

$$M_{cr0}^{(a)} = \frac{\pi}{0.5L}\sqrt{EI_y\left(GJ + \frac{\pi^2 EI_w}{(0.5L)^2}\right)} \tag{92}$$

$$M_{cr0}^{(a)} = \sqrt{4F_y}\sqrt{F_t + 4F_w}$$

$$M_{cr0}^{(b)} = \frac{\pi}{\sqrt{5/41}\,L}\sqrt{EI_y\left(GJ + \frac{\pi^2 EI_w}{\left(\sqrt{5/41}\,L\right)^2}\right)} \tag{93}$$

$$M_{cr0}^{(b)} = \sqrt{\frac{41F_y}{5}}\sqrt{F_t + \frac{41F_w}{5}}$$

$$M_{cr0}^{(c)} = 81\frac{h}{2}F_y + \sqrt{82F_y}\sqrt{F_t + F_w + 81\left(\frac{h}{2}\right)^2 F_y} \tag{94}$$

$$M_{cr0}^{(d)} = \sqrt{82F_y}\sqrt{F_t + F_w} \tag{95}$$

$$M_{cr0}^{(e)} = -81\frac{h}{2}F_y + \sqrt{82F_y}\sqrt{F_t + F_w + 81\left(\frac{h}{2}\right)^2 F_y} \tag{96}$$

Some of the M_{cr0} formulae can be interpreted by the equivalent length concept. In case (a), the equivalent length factors both for the lateral translation and twisting rotation are $\sqrt{1/4} = 0.5$, in perfect agreement with the engineering expectation. In case (b) the equivalent length factors are $\sqrt{5/41} = 0.3492$, i.e., the equivalent buckling length is approx. one-third of the beam length. In case (d), the buckling length for the twist is equal to the length, while the buckling length factor for the lateral translation is $\sqrt{1/82} = 0.1104$. In cases (c) and (e) the equivalent lengths cannot readily be determined.

The critical moment formulae with the prebuckling deflection are listed as follows:

$$M_{cr}^{(a)} = M_{cr0}^{(a)} / \sqrt{(1 - r_{yx})} \tag{97}$$

$$M_{cr}^{(b)} = M_{cr0}^{(b)} \Big/ \sqrt{(1 - r_{yx})\left(1 + \frac{16}{25}r_{yx}\right)} \tag{98}$$

$$M_{cr}^{(c)} = \frac{81\frac{h}{2}F_y(1 - r_{yx}) + \sqrt{82F_y(1 - r_{yx})}\sqrt{(F_t + F_w)(1 + 81r_{yx}) + 81\left(\frac{h}{2}\right)^2 F_y}}{(1 - r_{yx})(1 + 81r_{yx})} \tag{99}$$

$$M_{cr}^{(d)} = M_{cr0}^{(d)} / \sqrt{(1 - r_{yx})(1 + 81r_{yx})} \tag{100}$$

$$M_{cr}^{(e)} = \frac{-81\frac{h}{2}F_y(1 - r_{yx}) + \sqrt{82F_y(1 - r_{yx})}\sqrt{(F_t + F_w)(1 + 81r_{yx}) + 81\left(\frac{h}{2}\right)^2 F_y}}{(1 - r_{yx})(1 + 81r_{yx})} \tag{101}$$

It can be observed that in case (a) the moment increase is identical to the reference increase (eq. 81). Moreover, in cases (a), (b) and (d) the critical moment increase can be expressed by simple formulae, however, in cases (c) and (e) the moment increase cannot be easily understood from the formulae.

The analytical formulae suggest that in the case of TLS and BLS the critical moment and, thus, the critical moment increase is dependent on the h section depth, too. Therefore, even

if the I_y/I_x ratios for two otherwise identical beams would be the same, the critical moment (and moment increase) is dependent on h. However, it is easy to understand that it is not the section depth that really matters, but the position of the lateral support. Since in the case of TLS and BLS this position is plus or minus h/2, that is why h is directly included in the moment formulae.

4.5.3 Numerical results

To make the obtained results more understandable, and to compare the analytical and FEM solutions, sample numerical results are summarized in Table 4.2. The results are provided for two beam lengths: a short one (i.e., 5000 mm) and a long one (30000 mm). These two lengths are selected to cover the cases when the length is short vs too long. Four I_y/I_x ratio values are selected, including exceedingly small and large ones.

In the upper part of the table, critical moment values are given to each considered shape, from (a) to (e). It is not surprising that the critical moments are strongly dependent on the assumed buckled shape. In the lower part of the table the governing (i.e., lowest) critical values are given, also indicating the shape to which they belong. From the lowest M_{cr0} and M_{cr} values the moment increases are calculated, and compared to the moment increases from beam FEM solutions.

In general, the analytical results agree well with the beam model results. Considerable difference can be observed only if the moment increase is exceptionally large, i.e., close to 100%, otherwise, the FEM-calculated and analytically calculated moment increase percentages differ by no more than 1-2%, but mostly less than 1%. Regarding the shapes in the case of ALS, shape (a) leads to the lowest critical moment values, both without and with considering the prebuckling deflection, and regardless of the member length. Shape (b) is never governing. Moreover, in many cases the buckled shapes without and with prebuckling deflection are different, i.e., there is mode switch.

The results show that sometimes the classic LTB shape is point-symmetric, which switches to a symmetric one, see e.g., the CLS type; however, in other cases the classic LTB shape is symmetric, but can be switched to point-symmetric, see e.g., BLS type. Since the nature of the buckled shapes, and especially the mode switch seems to have crucial role in the value of moment increase, these are further discussed in Section 4.6.

Table 4.2: Analytical results

L	mm	5000	5000	5000	5000	30000	30000	30000	30000
h	mm	500	300	200	150	500	300	200	150
I_y/I_x		0.05	0.15	0.39	0.75	0.05	0.15	0.39	0.75
$M_{cr0}^{(a)}$	kNm	2340	1554	1213	1071	175	161	155	152
$M_{cr0}^{(b)}$	kNm	4573	2870	2092	1749	265	236	224	218
$M_{cr0}^{(c)}$	kNm	90510	54440	36515	27626	2712	1785	1354	1153
$M_{cr0}^{(d)}$	kNm	6562	5101	4526	4296	757	715	694	683
$M_{cr0}^{(e)}$	kNm	750	642	670	749	218	290	358	407
$M_{cr}^{(a)}$	kNm	2398	1688	1548	2159	179	175	197	305
$M_{cr}^{(b)}$	kNm	4616	2976	2390	2896	267	244	255	361
$M_{cr}^{(c)}$	kNm	19165	4678	1798	1400	695	277	173	181
$M_{cr}^{(d)}$	kNm	3045	1515	1017	1099	351	212	156	175
$M_{cr}^{(e)}$	kNm	763	659	687	967	184	165	142	169
M_{cr0}^{ALS}	kNm	2340 a	1554 a	1213 a	1071 a	175 a	161 a	155 a	152 a
M_{cr}^{ALS}	kNm	2398 a	1688 a	1548 a	2159 a	179 a	175 a	197 a	305 a
increase	%	2.48	8.65	27.61	101.5	2.48	8.65	27.61	101.5
inr, FEM	%	2.21	8.23	26.69	95.67	2.43	8.51	27.14	92.06
M_{cr0}^{TLS}	kNm	2340 a	1554 a	1213 a	1071 a	175 a	161 a	155 a	152 a
M_{cr}^{TLS}	kNm	2398 a	1688 a	1548 a	1400 c	179 a	175 a	173 c	181 c
increase	%	2.48	8.65	27.61	30.72	2.48	8.65	11.75	19.60
inr, FEM	%	2.21	8.23	26.62	28.78	2.44	8.48	9.93	18.36
M_{cr0}^{CLS}	kNm	2340 a	1554 a	1213 a	1071 a	175 a	161 a	155 a	152 a
$M_{cr}^{CLS}0$	kNm	2398 a	1515 d	1017 d	1099 d	179 a	175 a	156 d	175 d
increase	%	2.48	-2.51	-16.18	2.62	2.48	8.65	0.95	15.35
inr, FEM	%	2.21	-4.25	-16.48	2.14	2.46	8.87	0.52	14.87
M_{cr0}^{BLS}	kNm	750 e	642 e	670 e	749 e	175 a	161 a	155 a	152 a
M_{cr}^{BLS}	kNm	763 e	659 e	687 e	967 e	179 a	165 e	142 e	169 e
increase	%	1.69	2.63	2.53	29.14	2.48	2.76	-8.23	11.66
inr, FEM	%	1.6	2.63	2.91	29.55	2.44	1.42	-8.96	10.39

4.6 Shape analysis

4.6.1 Mode switch - LBA

To better understand the mode switch, the results are first analyzed in detail, focusing on when the mode switch occurs and how the buckled shapes differ depending on whether the

switch happens or not. The results are visualized in Fig. 4.8, where PP means that the buckling mode is point-symmetric both without and with the prebuckling effect. Similarly, SS means that the buckling mode is symmetric both without and with the prebuckling effect. PS identifies those cases when the mode is point-symmetric without the prebuckling deflections, but symmetric if the prebuckling deflection is considered; i.e., PS identifies the cases when mode switch happens. (Theoretically, SP could happen, too, but such a case has not been found among the investigated ones. Moreover, since the mode switch does not occur in the case of ALS, this intermediate support type is not discussed.)

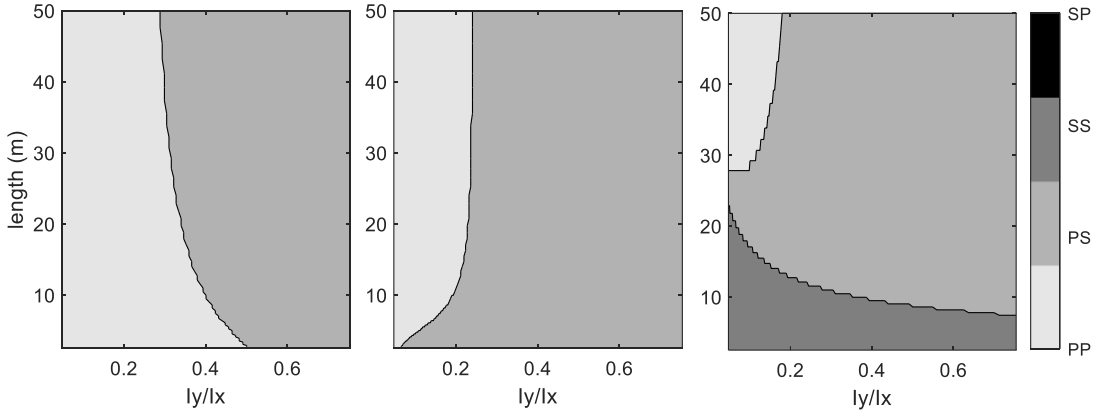

Figure 4.8: Overview of buckling shapes (left: TLS, middle: CLS, and right: BLS).

Looking at Fig. 4.8, it can be observed that the parts of the moment increase curves in Figs. 4.4-4.5 can be assigned to characteristic buckling shape scenarios. For example, in the cases of TLS and CLS, the left parts of the curves belong to PP, while the right (quasi-parabolic) parts of the curves belong to PS. The I_y/I_x threshold where the two lines join, i.e., where the behavior changes from PP to PS, is dependent on the length: the larger the length in the case of TLS, or the shorter the length in the case of CLS, the smaller the I_y/I_x threshold value, which is in accordance with the results obtained in section 4.4.2.

The most complex case however is BLS (which was also observed in section 4.4.2). If the beam is (at least, moderately) long and the I_y/I_x is (moderately) large, then the behavior is PS, characterized by the quasi-parabolic curve parts in the moment increase curves. When the beam is extremely long and I_y/I_x is small, the behavior is PP, characterized by the quasi-linear increasing line. (It seems that for beams that are too long, longer that 25m for the considered cross sections, the behavior of the BLS intermediate support becomes similar to that of the CLS case.) For shorter beams, the behavior is SS, i.e., the buckling mode is symmetric either the

prebuckling deflection is considered or not for low I_y/I_x ratios (if the beam is too short, all cross sections have the SS behavior). In these SS cases, the tangent of the line segment (of the moment increase curve) is proportional to the inverse of the beam length: the larger the length, the smaller the tangent. In most of the lengths the tangent is negative, but it becomes positive if the beam is short enough.

The above explanation is further illustrated and justified by Figs. 4.9-4.10., for TLS, CLS, and BLS, respectively. The composition of selected moment increase curves is shown, obtained by considering higher buckling modes from the buckling analyses. It can be observed that the PP curves are approximately identical to the reference moment increase curve, that is (i) they are negligibly dependent on the length, and (ii) they are independent of the vertical position of the lateral support. The PS and SS curves are dependent on the length and the position of the lateral support.

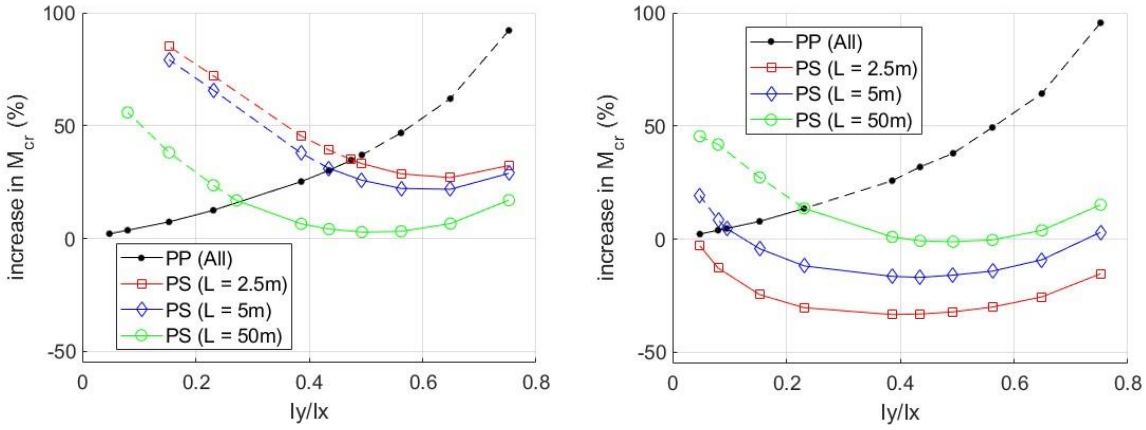

Figure 4.9: Moment increase curves for the various buckling shape scenarios: TLS (left) and CLS (right).

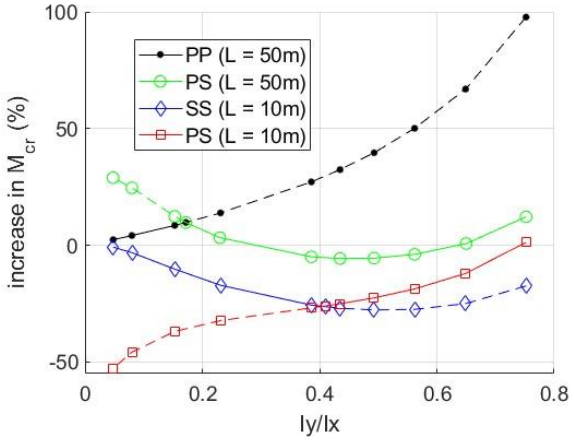

Figure 4.10: Moment increase curves for the various buckling shape scenarios: BLS.

Moreover, the threshold values of the I_y/I_x ratio can be found as the intersection of the curves that belong to the various scenarios. However, the final moment increase curve is not necessarily the lower envelop of the curves, since the final curve is determined by the lowest M_{cr0} and M_{cr} values, not by the lowest moment increase values (see e.g., the BLS, L = 10 m case). Therefore, from the results it can be concluded that the moment increase due to the prebuckling deflections is strongly determined by the buckled shapes, which are dependent on the beam length and the vertical position of the lateral support.

4.6.2 Mode switch - GNIA

In this Section, GNIA results are presented. The calculations are performed by FEM, using the same models as used in the LBA. The initial imperfect shape of the beam is identical to an eigen-shape from a classic LBA (without prebuckling deformation). In most cases the first eigen-mode is employed, though the effect of considering higher eigen-modes is also studied (see Section 4.6.3). Unlike when GNIA is applied in design, here, GNIA is applied to approximate the elastic critical moment, hence, the role of the initial imperfection is to disturb the perfect straight shape in order to allow the FEM to find the secondary equilibrium path. Accordingly, in most of the presented cases the initial imperfection is extremely small, the amplitude being 0.001 mm, though the effect of applying larger imperfection amplitudes is also studied (see Section 4.6.4).

It is to mention that the GNIA can predict the critical moment, as discussed in Chapter 3. However, since the M_{cr} values calculated by the iterative LBA or by GNIA are practically identical, it is used here for the purpose of the shape analysis only, by showing how the initial shape is transformed into the final buckling shape (although some M_{cr} results are presented, they are just for understanding and explaining the behavior) . This transformation is illustrated by Figs. 4.11-4.16. In all these figures lateral translations of the cross-section centroids (UX) and twisting rotation of the cross-sections (ROTZ) are plotted along the member length, at selected load levels, with 'M_{cro}' identifying the initial shape calculated from classic LBA.

It is to highlight that all the shape curves are scaled to have the maximum (in absolute value) equal to 1; without this scaling the shapes of early sub-steps would mostly be invisible due to the differences in the values of deflections at different load levels, as can be seen in Fig. 4.11. It is to note that, obviously, the presented secondary displacements occur together with the primary displacements, which are practically linearly proportional to the load intensity, and not shown in these plots.)

Figs. 4.11-4.13 show three cases of PS behavior. All are calculated for the same length and cross-section, however, the position of the lateral support varies. In all these three cases the initial shapes are the same, however, the final shapes are different. More precisely, the final ROTZ shapes are still similar, all being (approximately) a half sine wave. The UX in TLS and BLS is characterized by a single lobe, but one is positive the other is negative (i.e., the centroid moves in opposite directions); meanwhile, in CLS the UX has three lobes since the centroid at the middle is restrained against lateral movement. So, even if the shapes follow the PS scenario, the actual shapes are dependent on the position of the discrete lateral support, which explains the differences in the trends between these three cases (even for the same PS scenario).

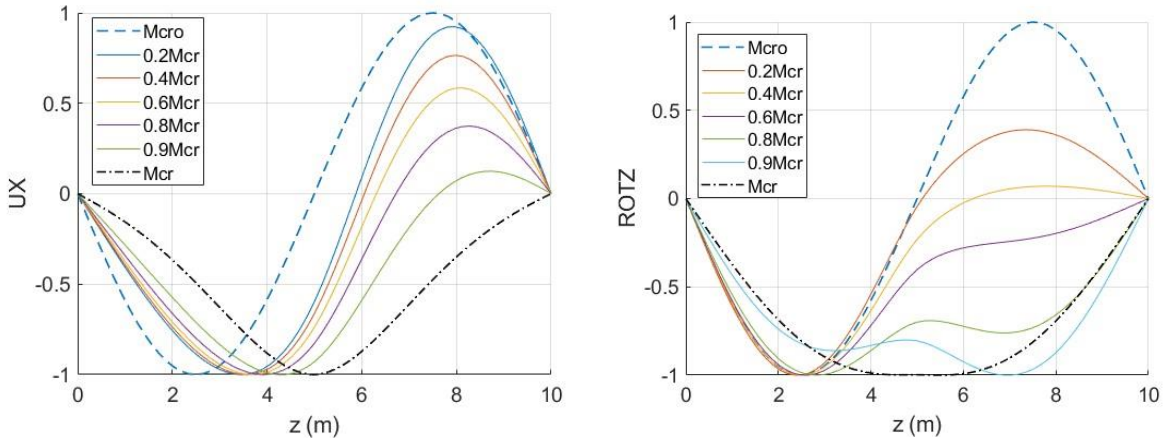

Figure 4.11: Deformed shapes from GNIA: TLS, L=10m, H=180mm, PS behavior

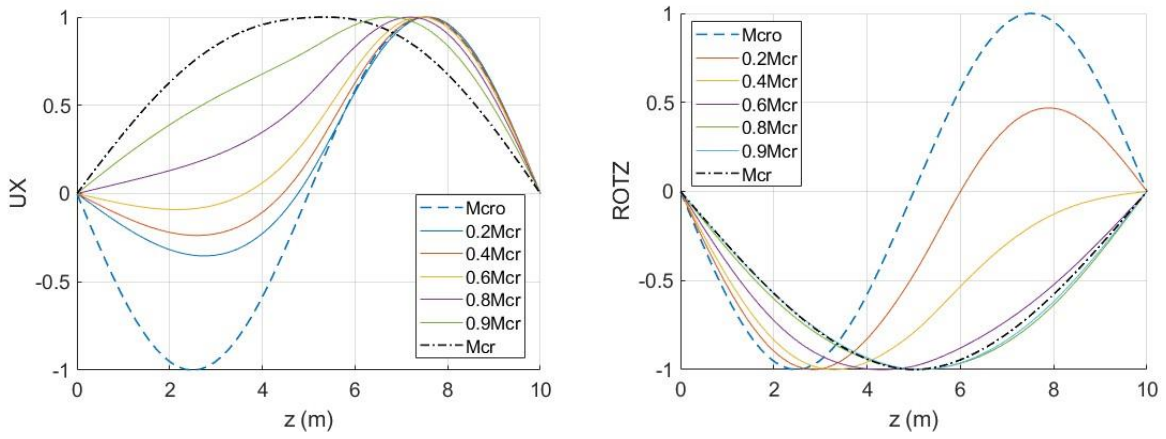

Figure 4.12: Deformed shapes from GNIA: BLS, L=10m, H=180mm, PS behavior

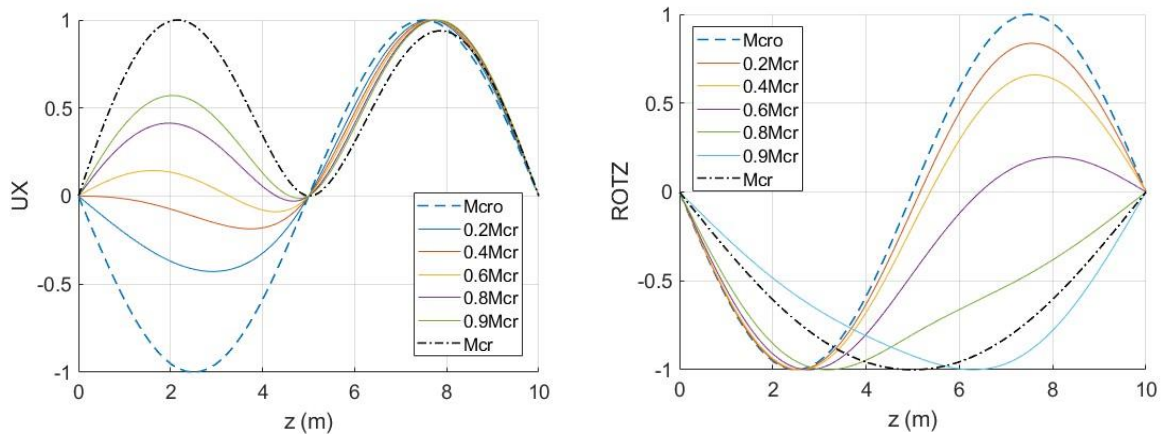

Figure 4.13: Deformed shapes from GNIA: CLS, L=10m, H=180mm, PS behavior

Fig. 4.14 shows the SS behavior, which in the investigated cases occurs only with BLS. As the plots show, the distribution of UX and ROTZ remains unchanged during the loading process. Partially similar phenomenon can be observed in the PP scenario, such as in the TLS case, shown in Fig. 4.15.

However, even if the LBA results suggest that CLS exhibits PP, the real behavior is quite different, as can be seen from Fig. 4.16. While UX hardly changes during the process, ROTZ does. The initial shape (of ROTZ) is point-symmetric with a full sine-wave, which first transforms into a symmetric one (characterized by a single lobe, but clearly not a half-sine wave,) then transforms back to point-symmetric again (full sine-wave), but opposite to the original one. This behavior, which could be identified as PSP, seems to be characteristic to CLS.

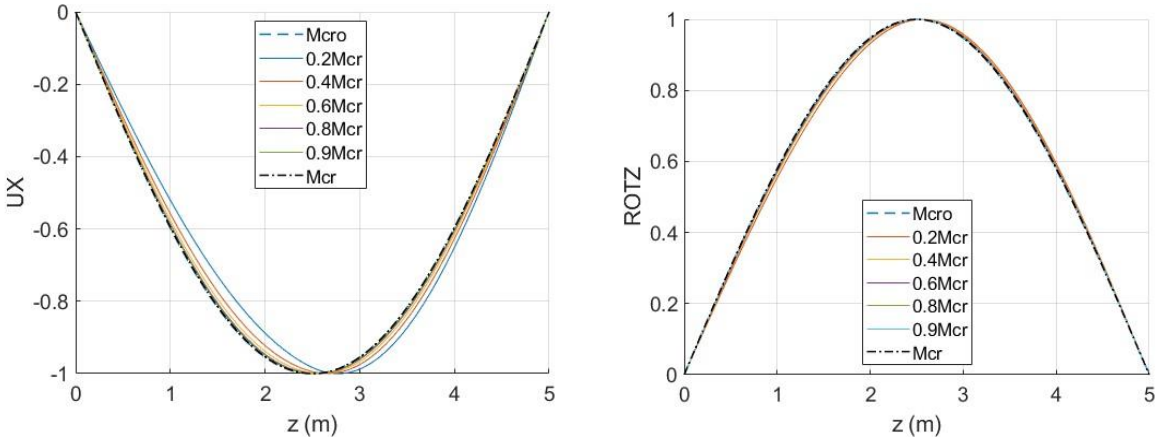

Figure 4.14: Deformed shapes from GNIA: BLS, L=5m, H=400mm, SS behavior

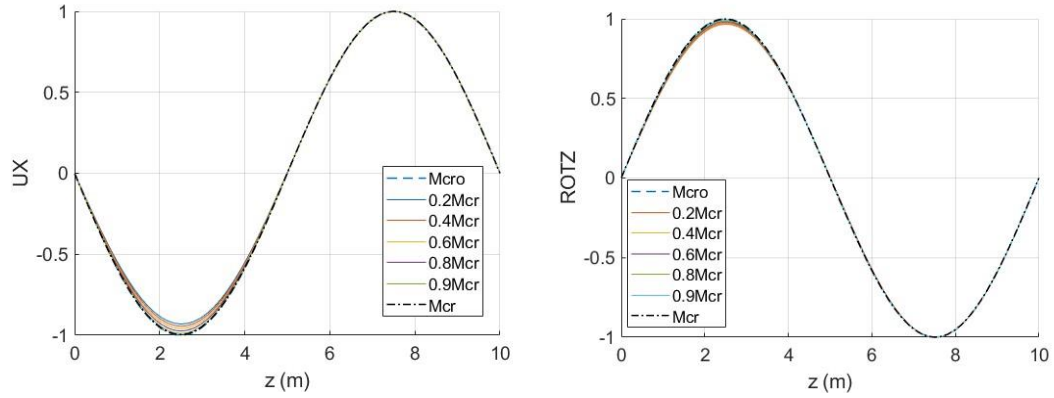

Figure 4.15: Deformed shapes from GNIA: TLS, L=5m, H=500mm, PP behavior

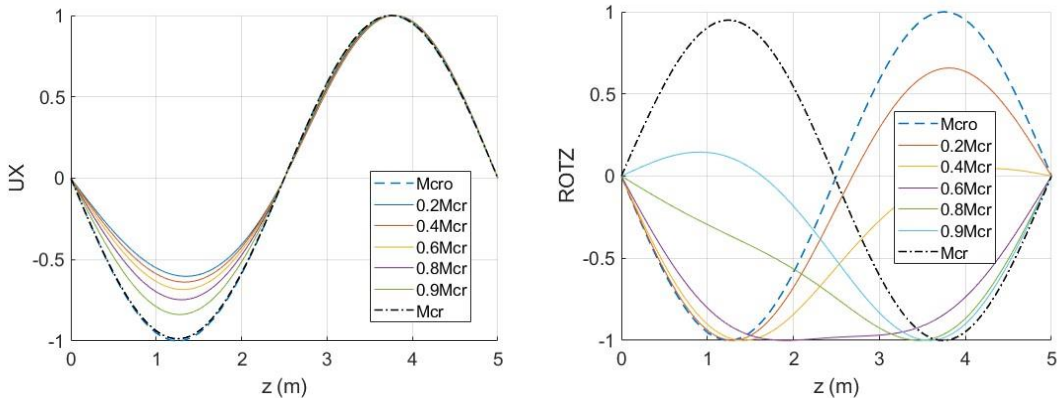

Figure 4.16: Deformed shapes from GNIA: CLS, L=5m, H=500mm, PSP behavior

4.6.3 The effect of initial shape

Though in certain cases the initial shape and the final shape are almost identical, i.e., the initial twist and out-of-straightness are simply amplified during the analysis, in many other cases the shape is significantly modified. This suggests that the initial shape itself is not crucially important. To prove this, several cases have been recalculated using the second or third (or even higher) classic buckling modes as initial shapes. (Nevertheless, the initial amplitude has been kept the same very small value.) Sample results are shown in Figs. 4.17-4.18 and 4.19-4.20, for TLS and BLS, respectively. As the plots show, though the shape transition of the beam is significantly influenced by the initial shape, the final shapes are hardly affected. (Note, the same cases with starting from the first mode are shown in Figs. 4.11 and 4.12 for TLS and BLS, respectively.)

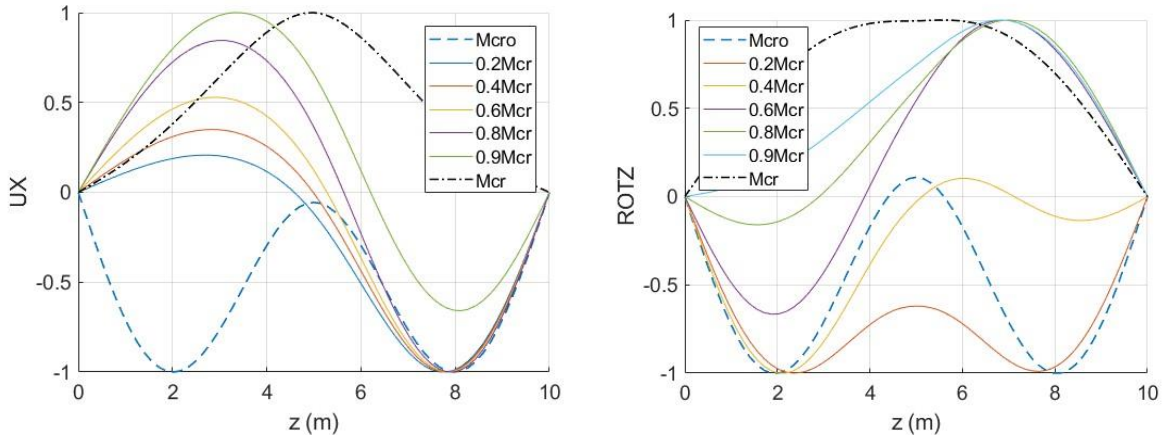

Figure 4.17: Deformed shapes from GNIA: TLS, L=10m, H=180mm, initial shape: second mode

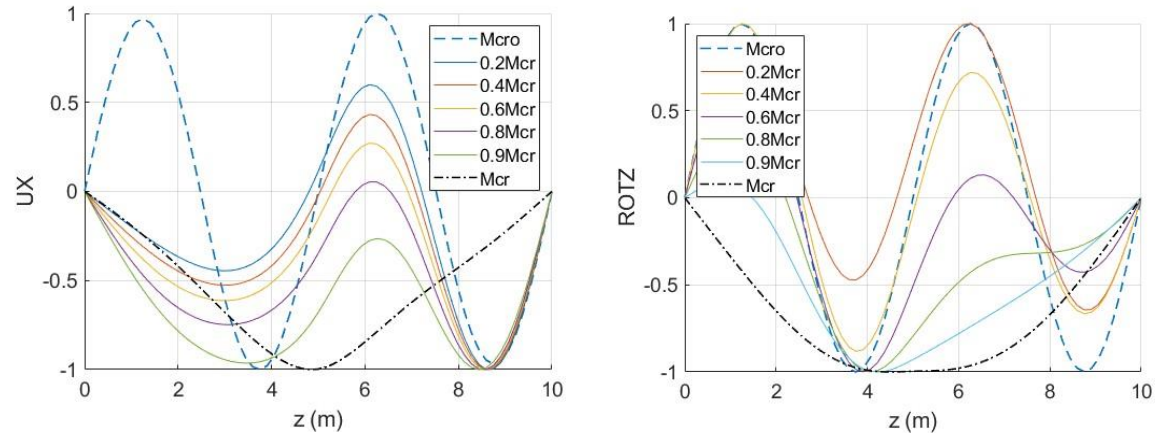

Figure 4.18: Deformed shapes from GNIA: TLS, L=10m, H=180mm, initial shape: third mode

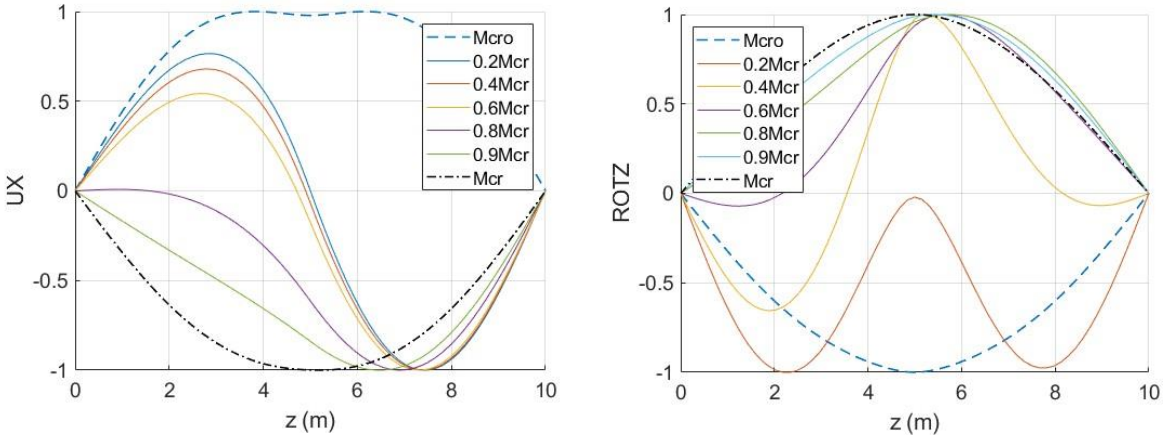

Figure 4.19: Deformed shapes from GNIA: BLS, L=10m, H=180mm, initial shape: second mode

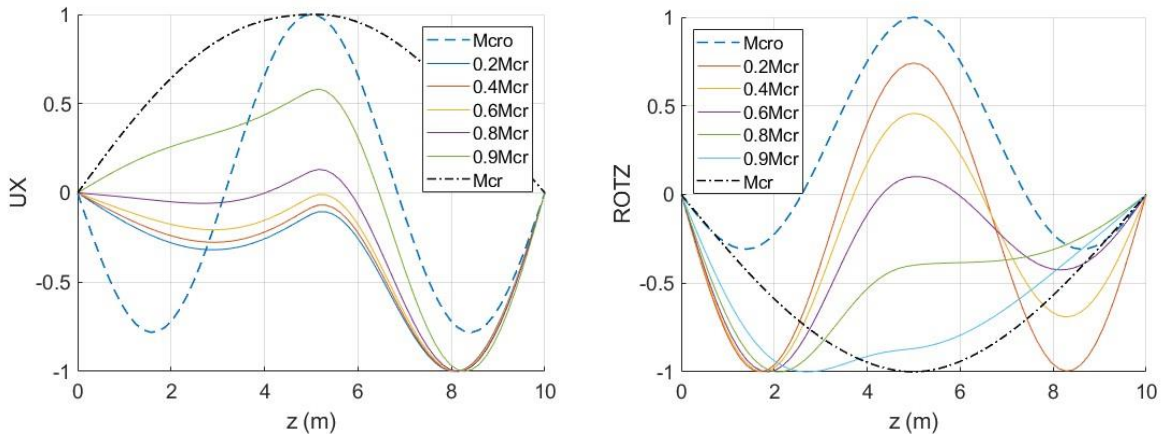

Figure 4.20: Deformed shapes from GNIA: BLS, L=10m, H=180mm, initial shape: third mode

The results suggest that the shape always converges to the same final shape regardless the initial shape. However, the initial shape determines how fast the load-displacement curve converges to the secondary equilibrium path, and it slightly affects the predicted M_{cr}value, too, as illustrated in Fig. 4.21. For example, in the actual case of TLS, mode 2 provides the fastest convergence and the largest M_{cr} (out of the first three modes), while in the actual case of BLS it is mode 3 that provides the fastest convergence and the largest M_{cr}.

Nevertheless, it can be concluded that if the initial imperfection is extremely small, then (i) the final buckling shape and the associated critical load value are insensitive to the actual initial shape, (ii) it is not necessarily the first mode that provides the best numerical performance in finding the final buckling shape.

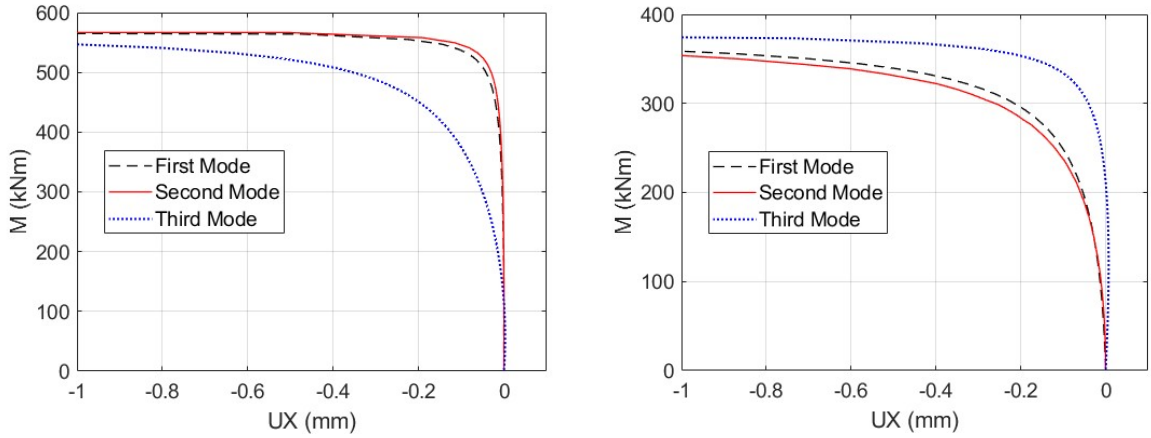

Figure 4.21: Load-displacement curves form GNIA: TLS (left) and BLS (right), L=10m, H=180mm

4.6.4 The effect of initial amplitude

Moreover, Figs. 4.21-4.24 show the final shapes together with the initial one for various amplitudes. As the plots shows, in certain cases the final shape is hardly affected by the initial amplitude, while in other cases it does. This observation can readily be connected to the 'amount' of shape transition involved (i.e., how much energy it takes to transition into the other mode). In certain cases, the initial shape hardly changes during the analysis, hence, it hardly matters how large the initial amplitude is, the FEM algorithm will easily find the secondary equilibrium path. However, in other cases the beam exhibits significant shape transition to reach its final shape; if the initial amplitude is large(r), the shape cannot fully be transformed before reaching the secondary equilibrium path.

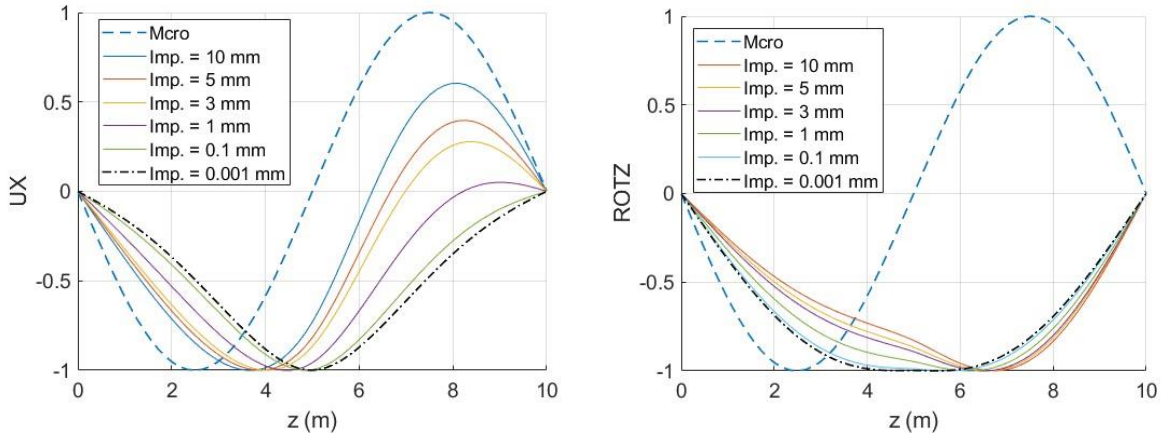

Figure 4.21: Load-displacement curves form GNIA for various imperfection values: TLS, L=10m, H=180mm

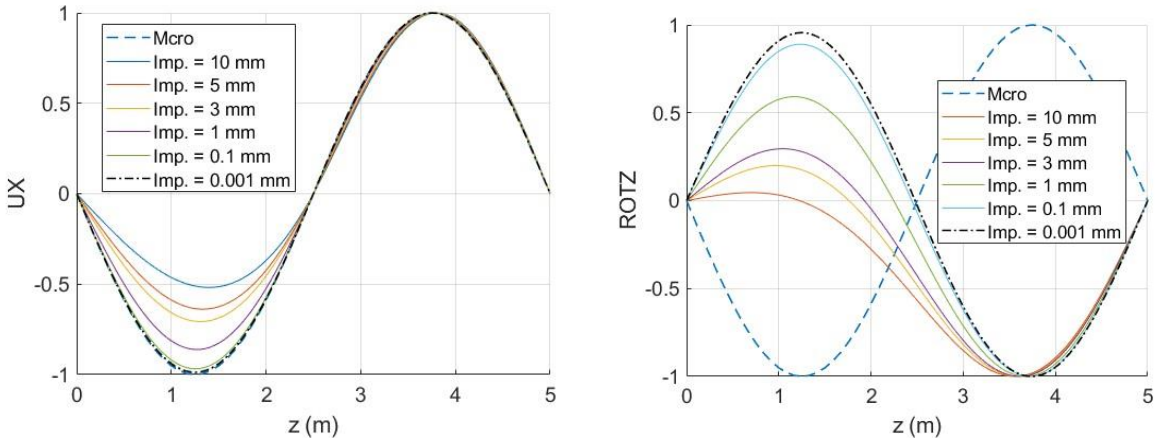

Figure 4.22: Load-displacement curves form GNIA for various imperfection values: CLS, L=5m, H=500mm

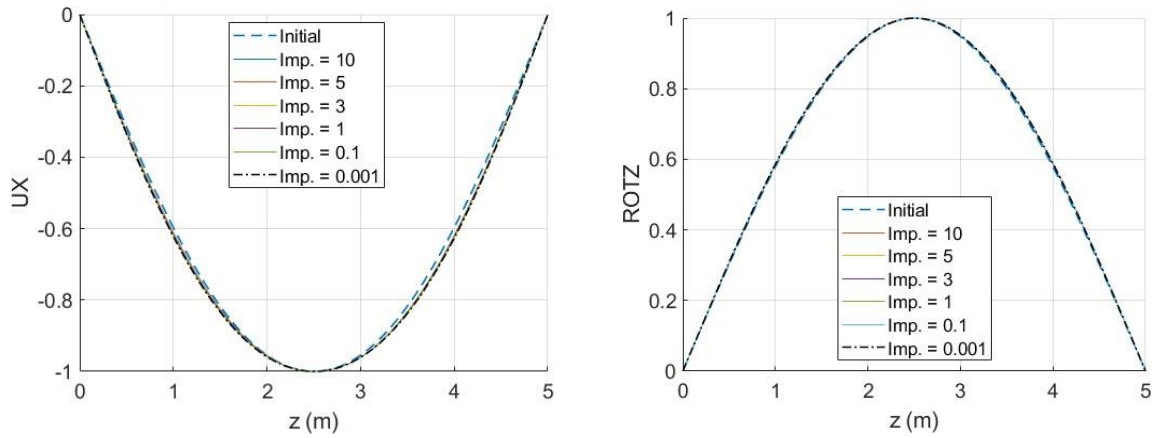

Figure 4.23: Load-displacement curves form GNIA for various imperfection values: BLS, L=5m, H=400mm

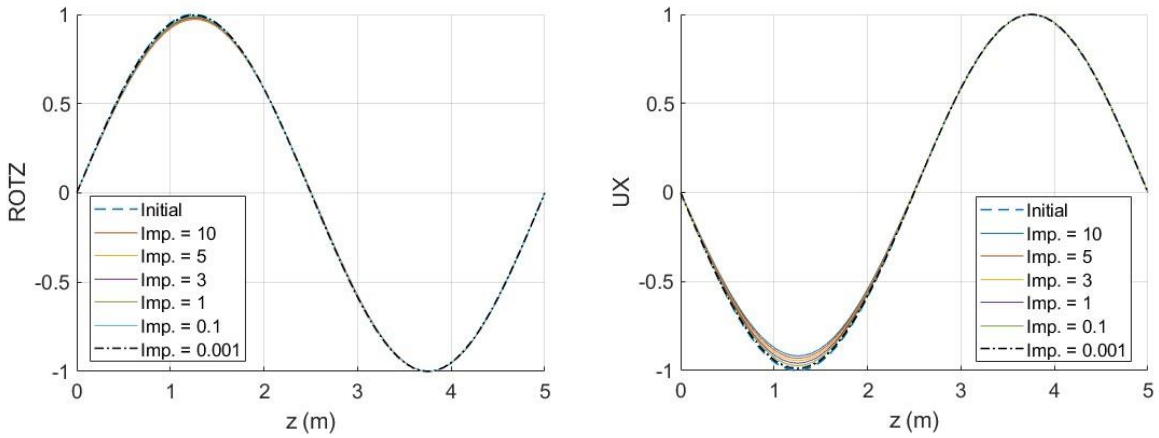

Figure 4.24: Load-displacement curves form GNIA for various imperfection values: TLS, L=5m, H=500mm

Regarding the resulting M_{cr} values, they also vary sometimes depending on the value of initial imperfection. Table 4.3 shows the M_{cr} values for different intermediate support cases and with having various initial imperfection values. It is observed that with higher initial imperfections, lower M_{cr} values result from the GNIA. Furthermore, it makes it more difficult to selecct a precise M_{cr} value. This makes it important to select the values of initial imperfections correctly in order for the results to be comparable with the LBA or the analytical solutions. It can be seen from Table 4.3 that the 'decrease' in M_{cr} due to larger imperfection values, is slightly affected by the type of intermediate supports.

Another interesting observation was made. In some cases (especially in TLS), if the initial imperfection is further increased, the M_{cr} value starts to increase again. Table 4.4 shows the results of further increasing the imperfection values, which was done on the TLS case, with L = 10 m, and H = 500 mm. In this case, the value of M_{cr} drops to 78.7% at 10 mm of initial

imperfection, but then increases again to reach 127.3% at 70 mm of initial imperfection, and then starts to decrease again by further increasing the initial imperfection.

Table 4.3: Increase in Mcr values from GNIA with various imperfection values for different mode switch cases

Imperfection	TLS – 10 – 180 (PS) % of Mcr	CLS – 5 – 500 (PSP) % of Mcr	BLS – 5 – 400 (SS) % of Mcr	TLS – 5 – 500 (PS) % of Mcr
0.0001	100	100	100	100
0.001	100	100	99.7	100
0.01	99.5	99.8	99.3	100
0.1	99.1	99.5	93.8	95.4
1	96.1	95.5	90.1	90.6
10	84.1	67.2	62.3	69.9

Table 4.4: M_{cr} for varying imperfection values for TLS, L = 10 m, H = 500.

Imperfection	Mcr	% of Mcr by LBA
0.0001	722	100
1	722	100
10	568	78.7
15	721	99.8
50	808	111.9
70	919	127.3
100	793	109.8
125	710	98.3

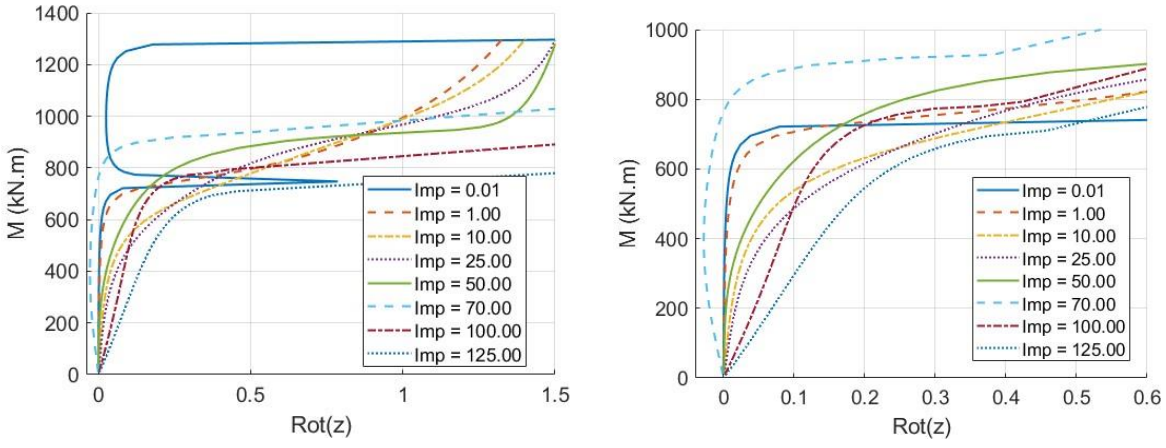

Figure 4.25: Load displacement cureves for TLS, L = 10 m, H = 500.

This phenomenon can be explained by a higher buckling mode, meaning that increasing the imperfection value to a certain level makes it easier for the beam to 'switch' into the higher

buckling mode. This was confirmed by the actual observed shapes, as they switch into a higher mode (but never fully) this is why the M_{cr} value never actually reaches the value of the second buckling mode, but starts to decrease again after a certain imperfection value. Figure 4.25 shows the load displacement curves of this case. It can be seen that if the imperfection value is too small, the algorithm is able to capture both the first and second buckling modes.

4.7 Efficiency of lateral supports

Intermediate lateral supports are widely used in structural engineering constructions. They are known to enhance the LTB behavior; occasionally, they can effectively prevent LTB type instability. It is also common knowledge that the position (e.g., at the top or bottom flange, etc.) and type (e.g., continuous or discrete, or, against twist and/or lateral translation, or, rigid or elastic, etc.) of the intermediate support strongly influences its efficiency. Based on the here-presented results, however, a further aspect is revealed: the efficiency of intermediate supports is highly dependent on whether the prebuckling deflections are disregarded or considered.

To illustrate this, Figs. 4.26-4.28 show the efficiency for three sample cases: two simple supported beams with different lengths and a clamped-clamped (i.e., minor-axis rotation and warping prevented) beam, all with various I_y/I_x ratios and various discrete lateral supports. The efficiency is expressed by the $M_{cr0}/M_{cr0(NLS)}$ or $M_{cr}/M_{cr(NLS)}$ ratio, where M_{cr0} and M_{cr} are the critical moments with the lateral supports, while $M_{cr0(NLS)}$ and $M_{cr(NLS)}$ are the critical moments without any lateral intermediate support.

In these actual samples, if the prebuckling effect is disregarded, then the actual benefit of the lateral support is dependent on the beam configuration, but almost any of the considered lateral supports are equally efficient except for short(er) PrPw-PrPw beam with BLS support. If the prebuckling effect is considered, the efficiency of the lateral support is more diverse. As expected, ALS is the most efficient and BLS is the least efficient, but the actual $M_{cr}/M_{cr(NLS)}$ value is strongly dependent on the problem parameters: it can be as high as 3.3, but in many cases, it is hardly greater than 1.

The general observation, therefore, is that though in some cases the efficiency of the lateral support is the same whether the prebuckling effect is considered or not, more often than not the calculated efficiency is rather different if based on the results of classic LBA or if based on the results of a more advanced analysis including the effect of prebuckling deflections.

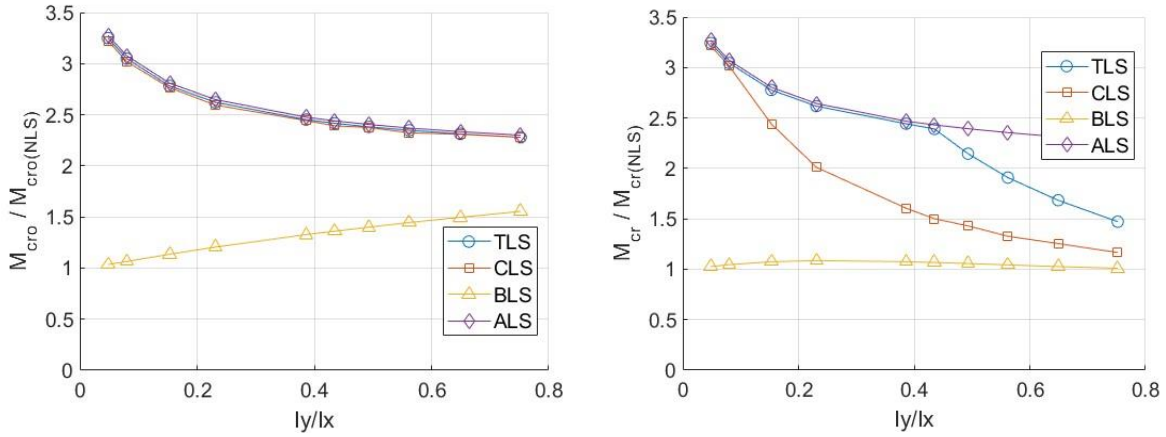

Figure 4.26: Ratio of critical moments with and without intermediate support for Mcr0 (left) and Mcr (right), for L = 5 m, PrPw-PrPw.

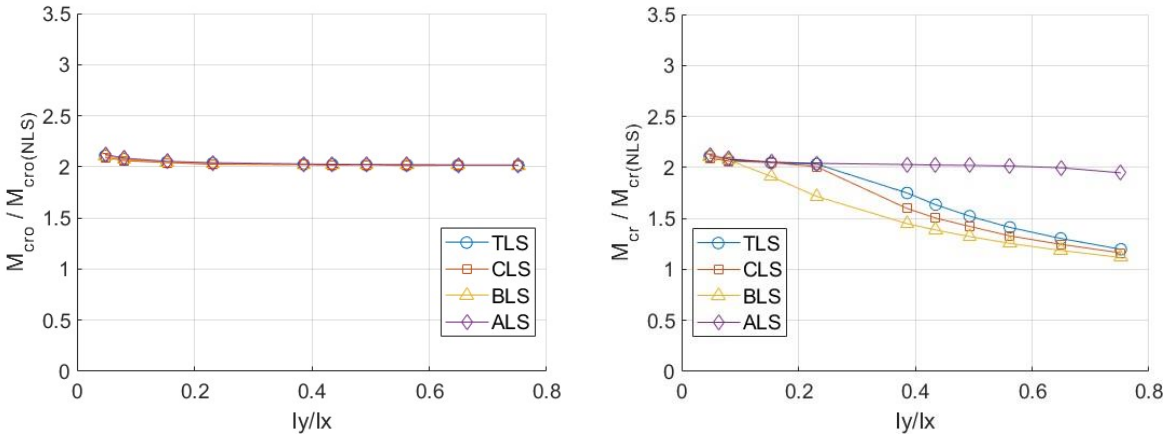

Figure 4.27: Ratio of critical moments with and without intermediate support for Mcr0 (left) and Mcr (right), for L = 30 m, PrPw-PrPw.

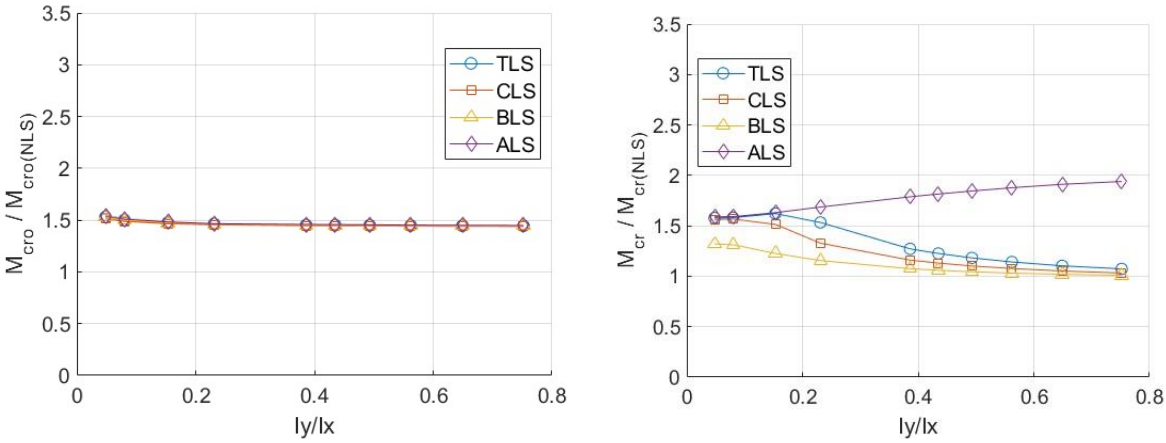

Figure 4.28: Ratio of critical moments with and without intermediate support for Mcr0 (left) and Mcr (right), for L = 30 m, FrFw-FrFw.

In the reported research the LTB behavior is investigated using numerous assumptions and simplifications, such as: the material is perfectly elastic and homogeneous, the effect of imperfections is disregarded, only classic beam-type displacements are assumed (i.e., the effect of shear of localized plate bending deformations are disregarded), etc. Real beams are affected by all these factors. Still, it is a common notion that the results from an idealized elastic analysis are representative, even though approximate, if the beam cross-section is compact and the beam is slender. In other words, it is a reasonable expectation that the M_{cr} values should approximate the real LTB capacity in the case of locally compact but globally slender beams. However, the presented results prove that the critical moment value is strongly affected whether the prebuckling deflections are considered or not: depending on the structural configuration the M_{cr} can be significantly larger than M_{cr}, but can also be significantly smaller, too, the M_{cr}/M_{cr0} ratio being in the 0.6-2.0 range.

Similar conclusions can be reached observing the efficiency of the intermediate lateral supports. The calculated efficiency of the lateral support is sometimes significantly different depending on whether the prebuckling effect is considered or not. For example, in the FrFw-FrFw case shown in Fig. 4.28, for large and moderately large I_y/I_x ratios, the efficiency of BLS is 50% and 0% without and with considering the prebuckling effect, respectively; however, the efficiency of ALS is 50% and 80% without and with considering the prebuckling effect, respectively. In other words, the classic analysis predicts the same 50% moment increase for both BLS and ALS, but a more realistic prediction is 0% for BLS and 80% for ALS. Again, the conclusion is that it can cause a drastic difference in the elastic results whether the prebuckling effect is considered or not. The results, therefore, suggest that if the critical moment is calculated by a classic LBA, the obtained result is not necessarily a good predictor of the capacity even if the behavior is elastic.

4.8 Summary

In this chapter, lateral-torsional buckling of simple beams with intermediate discrete lateral supports were investigated. Four variants of the lateral supports were considered, depending on the vertical position of the lateral support, and whether the twisting rotation is restrained or not. The behavior was studied by finite element analyses, using both beam and shell finite elements. Additionally, analytical solutions were also derived. Several observations were made:

Excellent agreement was found between the results from the derived analytical formulae and the finite element buckling analysis if beam finite elements are used. When the beam is modelled by shell finite elements, the results are still in reasonable agreement, though the effect of non-beam-like deformations (primarily: localized plate bending and shear deformations) is necessarily included in the result, causing noticeable differences.

Both the numerical results and the derived analytical formulae clearly show that the intermediate discrete lateral support has an important effect on how the prebuckling deflections modify the critical moment. In the case of beams with intermediate lateral support, the suggestion of multiple previous papers that the prebuckling effect is always positive and the critical moment increase can be approximated by the $1/\sqrt{1-I_y/I_x}$ ratio can be justified only if the intermediate support prevents both the lateral translation and the twisting rotation. In other cases, the moment increase is (or can be) significantly smaller; in fact, the increase is frequently negative, i.e., the prebuckling deflection can decrease the critical moment.

It was found that the discrepancies between these cases can be explained by the buckling shapes, meaning that the buckling shape can be different when considering the prebuckling deformations, suggesting a 'mode switch' that occurs sometimes during the loading of the beam. To better understand the behavior, geometric GNIA was performed, too. This type of the analysis reveals how the final buckling shape is formed as the load gradually increases.

The main observations are as follows: (i) the presence of a mode switch is confirmed, as the beam starts with the shape of LBA without prebuckling deformations, it can gradually switch into a different shape (ii) regardless of the initial shape, the beam will always switch to the same final shape if initial imperfection values are small, however, the rate of which it converges can vary, and the M_{cr} value can be slightly affected (iii) the value of initial imperfection can significantly affect the M_{cr} value, as well as the resulting buckling shape

Finally, the practical use of intermediate supports was investigated. If the prebuckling deformations are not considered, the discrepancies in M_{cr} between the different cases is limited. However, when considering prebuckling deformations, significant discrepancies can be observed. In some cases, the increase in M_{cr} due to intermediate support can be little to none, while in other cases it can be up to 100%. The buckling mode is the main factor that affects these results.

Chapter 5: Conclusions and Thesis Statements

5.1 Conclusions

This research investigates the effect of prebuckling deformations on the lateral torsional buckling of thin-walled steel beams. Classical solutions which are still used nowadays neglect the prebuckling effects, and although it was shown in previous studies that it can have a significant influence on the solution if the beam is not too deep, the topic is still far from being fully studied, with only a handful of papers investigating it, which are mostly limited to the most basic case, a doubly symmetric single span beam with forked supports, constant moment distribution, and no intermediate lateral supports.

Upon reviewing the available literature on the topic, discrepancies were found in the given analytical solutions for the seemingly same case. These discrepancies were found to be due to several factors during the analytical solution, chapter 2 provided a detailed overview of the analytical derivations for the basic case, showing when it's appropriate to do certain simplifications and giving the most suitable formulae. The effect of torsional rigidity is also considered in chapter 2, providing analytical solutions for open and closed doubly symmetric steel sections.

Chapter 3 investigates the effect of end supports. Various closed formed solutions are given for 5 different end support conditions. Numerical FEM solutions are also introduced using both beam and shell elements, and using two types of analysis, the GNIA, and a proposed iterative LBA process. The results of the various methods were found to be in good agreement, with some discrepancies found due to (i) the analytical solution needing more terms in the shape functions in some boundary conditions, and (ii) the localized deformations in the shell element. More refined analytical solutions are given, and a simple local deformations index was proposed. It was found that the effect of prebuckling deformations is highly influenced by the end supports, and it is even negative in some cases unlike what is suggested in the literature.

The next step in the research was investigating the effect of intermediate lateral supports. Using the methods developed earlier, several types of intermediate supports were considered: the lateral restrain at the top, bottom, or centroid of the beam, as well as everywhere on the section, preventing the torsional rotation as well. The results showed high discrepancies between these different types of supports, with some of them increasing the critical moment by up to more than 80% when accounting for prebuckling deformations, while others cause a

decrease that can be up to 40%. These discrepancies were also found to be present in the same case, when changing some parameters, like the length, cross section, or end supports.

To understand the causes for these differences, a study on the buckled shapes was conducted using LBA (classical or iterative), where it was found that sometimes, the buckled shapes can differ within the same case depending on whether the prebuckling deformations are considered or not, as sometimes they are symmetric if classical solutions are used, but point-symmetric if prebuckling deformations are considered. This suggests a 'mode switch' that happens during the loading of the beam before it reaches the buckling load. To confirm that, non linear (GNIA) analysis study was conducted with carefully observing the buckled shape for various sub-steps. The mode switch was confirmed and studied in detail.

Although this study provides valuable insights into the effect of prebuckling deformations on the LTB of beams considering various factors, the topic still needs further investigations to fill the gaps. For instance, other boundary conditions can be considered, such as cantilevers, fixed beams at both ends (about the primary rotations), or multi-span beams. Other loading conditions can also be investigated, such as varying moment distributions, or concentrated forces. Other types of intermediate supports can be studied, such as lateral restrains at varying heights, at different locations across the length, or multiple lateral supports. Other types of buckling can also be considered, such as combined global and local buckling. These factors and others are intended as topics for future studies.

5.2 Thesis Statements

- **Thesis 1**

I have conducted an analytical study on the lateral torsional buckling of beams considering the prebuckling effect. I have summarized most of the available analytical formulae in the literature, highlighting the variations between them (even for the seemingly same case), showing that the solution is far from unambiguous. I rederived the different formulae, identifying the important factors in the analytical derivations which influence the critical moment formula. By doing so, I explained the differences between the formulae found in the literature. Furthermore, by doing the analytical study, I showed that several further variants can be derived (but not all of them are accurate). I defined the requirements for the approximations and when it is appropriate to do them. I have distinguished between cross sections with high and low torsional rigidities in the analytical derivations. By doing so, I have shown that the

torsional rigidity of the section has an important, but unexplored effect, that is why open and closed section beams are differently affected by the prebuckling effect.

- **Thesis 2**

I have conducted a numerical study for the validation of the analytical solutions. For that purpose, I developed beam and shell finite element models, which are suitable for considering the prebuckling deformations. I pointed out some important modelling aspects that have (or might have) significant influence on the results when LTB with prebuckling effect is studied. I have shown that classical models used for LBA might not be suitable for an FEM analysis that consider prebuckling deformations, and special considerations must be made in order for the results to be comparable with the analytical solutions (namely: loading application, supports in beam and shell FEM models, and nonlinear static analysis in iterative LBA).

I have used two types of analysis for the numerical solutions. First, I proposed an iterative LBA methods that alternate between static analysis for inducing prebuckling deformations, and linear buckling analysis that obtain a critical moment value. I have shown that convergence occurs, leading to critical moment value that's close to the analytical solutions. I have shown that using a linear analysis in the static analysis step produces error, and non-linear analysis lead to better results. Then, I have conducted GNIA with very small imperfections, leading to critical moment values that are very close to the results from iterative LBA method, validating the use of such an algorithm. I have compared the shell and beam FEM methods, highlighting that the effect of non-beam-like deformations is significantly magnified when prebuckling deformations are considered.

- **Thesis 3**

I have considered other boundary conditions than the simple forked support case which was mostly discussed in the literature. I have derived closed formed analytical solutions for various boundary conditions, and I have created numerical models for these different boundary conditions cases. I have conducted a parametric study using the proposed analytical and numerical solutions. I have compared the results from all the proposed methods accounting for the combined effects of (i) prebuckling deformations, (ii) boundary conditions, and (iii) torsional rigidity.

Using the results, I have shown that the different methods used agree to an acceptable degree, validating the derived analytical solutions for most cases, with some inaccuracies,

especially when rotational fixities are introduced. I have shown that the source of these inaccuracies is the approximative nature of the shape functions used. I have derived enhanced solutions based on more accurate shape functions, giving more accurate results. I have shown that the end supports have a significant effect on how the prebucking deformations influence the solution, highlighting that proposed formulae in the literature are only valid for the simple forked support case.

I have shown that unlike what is suggested by literature, the effect of prebuckling deformations is not always positive, and can be negative in certain support cases. I have shown that the length of the beam influences the solution in some boundary condition cases, which is present in the FEM solution, but can only be captured in the analytical solution if the enhanced shapes are used. I have shown that longer beams require more terms in the shape functions to produce accurate results. I have shown that the effect of non-beam-like deformations in the shell element solution is further heightened when fixity is introduced to the twisting rotation at the end of the beam.

- **Thesis 4**

I have considered the intermediate lateral and torsional supports, I have derived analytical closed formed solutions for the critical moment of beams considering prebuckling deformations for four cases: (i) lateral support at the top flange (ii) lateral support at the bottom flange (iii) lateral support at the centroid, and (iv) lateral support with twisting rotation fixity. I have created numerical models for these cases and conducted a parametric study using the various methods.

Using the results, I have shown that the location of the intermediate support has a drastic effect on how the prebuckling deformations affect the solution. The differences can vary between a significant increase in the critical moment to a significant decrease (compared to the case when prebuckling deformations are not considered) depending on which kind of intermediate support is used. I have shown that the reason for these discrepancies is in the buckling shape, which vary depending on the type of intermediate support. I have shown using both the LBA and the analytical solutions that the buckling shape can differ depending on whether or not the prebuckling deformations are considered, suggesting the presence of a ‘mode switch’ as the load increases.

I have further investigated the mode switch behavior using the GNIA method, plotting and observing the transitioning from one mode to another during the non-linear analysis, and

confirming the mode-switch phenomena. I have investigated the effect of the initial shape and initial imperfection value on the mode-switch, showing that if the initial imperfection value is small, the beam will always switch to the same shape regardless of the initial shape, but larger initial imperfection values affect the final shape as well as the critical moment value. Finally, I have studied the practical effectiveness of the use of intermediate lateral supports, highlighting the variations between little to know advantage, to high advantage, depending on the type of the intermediate support, the cross section, and length of the beam

Publications of the author

Journal Papers

[AGA1] Abureden. G.A., Adany, S. (2025). The Effect of Torsional Rigidity and Approximations in Analytical Solutions for the Critical Moment of Beams Considering Prebuckling Deflections. Periodica Polytechnica Civil Engineerin. https://doi.org/10.3311/PPci.39445

[AGA2] Abureden. G.A., Adany, S. (2025). Influence of prebuckling deflections on the elastic lateral-torsional buckling of thin-walled beams with various end supports: analytical and numerical investigations in the case of doubly-symmetric cross-sections. Thin-Walled Structures, 113025. https://doi.org/10.1016/j.tws.2025.113025

[AGA3] Abureden. G.A., Adany, S. (2025). Elastic lateral-torsional buckling of single-span doubly symmetric I-section beams with intermediate discrete lateral support considering prebuckling deflections. Thin-Walled Structures, 11317. https://doi.org/10.1016/j.tws.2025.113179

Conference Papers

[AGA4] Abureden. G.A., Adany S. (2023). The effect of prebuckling deflections on the lateral-torsional buckling of beams: numerical studies. ce/papers, 6(3-4), 1686-1690.

[AGA5] Abureden. G.A., Adany S. (2023). On the effect of prebuckling deflections on the lateral-torsional buckling of beams. Proceedings of the Ninth International Conference on Thin-Walled Structures (ICTWS2023), Nov 29 – Dec 1, 2023, Sydney, Australia.

[AGA6] Abureden. G.A., Adany S. (2024). Critical moment of doubly-symmetric beams with prebuckling deflection: The effect of end supports. In Proceedings of the Annual Stability Conference, Structural Stability Research Council. San Antonio, Texas.

[AGA7] Abureden. G.A., Adany S. (2024). Critical moment of doubly-symmetric beams with prebuckling deflection: The effect of intermediate supports. In Proceedings of the Annual Stability Conference, Structural Stability Research Council. Louisville, Kentucky.

References

[1] Euler, Leonard (1744). *Methodus inveniendi lineas curvas maximi minimive proprietate gaudentes sive solutio problematis isoperimetrici latissimo sensu accepti [A method of finding curved lines enjoying the maximum-minimum property, or the solution of the isoperimetric problem in the broadest sense]* (in Latin). Geneva, Switzerland: Marc Michel Bousquet et Cie.

[2] Michell, A. G. (1899). XXXII. Elastic stability of long beams under transverse forces. *The London, Edinburgh, and Dublin Philosophical Magazine and Journal of Science*, *48*(292), 298-309.

[3] Bleich, F. (1952). Buckling strength of metal structures. *Mc Graw-Hill Book Company, Inc., Cardnr. 51-12588*.

[4] Chajes, A., & Winter, G. (1965). Torsional-flexural buckling of thin-walled members. *Journal of the Structural Division*, *91*(4), 103-124.

[5] Hancock, G. J. (1997). Design for distortional buckling of flexural members. *Thin-walled structures*, *27*(1), 3-12.

[6] Fan, S., Dong, D., Zhu, T., Wang, J., & Hou, W. (2022). Experimental study on stainless steel C-columns with local-global interaction buckling. *Journal of Constructional Steel Research*, *198*, 107516.

[7] Gioncu, V. (1994). General theory of coupled instabilities. *Thin-Walled Structures*, *19*(2-4), 81-127.

[8] Timoshenko, S. P. (1906). Lateral buckling of I-beams under the influence of forces acting in the plane of largest rigidity. *Proc. St. Petersburg Polytechnical Institute*, *4*(5), 151-219.

[9] Timoshenko, S. P. (1908). On the Subject of Buckling. *Proceedings Kiev Polytechnic Institute,* **8**, 181-212. *Strength of materials.* Part 1. Kiev.

[10] Timoshenko S. (1913) „Sur la stabilite des Systemes elastiques", Annls Ponts Chauss, 1st Part, *Memoires et Documents*, 9th Series, 13, 496—566; 16, 72—132, 372-412.

[11] Timoshenko, S.P. and Gere, J.M. (1961) Theory of Elastic Stability. Second Edition, McGraw-Hill Book Co. Inc., New York.

[12] Vlasov, V. Z. (1961). *Thin-walled elastic beams.* 2nd Ed., Israel Program for Scientific Translation, Jerusalem, Israel.

[13] Bažant, Zdeněk & Cedolin, Luigi. (2010). Stability of Structures: Elastic, Inelastic, Fracture and Damage Theories. 10.1142/7828.

[14] Lagrange, J.L.: Méchanique Analytique. La Veuve Desaint, Paris (1788)

[15] Taliaferro, S. D. (1980). An inversion of the Lagrange-Dirichlet stability theorem. *Archive for Rational Mechanics and Analysis*, *73*, 183-190.

[16] Leine, R. I. (2010). The historical development of classical stability concepts: Lagrange, Poisson and Lyapunov stability. *Nonlinear Dynamics*, *59*, 173-182.

[17] Galambos, T. V. (2016). *Structural members and frames*. Courier Dover Publications.

[18] Ioakimidis, N. I. (2018, February). The energy method in problems of buckling of bars with quantifier elimination. In *Structures* (Vol. 13, pp. 47-65). Elsevier.

[19] Hajdú, G., Pasternak, H., & Papp, F. (2023). Lateral-torsional buckling assessment of I-beams with sinusoidally corrugated web. *Journal of Constructional Steel Research*, *207*, 107916.

[20] Luo, L., Zhang, Y., Pan, C., Zheng, N., & Xu, C. (2024). Lateral torsional buckling in H-shaped steel beams considering the combined action of bending and torsion. In *Structures* (Vol. 66, p. 106935). Elsevier.

[21] Cai, J., Le Grognec, P., & Nême, A. (2023). Analytical and numerical study of the lateral buckling of an imperfect pipe accounting for torsional effects. *Ocean Engineering*, *271*, 113686.

[22] Gavin, H. P. (2012). Review of Strain Energy Methods and Introduction to Stiffness Matrix Methods of Structural Analysis.

[23] Love, A. E. H. (2013). *A treatise on the mathematical theory of elasticity*. Cambridge university press.

[24] Pi, Y. L., Trahair, N. S., & Rajasekaran, S. (1991). Energy equation for beam lateral buckling. *NASA STI/Recon Technical Report N*, *93*, 21019.

[25] Hrennikoff, Alexander (1941). "Solution of problems of elasticity by the framework method". *Journal of Applied Mechanics*. **8** (4): 169–175. 1941JAM.....8A.169H. doi:10.1115/1.4009129.

[26] Courant, R. (1943). "Variational methods for the solution of problems of equilibrium and vibrations". *Bulletin of the American Mathematical Society*. **49**: 1–23. 10.1090/s0002-9904-1943-07818-4.

[27] Nikishkov, G. P. (2004). Introduction to the finite element method. *University of Aizu*, 1-70.

[28] Logan, D. L. (2011). *A first course in the finite element method* (Vol. 4). Thomson.

[29] Belytschko, J. F. T. (2007). *A first course in finite elements*.

[30] Koutromanos, I. (2018). *Fundamentals of finite element analysis: Linear finite element analysis*. John Wiley & Sons.

[31] Liu, W. K., Li, S., & Park, H. S. (2022). Eighty years of the finite element method: Birth, evolution, and future. *Archives of Computational Methods in Engineering*, *29*(6), 4431-4453.

[32] Bucalem, M. L., & Bathe, K. J. (1997). Finite element analysis of shell structures. *Archives of Computational Methods in Engineering*, *4*, 3-61.

[33] Chapelle, D., & Bathe, K. J. (1998). Fundamental considerations for the finite element analysis of shell structures. *Computers & Structures*, *66*(1), 19-36.

[34] Sifakis, E., & Barbic, J. (2012). FEM simulation of 3D deformable solids: a practitioner's guide to theory, discretization and model reduction. In *Acm siggraph 2012 courses* (pp. 1-50).

[35] Cohen, G., Hauck, A., Kaltenbacher, M., & Otsuru, T. (2008). Different types of finite elements. *Computational Acoustics of Noise Propagation in Fluids-Finite and Boundary Element Methods*, 57-88.

[36] Stemple, A. D., & Lee, S. W. (1988). Finite-element model for composite beams with arbitrary cross-sectional warping. *AIAA journal*, *26*(12), 1512-1520.

[37] Shkolnikov, M. B. (2006). Three-Dimensional FEM Beam Elements. *SAE Transactions*, 1127-1140.

[38] Ádány, S. (2016). Shell element for constrained finite element analysis of thin-walled structural members. *Thin-Walled Structures*, *105*, 135-146.

[39] Ádány, S. (2014). Flexural buckling of simply-supported thin-walled columns with consideration of membrane shear deformations: Analytical solutions based on shell model. *Thin-Walled Structures*, *74*, 36-48.

[40] Ziegler, H. (1956). On the concept of elastic stability. *Advances in Applied Mechanics*, *4*, 351-403.

[41] Bin Kamarudin, M. N., Mohamed Ali, J. S., Aabid, A., & Ibrahim, Y. E. (2022). Buckling analysis of a thin-walled structure using finite element method and design of experiments. *Aerospace*, *9*(10), 541.

[42] Shinozuka, M., & Astill, C. J. (1972). Random eigenvalue problems in structural analysis. *AIAA journal*, *10*(4), 456-462.

[43] Ringertz, U. T. (1997). Eigenvalues in optimum structural design. *Large-Scale Optimization with Applications: Part I: Optimization in Inverse Problems and Design*, 135-149.

[44] Haffar, M. Z., Horáček, M., & Ádány, S. (2023). Analytical GNI Analysis for Lateral-torsional Behavior of Thin-walled Beams with Doubly-symmetric I-Sections. *Periodica Polytechnica Civil Engineering*, *67*(1), 211-223.

[45] Young, T. (1807) "A course of lectures on natural philosophy and the mechanical arts", Royal Institution of Great Britain, London.

[46] Ayrton W.E., Perry J. (1886) "On struts", The engineer, 62(464–465), pp. 513-515.

[47] Maquoi R., Rondal J. (1978) "Mise en Equation des Nouvelles Courbes Européennes de Flambement", Construction Métallique. Vol 15; No 1; pp. 17-30.

[48] CEN, EN 1993-1-1:2005, "Eurocode 3, Design of Steel Structures, Part 1-3: General rules and rules for buildings".

[49] Quan, C., Walport, F., Kucukler, M., & Gardner, L. (2022). Out-of-plane Stability Design by GMNIA–Equivalent Imperfections and Strain Limits. *ce/papers*, *5*(4), 320-329.

[50] Sadovský, Z., & Kriváček, J. (2020). Influential geometric imperfections in buckling of axially compressed cylindrical shells–A novel approach. *Engineering Structures*, *223*, 111170.

[51] Sadovský, Z., Kriváček, J., & Sokol, M. (2021). Imperfection sensitivity of axially compressed cylindrical shells under varying dimensions. *Engineering Structures*, *247*, 113133.

[52] Prandtl, L. (1899) „Kipperscheinungen", Dissertation, Nürnberg, 1899.

[53] Timoshenko, S. (1910). „Einige stabilitätsprobleme der elastizitätstheorie", Zeitschrift für Mathematik und Physik, 58, 337-385.

[54] Chwalla E., (1939) „Die Kipp-Stabilitat gerader Trager mit doppelt symmetrischen I-Querschitt", Forsch. Geb. Stahlbaues, Verlag von Julius Springer, Berlin, No. 2.

[55] Davidson J.F. (1952) „The elastic stability of bent I-section beams", Proc. Roy. Soc. London, Series A, Vol 212, pp. 80-95.

[56] Pettersson, O. (1952) „Combined bending and torsion of beams of monosymmetrical cross section", Bull. No. 10, Div. of Building Statics and Struct. Eng., Royal Institute of Technology, Stockholm, Sweden.

[57] Kerensky O.A., Flint A.R., Brown W.C. (1956) „The basis for design of beams and plate girders in the revised British Standard 153", Proceedings - Institution of Civil Engineers, Paper No 48, pp. 396–461.

[58] Clark J.W., Knoll A.H. (1958) „Effect of deflection on lateral buckling strength", J. Eng. Mech. Div. ASCE, 84(2), pp. 1596-1–1596-18.

[59] Trahair N.S. , Woolcock S.T. (1973) „Effect of major axis curvature on I-beam stability", J. Eng. Mech. Div. ASCE, 99(1), pp. 85-98.

[60] Vacharajittiphan, P., Woolcock, S.T., Trahair, N.S. (1974) „Effect of in-plane deformation on lateral buckling", Journal of Structural Mechanics, 3(1), pp. 29-60.

[61] Roberts, T.M., Azizian, Z.G. (1983) „Nonlinear analysis of thin-walled bars of open cross section", Int. J. Mech. Sci., Vol. 25, No. 8. pp. 565-577.

[62] Roberts T.M., Azizian Z.G. (1983) „Influence of pre-buckling displacements on the elastic critical loads of thin-walled bars of open cross section", Int. J. Mech. Sci., Vol. 25, No. 2. pp. 93-104.

[63] Pi Y.L., Trahair N.S. (1992) „Prebuckling Deflections and Lateral Buckling. I: Theory", J. Struct. Eng. Vol. 118. pp. 2949-2966.

[64] Pi Y.L., Trahair N.S. (1992) „Prebuckling Deflections and Lateral Buckling. II: Applications", J. Struct. Eng. Vol. 118. pp. 2967-2985.

[65] Trahair N.S. (1993) „Flexural-Torsional Buckling of Structures", Chapman and Hall, London, 1993.

[66] Torkamani M.A.M (1998) „Transaformation matrices for finite and small rotations", Journal of Engineering Mechanics, 124(3), pp. 359-362.

[67] Andrade A, Camotim D. (2004) „Lateral-torsional buckling of prismatic and tapered thin-walled open beams: assessing the influence of pre-buckling deflections, J Steel Compos Struct, Vol 4, pp. 281–301.

[68] Machado, S.P., Cortínez, V.H. (2005) „Lateral buckling of thin-walled composite bisymmetric beams with prebuckling and shear deformation", Engineering Structures, Vol 27, pp. 1185–1196.

[69] Mohri, F., Potier-Ferry, M. (2006) „Effects of load height application and pre-buckling deflections on lateral buckling of thin-walled beams", Steel and Composite Structures, Vol 6, No 5, pp. 1-15.

[70] Torkamani M.A.M., Roberts E.R. (2009) „Energy equations for elastic flexural–torsional buckling analysis of plane structures", Thin-Walled Structures, Vol 47, pp. 463-473.

[71] Mohri, F., Damil, M., Potier-Ferry, M. (2010) „Linear and non-linear stability analyses of thin-walled beams with monosymmetric I sections", Thin-Walled Structures, Vol 48, pp. 299-315.

[72] Attard, M.M., Kim, M-Y. (2010) „Lateral buckling of beams with shear deformations – A hyperelastic formulation", Int Journal of Solids and Structures, Vol 47, pp. 2825-2840.

[73] Erkmen, R.E., Attard, M.M. (2011) „Lateral–torsional buckling analysis of thin-walled beams including shear and pre-buckling deformation effects", Int Journal of Mechanical Sciences, Vol 53, pp. 918-925.

[74] Mohri, F., Damil, M., Potier-Ferry, M. (2012) „Pre-buckling deflection effects on stability of thin-walled beams with open sections", Steel and Composite Structures, Vol 13, No 1, pp. 71-89.

[75] Beyer A., Boissonade N., Khelif A., Bureau A. (2017) „Elastic stability of U-shaped members in bending considering pre-buckling displacements", J. Constructional Steel Research, Vol 135, pp. 230-241.

[76] Pezeshky, P., Mohareb, M., (2018) „Distortional lateral torsional buckling of beam-columns including pre-buckling deformation effects", Computers and Structures, Vol 209, pp. 93–116.

[77] Su Y., Zhao H., Liu S., Li R., Wang Y., Wang Y., Bian J., Huang Y. (2019) „Buckling of beams with finite prebuckling deformation", International Journal of Solids and Structures, Vol 165, pp. 148-159.

[78] Zhang, F., & Kim, M. Y. (2025). A simple but accurate FEM for lateral-torsional buckling loads of mono-symmetric thin-walled beams considering pre-buckling effects. Thin-Walled Structures, 206, 112676.

[79] Glauz, R.S. (2017) “Elastic lateral-torsional buckling of general cold-formed steel beams under uniform moment”, Thin-Walled Structures, Vol 119, pp. 586-592.

[80] Agüero, A, Pallares, F.J., Pallares, L. (2015) “Equivalent geometric imperfection definition in steel structures sensitive to lateral torsional buckling due to bending moment”, Engineering Structures, Vol 96, pp. 41-55.

[81] Abureden. G.A., Ádány S. (2025). Influence of prebuckling deflections on the elastic lateral-torsional buckling of thin-walled beams with various end supports: analytical and numerical investigations in the case of doubly-symmetric cross-sections. Thin-Walled Structures, Vol 210, May 2025, 113025.

[82] Abureden. G.A., Ádány S. (2023) “On the effect of prebuckling deflections on the lateral-torsional buckling of beams”, Proceedings of the Ninth International Conference on Thin-Walled Structures (ICTWS2023), Sydney, Australia, Nov 29 – Dec 1, 2023.

[83] Vlasov, V. Z. (1959). Thin-walled elastic beams. PST Catalogue, 428.

[84] Ziemian, R.D., McGuire, W., Liu, S.W., (2022). MASTAN2, V5.1.26, 2022.

[85] Ansys (2020), Ansys Inc., Release 2020 R1.

[86] Ádány S., Visy D. (2012) “Global Buckling of Thin-Walled Columns: Numerical Studies”, Thin-Walled Structures (2012), Vol 54, pp. 82-93.

[87] Haffar M.Z., Horacek M., Ádány S., (2023) “The effect of cross-section geometry on the lateral–torsional behavior of thin-walled beams: Analytical and numerical studies”, Vol 184.

[88] Nethercot, D.A. (1973). Buckling of laterally or torsionally restrained beams. Journal of the Engineering Mechanics Division, 99(4), pp. 773-791.

[89] Geng-Shu, T., Shao-Fan, C. (1988). Buckling of laterally and torsionally braced beams. Journal of Constructional Steel Research, 11(1), pp. 41-55.

[90] Yura, J.A., Helwig, T.A. (2010). Buckling of beams with inflection points. In Proceedings of the SSRC Annual Stability Conference, May 11-15, 2010, Orlando, FL, USA, pp. 761-780.

[91] Larue, B., Khelil, A., Gueury, M. (2007). Elastic flexural–torsional buckling of steel beams with rigid and continuous lateral restraints. Journal of Constructional Steel Research, 63(5), pp. 692-708.

[92] Khelil, A., Larue, B. (2008). Simple solutions for the flexural-torsional buckling of laterally restrained I-beams. Engineering structures, 30(10), pp. 2923-2934.

[93] Taras, A., Greiner, R. (2008). Torsional and flexural torsional buckling – A study on laterally restrained I-sections. Journal of Constructional Steel Research, 64(7-8), pp. 725-731.

[94] McCann, F. (2012). Stability of beams with discrete lateral restraints. Doctoral dissertation, Department of Civil and Environmental Engineering, Imperial College, London.

[95] Marin, C., Marin, A. (2012). Determination of the maximal buckling force for a straight beam with different supporting conditionsand symmetrically ends (I). The Romanian Review Precision Mechanics, Optics and Mechatronics, (41), 151.

[96] Nguyen, C. T., Joo, H. S., Moon, J., Lee, H. E. (2012). Flexural-torsional buckling strength of I-girders with discrete torsional braces under various loading conditions. Engineering Structures, 36, pp. 337-350.

[97] Nguyen, C. T., Moon, J., Lee, H. E. (2010). Lateral–torsional buckling of I-girders with discrete torsional bracings. Journal of Constructional Steel Research, 66(2), pp. 170-177.

[98] Lee, H. E., Nguyen, C. T., Moon, J. H., Joo, H. S. (2011). Lateral-torsional buckling of discretely-braced i-girder. Procedia Engineering, 14, pp. 264-271.

[99] Unterweger, H., Kettler, M., Loschan, S. (2017). 05.14: Lateral torsional buckling of steel beams: Effect of discrete flexible intermediate supports at the upper flange. ce/papers, 1(2-3), pp. 1143-1151.

[100] Unterweger, H., Taras, A., Loschan, S., Kettler, M. (2017). Influence of imperfections on the stability of beams with intermediate flexible supports. Journal of Constructional Steel Research, 136, pp. 140-148.

[101] Sahraei, A., Mohareb, M. (2016). Upper and lower bound solutions for lateral-torsional buckling of doubly symmetric members. Thin-Walled Structures, 102, pp. 180-196.